DANMARKS OG GRØNLANDS GEOLOGISKE UNDERSØGELSE RAPPORT 2010/24

The crustal velocity structure in southern Baffin Bay

Analysis of refraction seismic line 600 from the Merian 2008 cruise (MSM09/3)

Thomas Funck

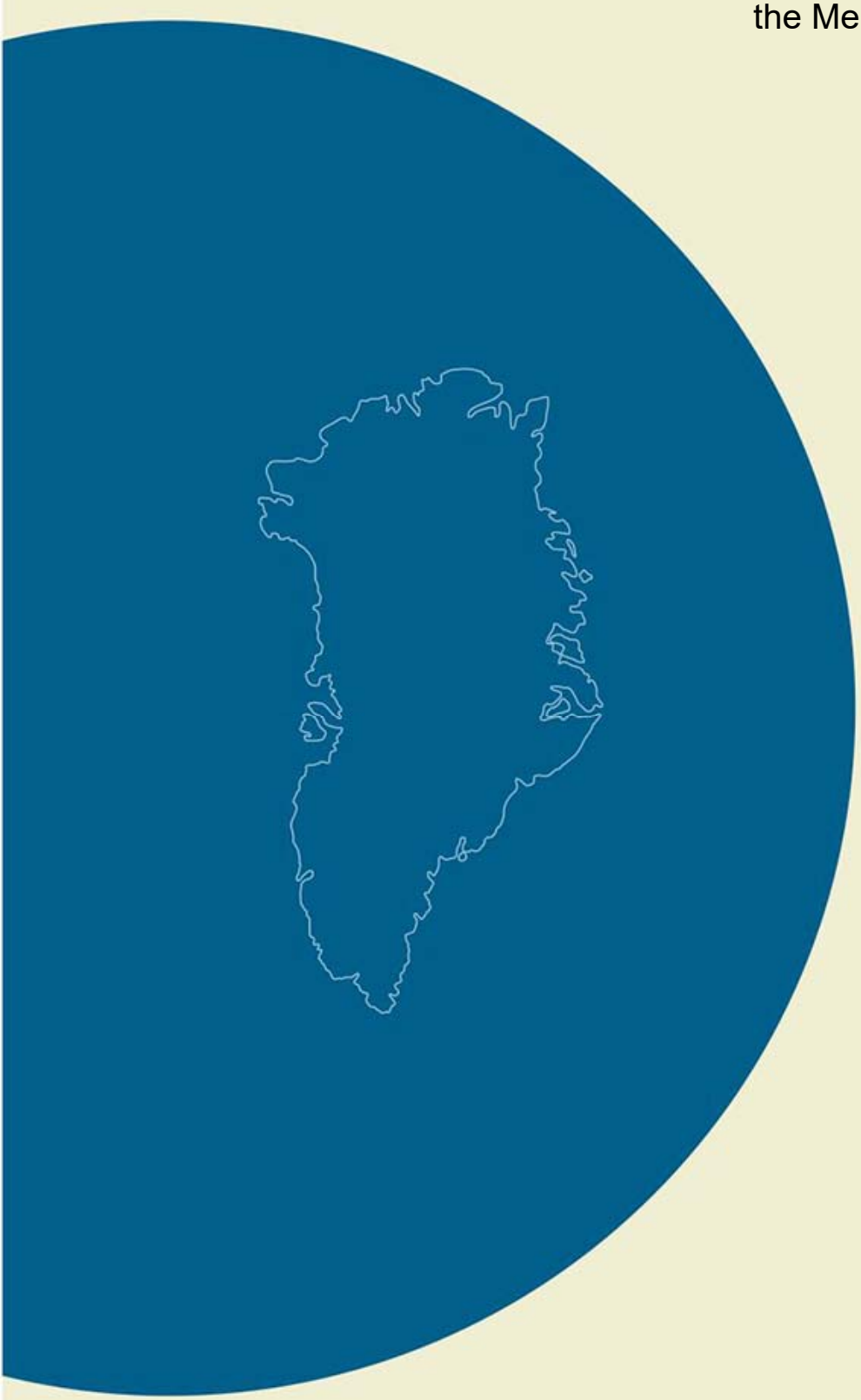

GEOLOGICAL SURVEY OF DENMARK AND GREENLAND
MINISTRY OF CLIMATE AND ENERGY

GEUS

DANMARKS OG GRØNLANDS GEOLOGISKE UNDERSØGELSE RAPPORT 2010/24

The crustal velocity structure in southern Baffin Bay

Analysis of refraction seismic line 600 from the Merian 2008 cruise (MSM09/3)

Thomas Funck

Released 23.12.2012

GEOLOGICAL SURVEY OF DENMARK AND GREENLAND
MINISTRY OF CLIMATE END ENERGY

GEUS

Contents

1. Summary

During the *Maria S. Merian* expedition MSM09/3 in 2008, a wide-angle reflection/refraction seismic experiment was carried out in southern Baffin Bay and Davis Strait. Line 600 is a 450-km-long transect from the shelf off Baffin Island, across the deep basin of southern Baffin Bay and onto the Greenland shelf where the line crosses the Hellefisk-1 well. Airgun shots from a 115 l array (7000 in^3) and with an average spacing of 156 m were recorded by 22 ocean bottom seismometers deployed along the line. The shots were also recorded by a 3450-m-long hydrophone cable, providing a coincident reflection seismic record along the line. A velocity model for the sediments, the crust and the uppermost mantle was developed by forward and inverse modelling of the observed travel times and by incorporation of the reflection seismic data, which constrains the geometry of sedimentary layers. Beneath the Baffin Island shelf, continental crust with velocities of 5.5 to 5.9 km/s (upper crust), 6.1 to 6.3 km/s (mid-crustal layer) and 6.6 to 6.9 km/s (lower crust) is observed. The maximum seismically constrained Moho depth is 15 km, but gravity modelling indicates a substantial crustal thickening towards the end of the line. The transition from continental to oceanic crust is abrupt without a transition zone. This is consistent with the interpretation that this portion of the margin represents a transform margin. The initial oceanic crust has a thickness of 6 to 7 km and is interpreted as a transform fault that can be correlated northward on the free-air gravity map. The remainder of the oceanic crust along line 600 has a thickness of 9 km, with the exception of a fracture zone (6 km) and another transform fault in the transition zone to the Greenlandic continental crust, where the crust of possible oceanic affinity is 4 km thick. Within this transform fault, a 5-km-deep basin with velocities of ~4.8 km/s is observed, probably representing volcanic material. Velocities within oceanic layer 3 are 6.8 to 7.2 km/s. Within layer 2, velocities are 5.5 to 6.0 km/s in the NW and SE but higher in the centre of the line (6.1 to 6.5 km/s) where there are positive magnetic anomalies. Proximity of line 600 to the extinct spreading axis in Baffin Bay indicates that the Iceland plume affected the study area well into the Eocene by creating thicker than normal oceanic crust (9 km compared to global average of 7 km). To the SE of the oceanic crust, 20-km-thick igneous crust has formed with velocities of 6.3 to 6.6 km/s and 6.8 to 7.3 km/s in the upper and lower section, respectively. This 25-km-wide zone coincides with a gravity high that can be traced through the entire length of Davis Strait into Labrador Sea. This gravity feature is interpreted to mark the position of a leaky transform fault within the Ungava Fault Zone, where plume-derived magma filled gaps that were formed during phases of transtension. The adjacent continental crust beneath the Hellefisk-1 well is characterized by upper and lower crustal velocities of 5.9 to 6.2 km/s and 6.5 to 6.8 km/s, respectively. The total thickness of the two layers varies between 9 and 14 km. Wide-angle reflections indicate the presence of an 8-km-thick high-velocity zone beneath the continental crust that can be correlated to the igneous crust of the leaky transform fault. This is consistent with interpretations that plume material was channelled southward through Davis Strait along lithospheric thin spots, as indicated by magmatic underplating and associated high seismic velocities at the base of the crust. Up to 4-km-thick Paleogene volcanic rocks (drilled at the Hellefisk-1 well) with velocities of 5.2 to 5.7 km/s cover the continental crust and the leaky transform fault. At the SE end of the line a low-velocity zone was discovered beneath the volcanic layer. However, velocities and composition within this zone are not constrained. Sediments have a maximum thickness of 6 km with velocities between 1.6 and 4.4 km/s.

Mantle velocities in the oceanic domain vary between 7.8 and 7.9 km/s, but may increase to 8.0 km/s beneath the Baffin Island continental crust.

2. Introduction

In 2008, the German research vessel *Maria S. Merian* carried out a geophysical study in Davis Strait and southern Baffin Bay (Fig. 1). The project was a collaboration between the Alfred Wegener Institute for Polar and Marine Research (AWI; Bremerhaven, Germany), the Federal Institute for Geosciences and Natural Resources (BGR; Hanover, Germany) and the Geological Survey of Denmark and Greenland (GEUS; Copenhagen, Denmark) with participation of Dalhousie University (Halifax, Canada).

The four main components of the program included the collection of wide-angle reflection/refraction seismic data with ocean bottom seismometers (OBS), the acquisition of reflection seismic data along the OBS transects and along additional tie lines, magnetic profiling and continuous gravity measurements. In addition, the onboard sediment echosounder (Parasound DS P-70) and swath bathymetric system (Kongsberg EM-120) were operated almost continuously while the ship was in the study area.

The Merian expedition was a component of the lead project "*Plate Tectonics and Polar Gateways in the Earth System (PLATES & GATES)*" of the International Polar Year (IPY 2007/08). The project title of the cruise was DAVIS GATE and the aim was to develop a tectonic and sedimentary reconstruction of the opening process of the oceanic gateway formed by the Davis Strait – a shallow water strait that separates the Baffin Bay in the north from the Labrador Sea in the south.

For these geodynamic reconstructions, knowledge of the deep crustal structure is essential and for this reason, refraction seismic data were collected. The data set will allow the nature of the crust in southern Baffin Bay to be determined, whether it consists of oceanic crust or of unroofed and partially serpentinized mantle as suggested for northern Baffin Bay (Reid & Jackson 1997). So far, the presumed spreading axis in Baffin Bay is only inferred from gravity data. With the new data, the position of the axis will be verified. Together with the mapping of the continent-ocean transition zone, important constraints for plate reconstructions will be obtained. Paleogene volcanism in the Davis Strait and southern Baffin Bay is associated with the Greenland-Iceland mantle plume. The refraction seismic data will provide information on the distribution and volume of this volcanism, both near the surface and as underplated layers at deep-crustal levels. This will also allow the interaction between the plume and the transform-rifted margin in the Davis Strait to be investigated. Analysis of the crustal extension and subsidence will help to constrain paleotopographic models of the region. This in turn will provide information on the water exchange from Baffin Bay to Labrador Sea. GEUS is leading the analysis of refraction seismic line AWI20080600 (below referred to as line 600) on which this report will focus.

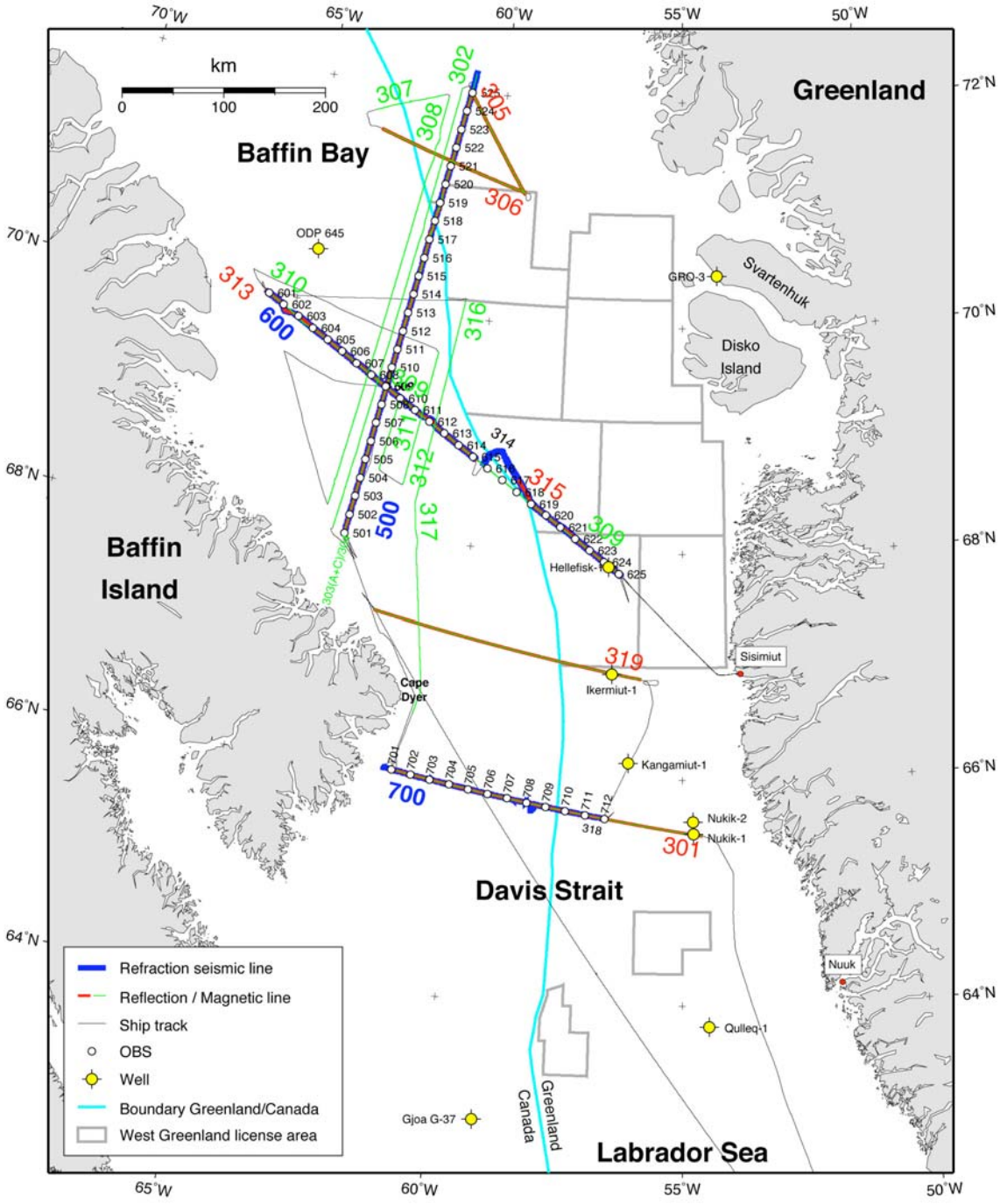

Figure 1. *Location map showing the profiles along which geophysical data were acquired during the MSM09/3 expedition. Gravity measurements were collected continuously during the cruise. In addition, while in the study area, the sediment echo-sounder and the swath-bathymetric system were in operation. For details see Gohl et al. (2009).*

3. Geological Setting

3.1 General Setting

Davis Strait is a bathymetric high between Baffin Island to the west and Greenland to the east that separates Labrador Sea from Baffin Bay (Fig. 2). The oldest undisputed sea-floor spreading magnetic anomaly in the Labrador Sea is magnetic chron 27 (61.3–60.9 Ma) (Chalmers & Laursen 1995). Other authors suggest that sea-floor spreading started during magnetic chron 33 (79.7–74.5 Ma) (Roest & Srivastava 1989) or between chron 29 and 31 (66–64 Ma) (Chian *et al.* 1995a). A reorientation of the spreading axis took place during magnetochron 24r (55.9–53.3 Ma), at the same time that sea-floor spreading initiated between Greenland and Europe. Spreading in the Labrador Sea ceased by magnetochron 13 (33 Ma) (Srivastava 1978). The continental stretching and rifting in the Labrador Sea and Davis Strait occurred over an extended period of time as indicated by dyke swarms in West Greenland. Based on the ages of these dykes, Larsen *et al.* (2009) identified several phases of tectonomagmatic activity: initial stretching from the Late Triassic to Late Jurassic (223 to 150 Ma), stretching and thinning in the Late Jurassic (150 Ma), further stretching and thinning in the Early Cretaceous (140 to 133 Ma) followed by Paleogene thinning and break-up (63 to 50 Ma).

Baffin Bay is the northwest extension of the Labrador Sea spreading system. The transform margin in Davis Strait that links these two areas is characterized by the Ungava transform fault, a name that was first introduced by Kerr (1967). Later, the term Ungava fault zone (UFZ) became more commonly used. The position of the UFZ is taken to be along the SE side of a line of positive gravity anomalies. Davis Strait, unlike Labrador Sea and Baffin Bay, is bounded by volcanic margins. Onshore, Palaeogene volcanics crop out on either side of the strait in a short narrow belt near Cape Dyer on Baffin Island and in a wider zone in the Disko-Svartenhuk area of West Greenland. Storey *et al.* (1998) identified two main pulses of volcanism in West Greenland: one between 60.7 and 59.4 Ma and one between 54.8 and 53.6 Ma. The first pulse is probably related to the arrival of the Greenland-Iceland plume. Larsen & Saunders (1998) explain the almost simultaneous volcanism from 62 to 60 Ma in West Greenland (Storey *et al.* 1998), East Greenland (Larsen & Saunders 1998), and on the British Isles (Pearson *et al.* 1996) by rapid lateral flow of a small plume head that impinged on the continental lithosphere. Continental break-up of East Greenland from NW Europe occurred at 56 Ma (Larsen & Saunders 1998) and caused a reorientation of the spreading axis in Labrador Sea (Srivastava 1978). Storey *et al.* (1998) suggested that the second pulse of volcanism in West Greenland could be related to this reorientation of the spreading axis, during which remnants of the plume could have generated melts along the UFZ. Volcanic layers, lava flows and seaward dipping reflectors (SDR) are mapped in large areas of Davis Strait (Skaarup *et al.* 2006, Chalmers & Laursen 1995, Chalmers 1997). In addition, volcanic rocks were drilled in the Hekja O-71 (Klose *et al.* 1982), Ralegh N-18 (BASIN database, Geological Survey of Canada, Dartmouth, Nova Scotia, Canada), and Gjoa G-37 (Klose *et al.* 1982) wells. Laser Argon dating of basaltic rocks from the Gjoa well yielded ages of 59.5 Ma (Williamson *et al.* 2001), which relates those rock samples to the first pulse of volcanism.

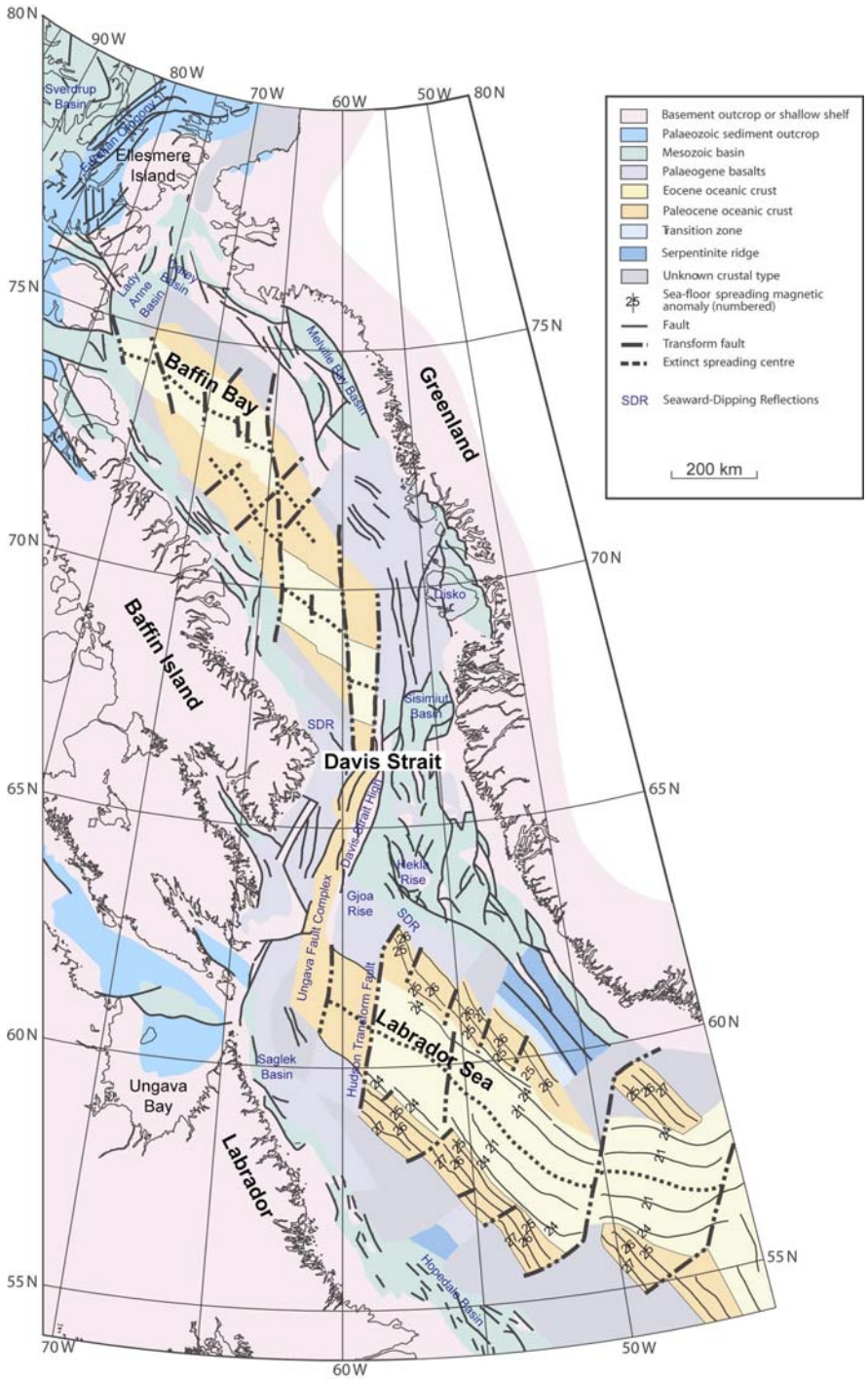

Figure 2. *Geological map of the offshore region between Canada and Greenland (from Chalmers & Oakey 2007).*

Baffin Bay forms a sedimentary basin that extends from Davis Strait in the south to Nares Strait in the north. The sediment thickness is up to 12 km in northern Baffin Bay (Reid & Jackson 1997). The nature of the crust in Baffin Bay is disputed. Keen *et al.* (1974) provide evidence that the Baffin Bay crust was created by seafloor spreading, which is supported by refraction seismic velocity models that are compatible with oceanic crust (Keen & Barrett 1972). In contrast, Reid & Jackson (1997) interpret their velocity model as evidence for serpentinised mantle in northern Baffin Bay in support for amagmatic conti-

nental rifting and separation. Serpentinised mantle is often observed in ocean-continent transition zones of non-volcanic continental margins (e.g., Funck *et al.* 2003, 2004) or at ultra-slow spreading ridges (Jokat *et al.* 2003). Chalmers and Pulvertaft (2001) point out that there are no unequivocal magnetic anomalies in Baffin Bay that can be related to sea-floor spreading. Absence of these anomalies could be related to oblique spreading or to a blanketing effect of up to 12 km of sediments. The position of the extinct spreading axis and of the transform faults in Fig. 2 is determined from gravity and magnetic anomaly maps (Chalmers & Pulvertaft 2001, Chalmers & Oakey 2007).

3.2 Previous Geophysical Studies

The coverage by refraction and regional deep reflection seismic data is variable along the ocean basins west of Greenland. The most detailed picture is available for the Labrador Sea, where a number of refraction profiles define the non-volcanic nature of the conjugate continental margins of Labrador and SW Greenland (e.g., Chian & Louden 1994, Chian *et al.* 1995b). In addition, long regional reflection seismic lines were acquired by BGR, the Geological Survey of Canada (GSC) and LITHOPROBE (e.g., Chalmers & Laursen 1995, Chian *et al.* 1995a, Hall *et al.* 2002).

In the Baffin Bay, modern refraction seismic lines with ocean bottom seismometers are limited to the entrance of the Nares Strait (Jackson & Reid 1994, Reid & Jackson 1997), where Reid & Jackson (1997) interpret velocities of 6.8 km/s as indication for serpentinized mantle rather than oceanic crust. The remainder of the Baffin Bay is only covered by short sonobuoy profiles (Fig. 2), which show velocities compatible with oceanic crust (Keen & Barrett 1972).

In the southern Davis Strait, two lines from the Nugget experiment (Funck *et al.* 2007; Gerlings *et al.* 2009) and a line along the Greenland coast (Gohl & Smithson 1993) provide some information on the crustal structure in that region. Nugget line 1 (Fig. 2) shows that the Davis Strait is underlain by thinned continental crust with the exception of an area around the UFZ, where crust of an oceanic affinity was observed (Funck *et al.* 2007). The oceanic crust is associated with pronounced gravity and magnetic anomalies that can be correlated through Davis Strait. This suggests that the UFZ acted as a leaky transform fault during phases of transtension. The 7 to 12-km-thick continental crust on Nugget line 1 is underlain by a ~5 km thick high-velocity zone (HVZ) that Funck *et al.* (2007) associate with southward flow of plume material along lithospheric thin spots, similar to a model suggested earlier by Nielsen *et al.* (2002).

While Funck *et al.* (2007) found no evidence for a HVZ beneath the thicker continental crust close to Greenland, Gohl & Smithson (1993) identified an up to 8-km-thick HVZ at the base of the Greenlandic crust, where the Moho depth varies between 30 to 42 km. Gohl & Smithson (1993) interpret the HVZ to be associated with hot-spot magmatism in the Davis Strait and Baffin Bay region. This magmatism is also observed along Nugget line 2 (Fig. 2), which extends from southern Davis Strait into northern Labrador Sea. Here, Gerlings *et al.* (2009) observed a 12-km-thick oceanic crust that is overlain by an up to 2-km-thick sequence of Palaeogene basalts. This is in the area of BGR line 77-6, where Chalmers & Laursen (1995) identified seaward-dipping reflections that are indicative of volcanic-style margins. However, the volcanism is limited to the northernmost part of Labrador Sea. Far-

ther south, the continental margins have a non-volcanic character with serpentinised mantle in the continent-ocean transition zone (Chian *et al.* 1995b).

4. Wide-Angle Seismic Experiment

4.1 Data Acquisition and Processing

The DAVIS GATE project was carried out in September and October 2008 onboard the German research vessel *Maria S. Merian* (Gohl *et al.* 2009). At that time of the year, the Baffin Bay is relatively ice-free with the exception of isolated icebergs. As trade-off, one has to accept reduced daylight, increased frequency of storms, temperatures close to the freezing point and precipitation in form of snow. Three refraction seismic lines were collected during the cruise (lines 500, 600 and 700; Fig. 1). This report is on line 600, a 450-km-long transect (Fig. 3) from the shelf off Baffin Island, across the southern Baffin Bay and onto the shelf off West Greenland. Close to the southeastern termination of line 600, the location of the 3201-m-deep Hellefisk-1 well was crossed.

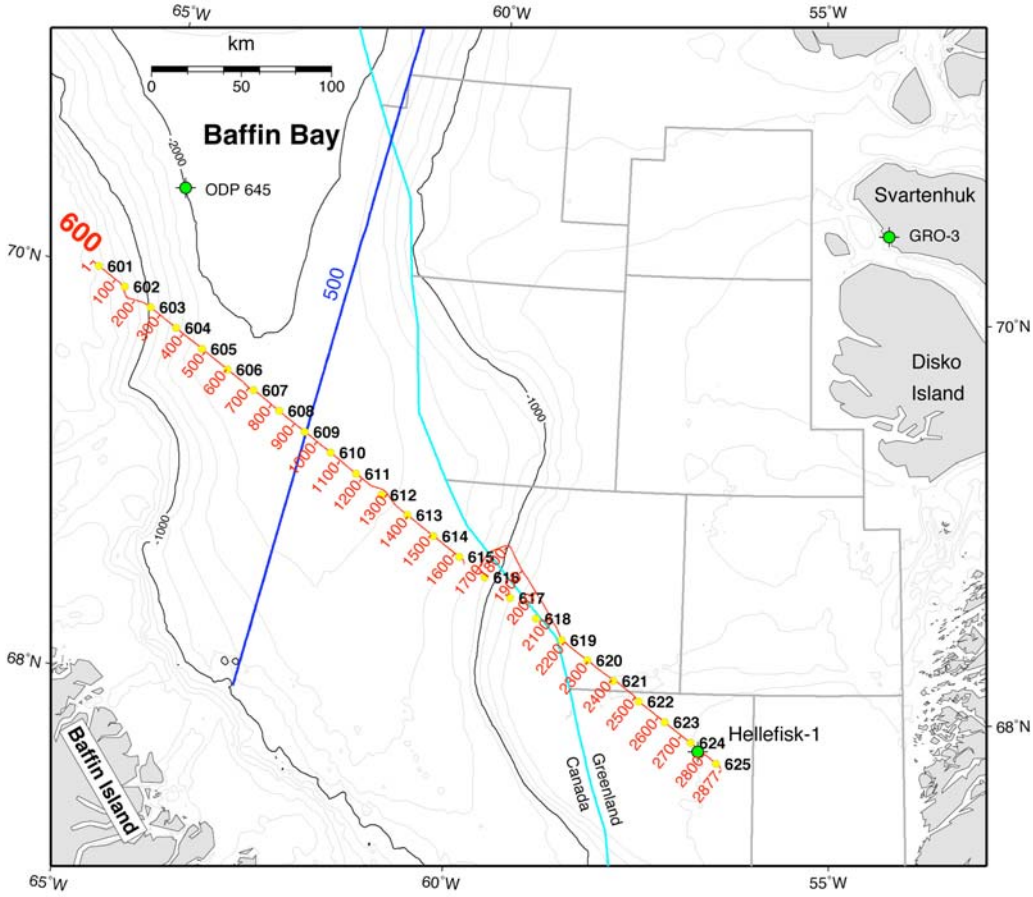

Figure 3. *Location map of line 600 (full name: AWI20080600) of the MSM09/3 expedition. Line 600 is shown in red, shot positions are labelled for every 100th shot point. Yellow circles indicate the location of ocean bottom seismometers (OBS), the dark blue line marks refraction line 500 and green circles indicate well locations. License areas and the boundary between Canada and Greenland are shown as light blue and grey lines, respectively. The bathymetry is plotted with solid lines; the contour interval is 200 m. Digital navigation for the shots and OBS can be found on the CD-ROM attached to this report.*

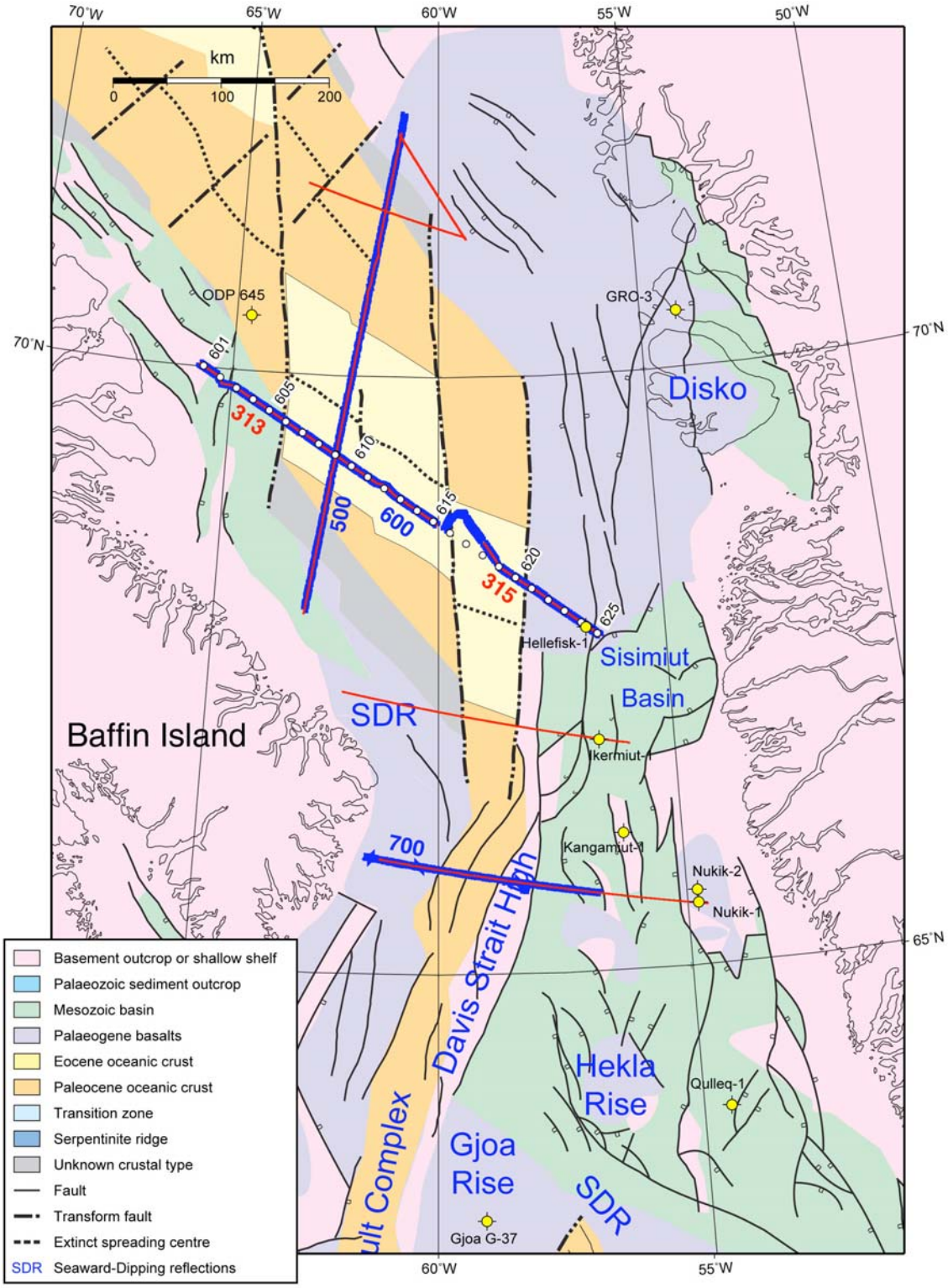

Figure 4. *Geologic map of the southern Baffin Bay, the Davis Strait region and the northernmost Labrador Sea (Chalmers & Oakey 2007). Blue lines indicate the location of the MSM09/3 refraction seismic lines (AWI20080[500/600/700]) with white circles showing the position of ocean bottom seismometers (OBS) along line 600. MSM09/3 reflection seismic lines (BGR08-[301to319]) are shown in red. Wells are indicated by yellow circles.*

Fig. 4 shows the location of line 600 in a geological context using the most up-to-date regional geology map compiled by Chalmers & Oakey (2007). The characterization of basement types is primarily based on reflection seismic data, potential field data and plate reconstructions since refraction seismic data are scarce in this area (see 3.2 Previous Geophysical Studies). The map was used for planning the location of the refraction lines of the MSM09/3 expedition with the goal to verify the crustal affinity in key areas, such as the northern extension of the Ungava Fault Zone.

A total of 25 ocean bottom seismometers (OBS) were deployed at equal distances along the line (18.4 km spacing). The instruments were provided by IFM-GEOMAR (Kiel, Germany) and contained either a Marine Broadband Seismic Recorder (MBS) or a Marine Longtime Seismocorder (MLS) data logger manufactured by SEND GmbH. Each instrument was equipped with a three-component Mark (4.5 Hz) seismometer and a HighTech (HTI) or E-2PD hydrophone by OAS (Gohl *et al.* 2009).

The seismic source consisted of two G-gun sub-arrays, each with four two-gun clusters, and two Bolt 800CT airguns towed at 6 m depth. The volume of individual G-guns ranged from 1.1-4 l (70 to 250 in^3) and the total volume was 50 l (3100 in^3) with a nominal working pressure of 145 bar (2100 psi). The two Bolt 800CT airguns each had a volume of 32 l (1953 in^3) and were used to boost the low frequencies. However, the Bolt guns could only be operated at a pressure of 80 bar (1160 psi) due to technical problems with the shot trigger signal. The shot interval was one minute, which resulted in an average shot spacing of 156 m at a variable ship speed of 4 to 5 knots. For navigation, the ship's GPS system was used with an accuracy of 10-20 m (Gohl *et al.* 2009).

The shots were simultaneously recorded by a digital hydrophone streamer with an active length of 3450 m. Originally, the plan was to shoot the line twice; once with a larger shot spacing for the refraction line (OBS) and a second time for the reflection seismic with a shorter shot spacing of 50 m. However, since the expedition was running short of time, shooting with the shorter spacing had to be abandoned. The purpose of the coincident reflection seismic lines was to assist the velocity modelling of the refraction seismic data by providing detailed information on the geometry of the basement and sedimentary layers. In addition, the interpretation of either data set greatly benefits from the other. The coincident reflection seismic data are shown in Appendix B.

During the shooting of line 600, the vessel encountered an area with active fishing just to the west of the boundary between Canada and Greenland. This happened at night during a heavy snow storm with a visibility well below 50 m. For this reason, the streamer had to be recovered and the ship detoured to the north into Greenlandic waters (Fig. 3), from where the ship followed the international boundary in a SE direction back to the original line. This resulted in a kink in the line with shots being offset by up to 23 km from the deployed positions of OBS 616, 617 and 618. As discussed later, the resolution of the velocity model is reduced in this zone.

After recovery of the OBS, the data were dumped to disk, corrected for OBS clock drift, converted to SEG-Y format, and debiased. Travel time picks of the direct wave were used to recalculate the position of the instruments at the seafloor using a least squares method and velocity-depth profiles for the water column obtained from CTD measurements. Shot-receiver ranges were calculated from the new OBS locations. Record sections were produced for all hydrophone and geophone components to aid digitising the travel times on a computer screen. In Appendix A, the component (hydrophone or vertical geophone) with

the highest signal-to-noise ratio is shown for each OBS, displayed with a band-pass filter from 8 to 24 Hz (corner frequencies 2-8-24-36 Hz). This filter reduces noise signals with a frequency of 4 to 5 Hz, which were observed on some records. Deconvolution improved the recognition of seismic phases to some extent but was less successful in the shallow water where the large Bolt guns produced significant reverberations. Trace amplitudes in the record sections (Figs A-1 to A-23) are weighted by their distance to the OBS to increase amplitudes for large offsets; travel times are plotted with a linear reduction velocity of 6.8 km/s.

4.2 Methodology

The goal of the analysis of the refraction seismic data was to obtain a two-dimensional velocity model for the sediments, basalts, crust, and uppermost mantle. Line 600 was shot along a great circle arc with the exception of the off-line shots when the ship had to deviate from the line due to fishing vessels. Reference point (x=0 km) in the model is the location of the first shot (70.021278°N and 65.835490°W). The OBS positions for the model were derived from the calculation of the distance between the reference point and the recalculated OBS position assuming spherical earth.

The *P* wave velocity model was developed using the program RAYINVR (Zelt & Smith 1992; Zelt & Forsyth 1994), which allows both for forward and inverse modelling. Initially, a forward model was developed from top to bottom (seafloor to mantle) by fitting the observed travel times that were digitised in the program ZPLOT (written by Colin A. Zelt). Layer boundaries within the sediments and the basement geometry were taken from the coincident reflection seismic record whenever the data quality allowed for this. However, the low fold of the reflection seismic data, the location of the seabed multiple, and the gap in the reflection data due to the deviation around fishing vessels, prevent a clear definition of the basement along most portions of line 600. After the development of the initial forward model, both layer boundaries and velocities within layers were optimised by using the inversion algorithm in RAYINVR. Gravity data were used to help defining the deep structures at the edges of the line without ray coverage (see 5.3 Gravity Modelling).

4.3 Seismic Data

Record sections for all instruments are displayed in Appendix A (Figs A-1 through A-23). Three OBS had technical problems, which prevented the recording of data (OBS 605, 606 and 621). Most records exhibit a high signal-to-noise ratio that allow for the identification of seismic phases down to the mantle (mantle refraction P_n) as for example on OBS 609 (Fig. A-7). The Moho reflection (P_mP) can be recognized on most records, in particular for OBS's on crust with oceanic affinity (e.g., OBS 609 to the SE; Fig. A-7) but also in the continental domain (e.g., OBS 624 to the NW; Fig. A-21). Most instruments between OBS 604 and 619 show a prominent refraction that is approximately horizontal when plotted with a reduction velocity of 6.8 km/s. This indicates the presence of a crustal layer with a velocity around 6.8 km/s, which is very typical for layer 3 in oceanic crust (White *et al.* 1992).

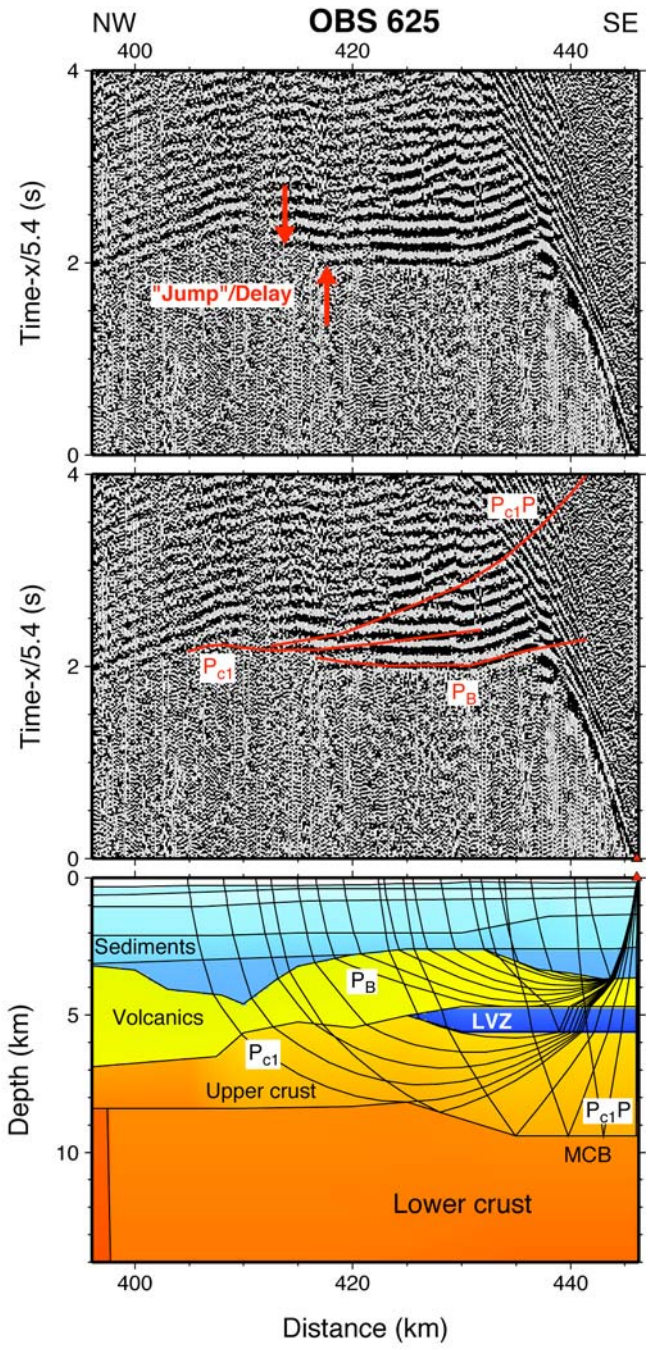

Figure 5. *(top) Part of record section of OBS 625 (hydrophone component) displayed with a reduction velocity of 5.4 km/s. The horizontal scale is distance along the velocity model. (middle) The same record shown together with calculated travel times (red lines) for some selected phases. (bottom) The corresponding velocity model (same colour scheme as in Fig. 7) with the ray paths of the selected phases. The red triangle marks the position of the OBS. For phase names see also Table 1. A description of the processing is given in the text. Abbreviations are LVZ, low-velocity zone; MCB mid-crustal boundary.*

Two important record sections are discussed here in more detail. OBS 625 (Fig. 5) at the SE end of line 600 shows a high-amplitude mid-crustal reflection ($P_{c1}P$). Such mid-crustal reflections are generally not observed in oceanic crust as there is a rather smooth transition from the upper, layer 2 to lower, layer 3 crustal velocities (cf. White *et al.* 1992). In contrast, mid-crustal reflections are very typical for continental crust (e.g., Funck & Louden 1999; Funck *et al.* 2000, 2003). Hence, this reflection is regarded as an indication for the presence of continental crust close to the Hellefisk-1 well. Further evidence is provided by the observed velocities (see 5.1 Velocity Model).

A second feature to be discussed for OBS 625 (Fig. 5) is the occurrence of a low-velocity zone that is revealed by a “jump” or time delay in the first arrivals some 30 km to

the NW of the OBS (at a distance of 417 km). At this distance, the refraction within the volcanic layer (labelled P_B) disappears and some 200 ms later another refraction (P_{c1}, within the upper crust) becomes the new first arrival. Such a time delay can only be generated by a layer between the volcanic layer and the upper crust with a velocity lower than in the volcanic layer. Unfortunately, due to the inherent nature low-velocity zones (LVZ), no refractions from within the LVZ can be observed. Hence, the velocity within the LVZ is unconstrained (see also 5.2 Model Resolution and Uncertainty).

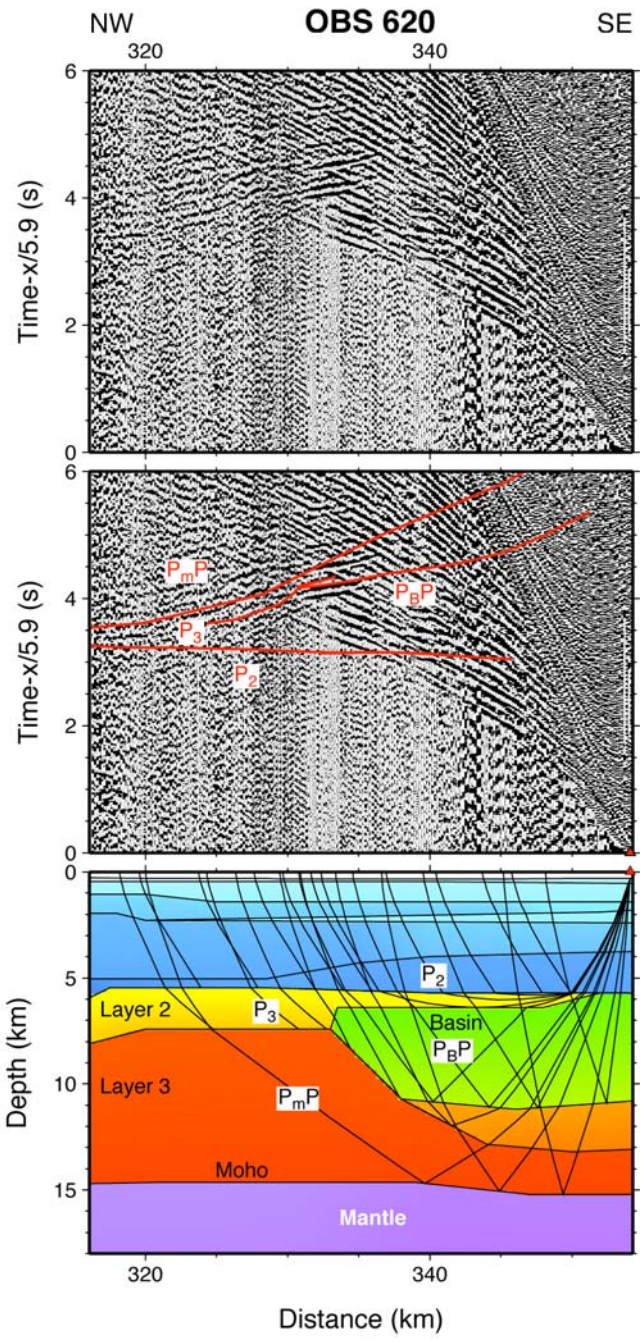

Figure 6. *(top) Part of record section of OBS 620 (hydrophone component) displayed with a reduction velocity of 5.9 km/s. The horizontal scale is distance along the velocity model. (middle) The same record shown together with calculated travel times (red lines) for some selected phases. (bottom) The corresponding velocity model (same colour scheme as in Fig. 7) with the ray paths of the selected phases. The red triangle marks the position of the OBS. For phase names see also Table 1. A description of the processing is given in the text.*

One OBS that was very difficult to model was OBS 620 (Fig.6). This was due to a very complex geometry close to that OBS with a deep basin that caused problems with phase identification. A strong reflection at a distance of 330 to 335 km was initially thought to be the Moho reflection P_mP. However, later it was determined to be a reflection from the base of the basin. The most important phase on this record is the P_2 refraction – a phase that is very difficult to spot due to its low amplitude. It is, however, easy to detect when the data are displayed with a reduction velocity similar to the phase velocity (5.9 km/s). The velocity is similar to that observed in the upper crust to the NW of OBS 619 (Fig. A-17). However, using a velocity of 5.9 km/s for the entire basin cannot explain the time delay for deep crustal phases observed on instruments farther to the SE (e.g., the pronounced delay of the first arrivals at 345 km on OBS 22; Fig. A-19). This is why velocities <5.9 km/s had to be used for the basin. To match the observed P_2 phase at OBS 620, a thin layer with a velocity of 5.5 km/s was introduced at the top of the basin.

5. Results

Below, the *P* wave velocity model for line 600 is presented. First, the model is described followed by a detailed account of the model resolution and uncertainties. Finally, two-dimensional gravity modelling is employed to check for consistency of the velocity model with the observed gravity data.

5.1 Velocity Model

The *P*-wave velocity model for line 600 is shown in Fig. 7. Although some interpretation of the observed velocity structure is given here, a more detailed account can be found in the next section (6. Discussion and Interpretation). The upper part of the model consists of a series of sediment layers that follow the general trends of reflectivity along the coincident reflection seismic data (see Appendix B). In the central part of the line in the deep basin of Baffin Bay, velocities within the sedimentary layers vary from 1.6 to 4.2 km/s and the total thickness reaches 6 km. The velocities of 1.6 km/s close to the seafloor are not constrained seismically. Refractions at such a velocity and depth interfere with the direct water wave, which makes detecting sediment refractions difficult or impossible. These low velocities indicate a high water content of the uppermost sediment layer. In the NW beneath the Baffin Island shelf, the lowermost sediment layer is modelled with a velocity of 4.3 to 4.4 km/s. On the Greenland side velocities are not as high; sediments above the volcanic basement reach a velocity of 3.8 km/s. However, the maximum sediment thickness on line 600 is slightly higher off Greenland than off Baffin Island with values of 6 and 5 km, respectively.

Volcanic rocks were drilled in the lower section of the Hellefisk-1 well. The velocity model (Fig. 7) shows velocities of 5.2 to 5.7 km/s that are consistent with a volcanic layer with a maximum layer thickness of 4 km. However, the volcanic sequence consists of two mounded structures, resulting in a variable layer thickness. Between these two mounds, the thickness is as little as 1 km. To the northwest, the layer pinches out at 365 km. Between 333 and 357 km another layer appears with velocities of 4.7 to 4.9 km/s and a thickness of 5 km. This layer forms a basin and given that it is surrounded by igneous crust and has a general proximity to the drilled volcanic sequence, a mainly basaltic composition is assumed. At the SE end of the line, a low-velocity zone (LVZ) is observed beneath the basalts. The modelled velocity is 4.1 km/s within the LVZ, but it should be emphasized here that the velocity within the LVZ is not constrained due to the absence of refractions; even the depth of the top of the LVZ is undefined. However, the reflection seismic data indicate the disappearance of high-amplitude reflections at that depth level. What can be said about the velocities in the this layer is that they are lower than within the overlying basalts (5.6 km/s). Thus. the composition of the layer remains unclear (basalts or non-volcanic sediments). Other, local LVZs are observed within the sedimentary column.

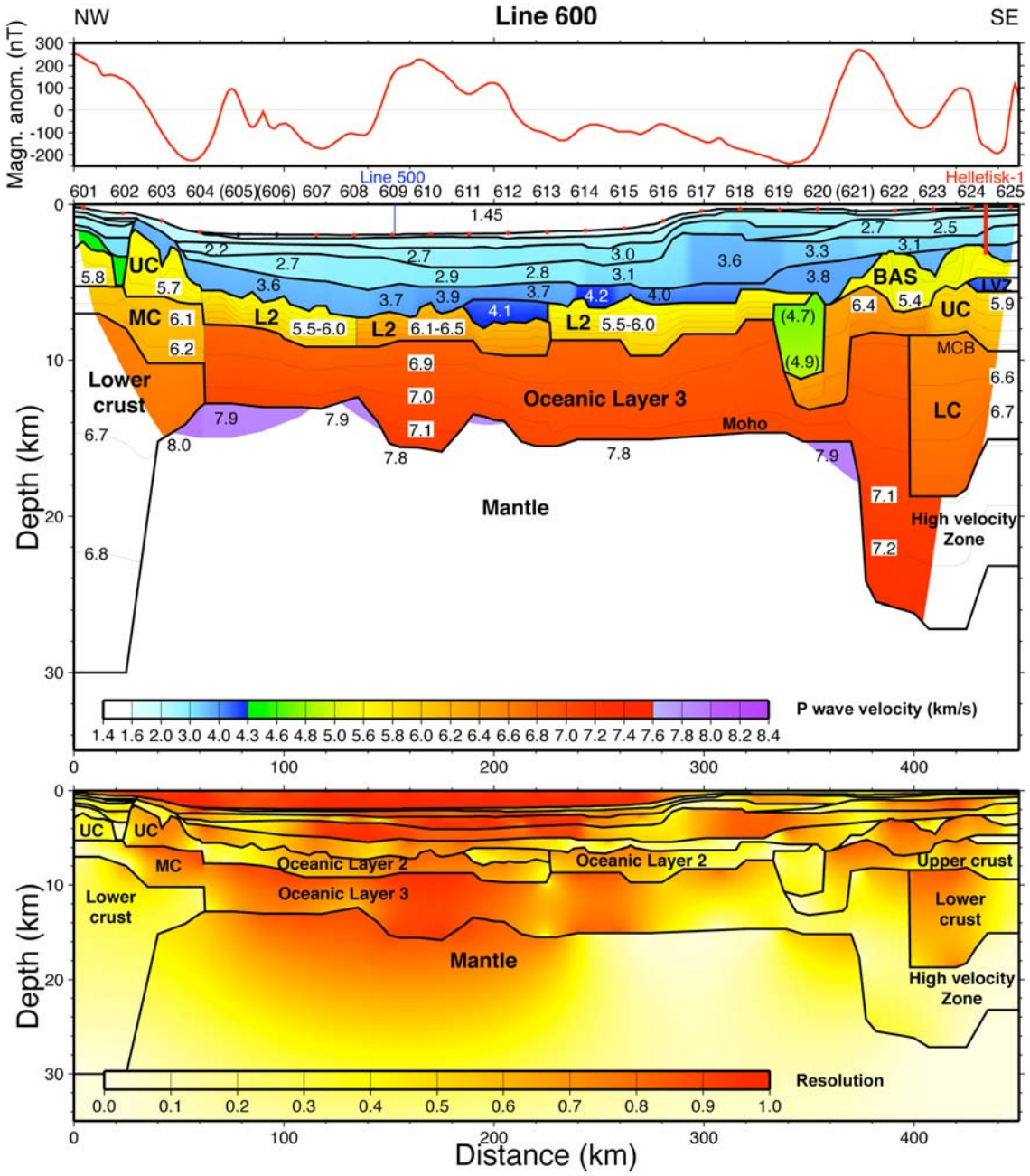

Figure 7. *Magnetic anomalies (top), P-wave velocities (middle), and diagonal values of the resolution matrix of the P wave velocity model (bottom) along line 600. Data source for the magnetic data: Verhoef et al. (1996). The outer parts of the velocity model with no ray coverage are shown in white, velocities are specified in km/s, the velocity contour interval is 0.1 km/s. Red circles show the location of OBS's that were used for the modelling, the black circles refer to non-functional OBS's. The location of the Hellefisk-1 well and the cross-point with refraction line 500 are indicated by a red and blue line, respectively. Abbreviations are BAS, basalts/volcanic rocks; MCB, mid-crustal boundary; L2, oceanic layer 2; LC, lower crust; LVZ, low-velocity zone; MC, mid-crustal layer; MCB, mid-crustal boundary; UC, upper crust.*

The basement layer shows large lateral variations both in velocity and in crustal thickness (Fig. 7). Between 0 and 60 km, the crust is modelled with three layers with velocities of 5.5-5.9 km/s in the upper crust, 6.1 to 6.3 km/s at mid-crustal levels and 6.6 to 6.9 km/s

within the lower crust. This velocity distribution and the occurrence of mid-crustal reflections are consistent with continental crust. Rough basement topography with three basement highs and a seaward shallowing of the Moho indicates that the crust has been faulted and thinned. The Moho depth is only constrained between 40 and 60 km where it shallows from 15 to 13 km.

At 60 km, a rather abrupt velocity change occurs as observed at OBS 604 (Fig. A-4), where completely different seismic phases are seen on either side of the instrument. Between 60 and 333 km, the crust is divided into an upper and lower crustal layer interpreted as oceanic layers 2 and 3 (Fig. 7). Velocities within layer 3 are fairly constant and around 6.8 km/s at the top and 7.0 to 7.2 km/s at the base as is typical for oceanic crust. Layer 2 velocities can be divided laterally into three segments: between 60 and 135 km velocities range from 5.5 to 6.0 km/s, between 135 and 227 km there is an increase to 6.1 to 6.5 km/s, and between 227 and 333 km velocities decrease again to 5.5 to 6.0 km/s. The thickness of layer 2 is generally around 2 km, but locally exceeds 3 km. The total oceanic crustal thickness varies from 5 to 9 km and the Moho reflection is located at depths between 13 and 16 km. The previously discussed basin is partly covered by a thin layer with a velocity of 5.5 km/s, which is similar to the adjacent oceanic layer 2. The exact thickness of this layer, which is assumed to be basaltic, is not determined seismically. To the SE of 352 km there is no evidence for this layer. Indeed, a better fit between observed and calculated travel times could be obtained by terminating this high-velocity layer at the SE part of the basin.

Crustal velocities beneath the basin (333 to 357 km) are not constrained seismically. However, reflections from the base of the basin and from the Moho give a thickness estimate of 4 km for the crust in this zone (Fig. 7). Farther to the SE, the crust thickens substantially; the Moho deepens from 15 km beneath the basin to 26 km between 380 and 400 km. In this zone, two crustal layers can be distinguished with velocities of 6.3 to 6.6 km/s and 6.8 to 7.3 km/s in the upper and lower layer, respectively. This crust is interpreted as thick igneous crust. Farther to the SE toward Greenland, crustal velocities decrease and this, together with the observations of mid-crustal reflections, suggest a continental character of the crust. In the upper continental crust, velocities range from 5.8 to 6.2 km/s while the lower crust exhibits velocities from 6.5 to 6.8 km/s. The upper crust is between 3 and 4 km thick, while the lower crustal thickness decreases from 10 km in the NW to 6 km in the SE. Beneath the continental crust, another layer was introduced into the model to explain a set of reflections ($P_{c2}P$) that originate from a depth level that is shallower than the Moho in the zone that is adjacent to the thick igneous crust. This was done by continuing the high velocities of the igneous crust beneath the continental crust and is interpreted as magmatic underplating. Velocities in this high-velocity zone (HVZ) are not constrained due the lack of refractions from this layer. However, the velocity change in the model from 6.8 km/s at the base of the lower continental crust to 7.1 km/s at the top of the HVZ yields in an impedance contrast that is sufficient to create detectable reflections. Funck *et al.* (2007) found a similar underplated layer in the southern Davis Strait, where the velocity was 7.4 km/s and was well resolved. This gives an idea of the possible range of velocities in the HVZ. Mantle velocities within the oceanic domain were modelled between 7.8 and 7.9 km/s. Beneath the continental crust off Baffin Island, mantle velocities of 8.0 km/s were used in the model.

5.2 Model Resolution and Uncertainty

There are several ways to assess the resolution and uncertainty of a velocity model. Here a formal error analysis for individual phases is given next to plots showing the ray coverage. In addition, the values of the diagonal of the resolution matrix for the velocity nodes are calculated. The resolution matrix is a good indicator that distinguishes between poor and well resolved parts of a model. Ideally, values of the resolution matrix are 1 but values >0.5 indicate reasonably well resolved model parameters (Lutter & Nowack 1990).

Phase	*n*	t_{rms}, s	χ^2 *(chi-square)*
Direct wave	1735	0.026	0.379
P_S (all sediment refractions)	3129	0.045	0.354
P_SP (all sediment reflections)	1337	0.096	1.683
P_B (refraction in basalt)	585	0.048	0.441
P_BP (reflection base basalt)	45	0.046	0.214
P_2 (refraction in oceanic layer 2)	1532	0.132	0.913
P_3 (refraction in oceanic layer 3)	3518	0.068	0.575
P_{c1} (refraction in upper crust)	747	0.066	0.724
$P_{c1}P$ (reflection base upper crust)	102	0.045	0.372
P_{c2} (refraction in mid-crustal layer)	882	0.090	0.859
$P_{c2}P$ (reflection base mid-crustal layer)	223	0.080	0.433
P_{c3} (refraction in lower crust)	30	0.035	0.197
P_mP (Moho reflection)	1670	0.077	0.619
P_n (refraction in mantle)	2177	0.113	0.876
All phases	17712	0.080	0.682

Table 1. *Number of observations (n), RMS misfit between calculated and picked travel times (t_{rms}), and normalized χ^2 for individual phases on line 600.*

The formal error analysis for individual phases on line 600 is summarized in Table 1. The normalized χ^2 is based on assigned pick uncertainties of 40-200 ms depending on the quality of each individual travel time pick. The assignment of pick uncertainties was done to the time of picking and primarily depends on the signal-to-noise ratio and on the interference of different seismic phases. Pick uncertainties are graphically indicated in Fig. 8. The model is generally well constrained with a total RMS misfit of 80 ms between calculated and picked travel times. This is close to the average travel time uncertainty of 83 ms. The normalized χ^2 of 0.682 is below the optimum value of 1 when travel times are fitted within the given pick uncertainty. This could indicate that either the model was fit to noise in the data or the pick uncertainties were overestimated. Looking at the χ^2 of individual phases, the refractions within the basalts and sediments have a low χ^2 (< 0.5), whereas the χ^2 of crustal and mantle phases is closer to 1. This could indicate that pick uncertainties were only overestimated for close-offset shots. Alternatively, information extracted from the coincident MCS data (in particular layer geometry of the sediments and basalts) has resulted in a better fit of the observed and calculated travel times than would have been possible by the refraction data alone.

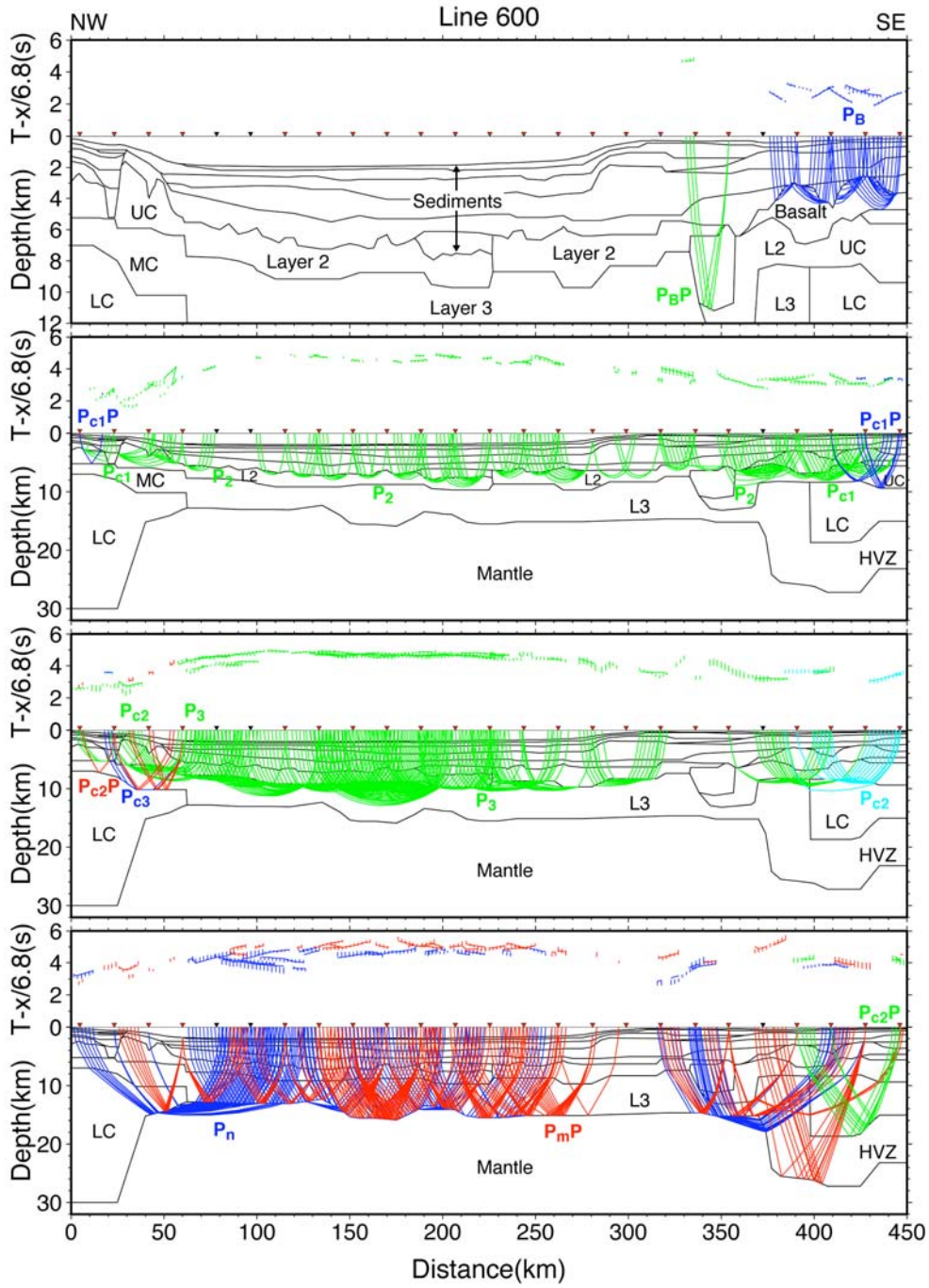

Figure 8. *Ray coverage along line 600 obtained from "point to point" (shot to OBS) ray-tracing for all travel time picks used for the modelling (only phases below basement are shown). The figure is divided into four panels for different depth levels. The lower part of each panel shows the layer boundaries of the velocity model together with the ray paths; the upper part visualizes the calculated travel times and the associated travel time picks (vertical bars with a height corresponding to the estimated pick uncertainty). Not every travel time pick and ray is plotted, a distance of 2 km between picks is used to keep the plot readable. Triangles mark the positions of the OBS's. For phase names see also Table 1. Detailed plots for each OBS are shown in Appendix A. Abbreviations are HVZ, high-velocity zone; L2, oceanic layer 2; L3, oceanic layer 3; LC, lower crust*; *MC, mid-crustal layer; UC, upper crust.*

The diagonal values of the resolution matrix of the velocity nodes are shown in a gridded version in Fig. 7 and show a close correlation with the ray coverage (Fig. 8). That is, areas with good and reversed ray coverage are characterized by high resolution values. Within the sedimentary column, velocities are generally well resolved, although there are some exceptions. In the area where the ship deviated from the track line (ca. 265 to 335 km), there are zones with reduced resolution that are caused by lack of observations (absence of close offset shots) or by complexities associated with the three-dimensionality introduced by the off-line shots. Large lateral variations were avoided within that zone. The picked phases often indicated a velocity consistent with areas close by, but with some offset in time. This indicates that the sediment thickness changes perpendicular to the line. In these cases, the offset was accepted because no consistent two-dimensional model could be found that would explain all the observations within this zone. Thus, the velocity model is representative for the location of the OBS rather than for the off-line shot locations. Phases that displayed these problems were not included in the error analysis. Another zone with poor resolution is within the sediments on the Baffin Island shelf between 0 and 30 km, where low-velocity zones occur and where not all ray-paths are reversed.

Velocities within the oceanic crust are well resolved (Fig. 7), but as before, the resolution decreases in the region where the ship deviated from the line during the shooting. Nevertheless, some P_3 rays sampled the lower crust in this region and are consistent with layer 3 velocities farther to the NW. Also the few P_2 observations are consistent with layer 2 velocities outside this zone. However, no P_n or P_mP phases are observed between 280 and 335 km, which could determine the Moho depth. As mentioned above, velocities within low-velocities zones cannot be resolved and a resolution value of 0.3 in the basin around 340 km indicates uncertainty in the velocities there. Reduced resolution within the crust close to the outer limit of the model coincides with a decrease of the number of reversed ray paths in these areas. The lower crust around 390 km has well resolved velocities at the top (resolution values of 0.7-0.8), but at the bottom and within the adjacent HVZ, velocities are only poorly resolved (see also 5.1). Mantle velocities display resolution values up to 0.9 in areas where P_n phases are observed. The plot with the ray coverage (Fig. 8) also indicates the segments of layer boundaries that are constrained by wide-angle reflections.

Absolute errors of the model can be estimated by perturbation of single nodes (velocity and boundary nodes) in the model and examination of the sensitivity of the travel times to these perturbations. No systematic tests were performed in this study, but such tests in similar settings with similar data quality generally indicate that the velocity error within the reasonably resolved parts of the crust is ±0.1 km/s and the error in Moho depth is on the order of 1 km (Funck et al. 2000). However, some tests were performed within the basin (333 to 357 km; Fig. 7). It was found that velocities that deviate ±0.4 km/s from the modelled 4.7 to 4.9 km/s can still explain most of the travel time observations, although it becomes increasingly difficult to fit all observations once the velocities are varied by more than ±0.2 km/s.

Line 600 offers another opportunity to check the accuracy of the velocity model since the line crosses the Hellefisk-1 well. Fig. 9 shows a comparison of the velocity model with the sonic log from the well. To reduce the scatter in the sonic log data, a median filter with a filter length of 20 m was used. It should also be noted that the log data were not used to adjust the velocity model; only the wide-angle reflections and refractions as well as the coincident reflection seismic data were used for the modelling. There is a general agreement between the two velocity curves but there are also deviations. For example, the velocity

model has different velocity gradients within layers, since the refractions primarily constrain velocities at the top of each layer. The layer at a depth of 1500 m and a sonic velocity of 4.5 km/s is completely missing in the velocity model because no refractions could be detected in the seismic data and, hence, such a layer is not required by the data. By missing this layer and having too low a velocity gradient in the underlying layer resulted in an underestimation of velocities. Thus, the top of the volcanic unit (velocities >5 km/s) is modelled 400 m too deep. However, in two-way travel time, the velocity model still fits the travel time to the top of the volcanic layer as can be seen when compared with the coincident reflection seismic (Fig. B-2). Velocities within the basalts compare fairly well (around 5.5 km/s). In summary, the comparison shows that the refraction data are unable to resolve the detailed velocity structure within the sediments but still match the long-wavelength features. It can also be seen that the absolute depth error of layer boundaries at the basement level is on the order of 400 to 500 m.

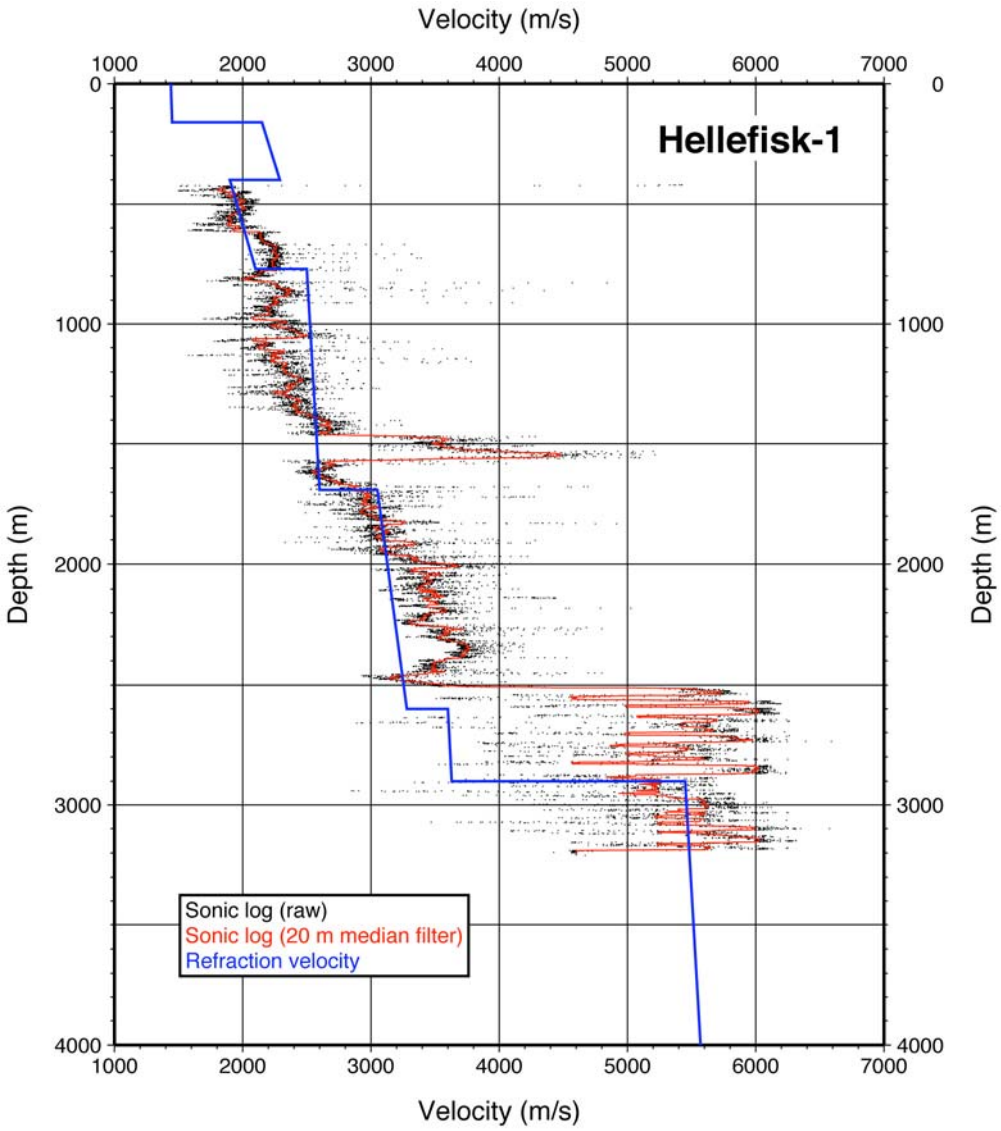

Figure 9. *Comparison of the sonic log velocities from the well Hellefisk-1 (GEUS database) with the velocities obtained from the modelling of the refraction seismic data along line 600.*

5.3 Gravity Modelling

Gravity modelling can provide additional constraints on velocity models, in particular in areas where the velocities are poorly resolved. In addition, gravity modelling can be used to verify how consistent the velocity model is with the gravity data. In this study, two-dimensional gravity modelling was performed along line 600 using the algorithm of Talwani *et al*. (1959). The observed gravity in the models (Fig. 10) are free-air gravity anomalies measured along the main line during the expedition, i.e. not along the deviation (kink) during the shooting. Ingo Heyde from the Federal Institute for Geosciences and Natural Resources (BGR; Hanover, Germany) kindly processed the ship's data and provided them for this study. Densities were obtained from conversion of the *P* wave velocities (Fig. 7) using the curve shown in Ludwig *et al.* (1970) and is approximated by

$$\rho = -0.00283v^4 + 0.0704v^3 - 0.598v^2 + 2.23v - 0.7$$

where ρ is the density in g/cm^3 and v is the *P* wave velocity in km/s. Densities of 1.03 and 3.30 g/cm^3 were used for the sea water and the mantle, respectively.

Model B (Fig. 10, top) is the starting model, in which the Moho is continued horizontally to the outer boundaries where there is no ray coverage. At the NW end of the line (between 0 and 40 km) the Moho depth was kept at 15 km. This depth is not compatible with the gravity data as the observed and calculated gravity deviate by up to 190 mgal. To compensate for that, the Moho depth was increased to 30 km at that end of the line (model C) and this resulted in a greatly reduced misfit. At the SE end of the line, a decrease of Moho depth by 4 km (model A) can reduce the misfit, although the calculated gravity is still too low. Further shallowing of the Moho in that area, however, started to affect the overall shape of the calculated gravity and was therefore not pursued. Instead, the mantle density was increased from 3300 to 3350 kg m^{-3} at the SE end of the line (model D; Fig. 10 bottom), assuming that the lithosphere beneath the continental crust might be colder and denser than in the oceanic domain. However, this assumption is questionable as this zone is affected by the mantle plume as indicated by the HVZ beneath the continental crust that is interpreted as magmatic underplating. In any case, such a density change greatly reduces the misfit between observed and calculated gravity in the southeast.

In a last modelling step, the misfit in the area of the basin at 340 km was investigated. As mentioned above, velocities within the basin are not well resolved and the velocity uncertainty may be up to 0.2 to 0.4 km/s. To obtain a good fit, the density had to be reduced from 2510 to 2310 kg m^{-3} (model E; Fig. 10 bottom). Although this decreases the misfit in the area of the basin, it seems unlikely that the density within the basin is that low. A reduction by 200 kg m^{-3} compared to the empirical formula by Ludwig *et al.* (1970) corresponds to a velocity decrease from 4.8 to 3.1 km/s. This is far too low to explain the observed travel times in the refraction seismic data. In addition, both density and velocity would be lower than in the overlying sediment layers.

In summary, even with some density adjustments, there is no perfect fit to the observed gravity data. Many of the deviations are likely due to three-dimensional effects that cannot be treated properly in a two-dimensional model. One example is the 4-km-deep sedimentary basin around 20 km (Fig. 10) that is required to model the observed delays of crustal phases in that zone. The basin has a pronounced signature in the calculated gravity, but cannot be seen in the observed gravity. This indicates that the basin has to be a local fea-

ture that violates the assumption of two-dimensionality in the gravity model. Fig. 11 shows a free-air gravity map of the study area. The map indicates that most features cross line 600 at an oblique angle. The most prominent departure from two-dimensionality the pronounced gravity high at OBS 620 that can be correlated southward all the way through the Davis Strait but disappears just to the north of the line.

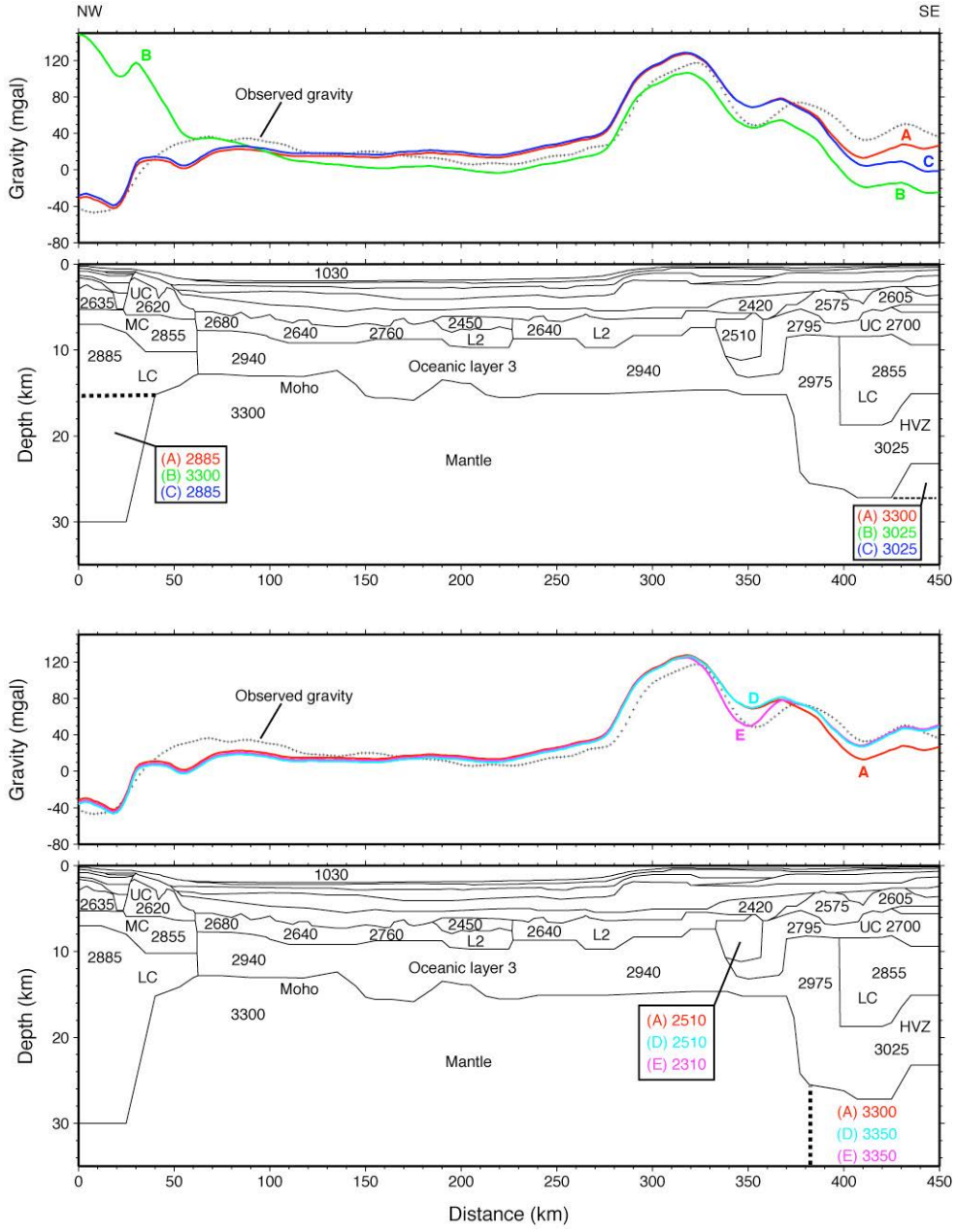

Figure 10. *Gravity modelling along line 600. The upper panel with models A through C explores the Moho geometry at the outer limits of the model with no constraints from the refraction seismic data (compare the ray-coverage in Figs 7 and 8). The lower panel with models A, D and E tests for lateral variations of the density in the mantle and within the basin around 350 km. The observed gravity is the free-air gravity measured during the MSM09/3 expedition (Ingo Heyde, Federal Institute for Geosciences and Natural Resources, Hanover, Germany, personal communication). All densities in the model are given in kg m^{-3}. For details see text. Abbreviations are HVZ, high-velocity zone; L2, oceanic layer 2; LC, lower crust*; *MC, mid-crustal layer; UC, upper crust.*

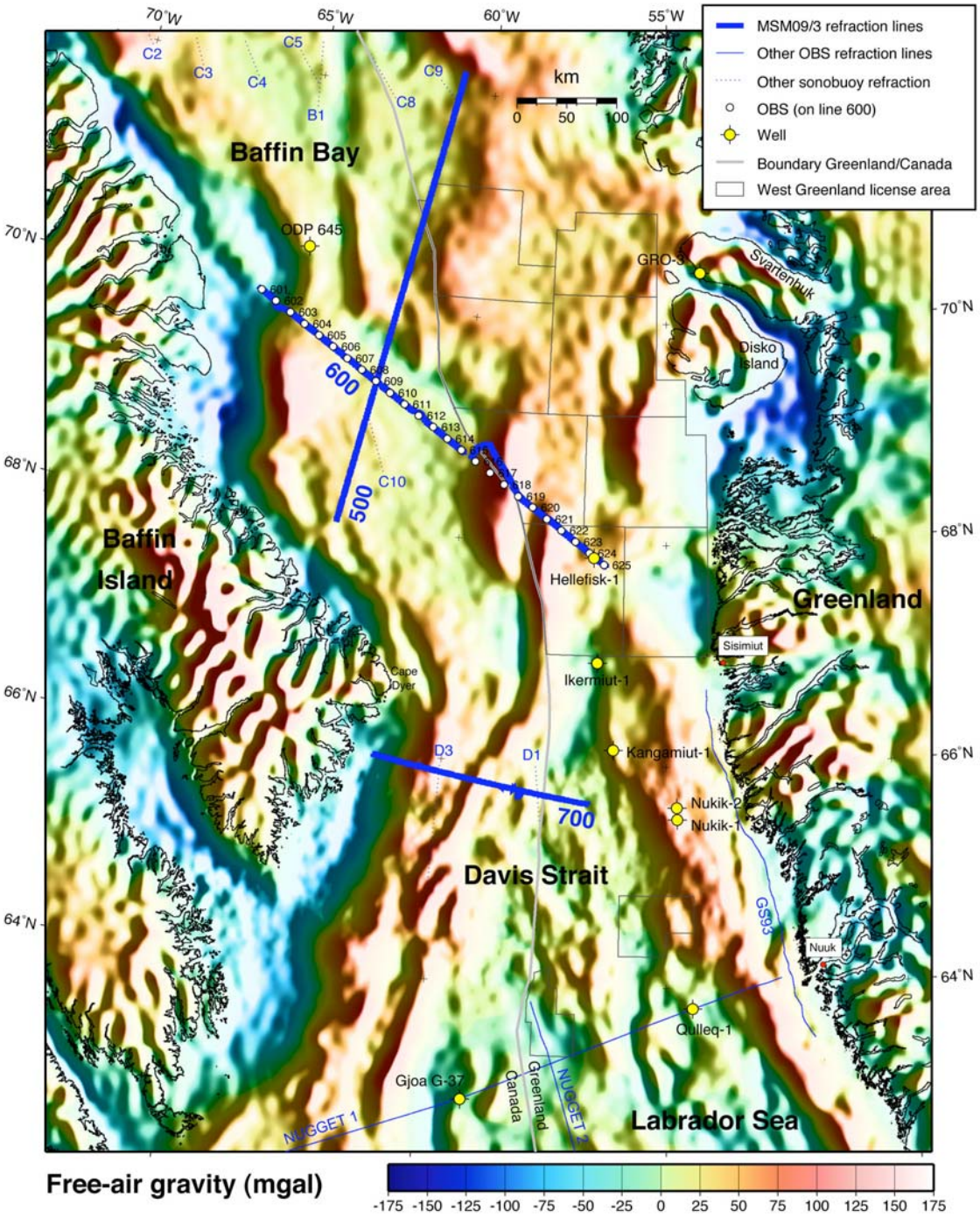

Figure 11. *Free-air gravity map with shading by artificial illumination from the east. Data source: Satellite altimetry, DNSC08 1-minute grid (Andersen et al. 2008). Bold blue lines refer to the MSM09/3 refraction seismic lines (AWI20080[500/600/700]) (Gohl et al. 2009); thin blue lines show the location of other refraction seismic experiments: GS93 (Gohl & Smithson 1993), Nugget 1 (Funck et al. 2007), and Nugget 2 (Gerlings et al. 2009); dashed blue lines indicate sonobuoy experiments: C1 to C10, B1 and D1 (Keen & Barrett 1972), D3 (Srivastava et al. 1982).*

6. Discussion and Interpretation

In section 5.1 (Results), the model for line 600 was presented with a description of the velocity distribution in the sediments, the crust, and the mantle. In addition, a first interpretation of the crustal structure was given. However, a more thorough discussion of the model is necessary and is presented in this chapter. The model is discussed in context of the regional geology as well as compared to studies in similar tectonic and geologic settings. The discussion starts in the NW off Baffin Island and then moves toward the SE following the segmentation of the crust indicated in Fig. 12.

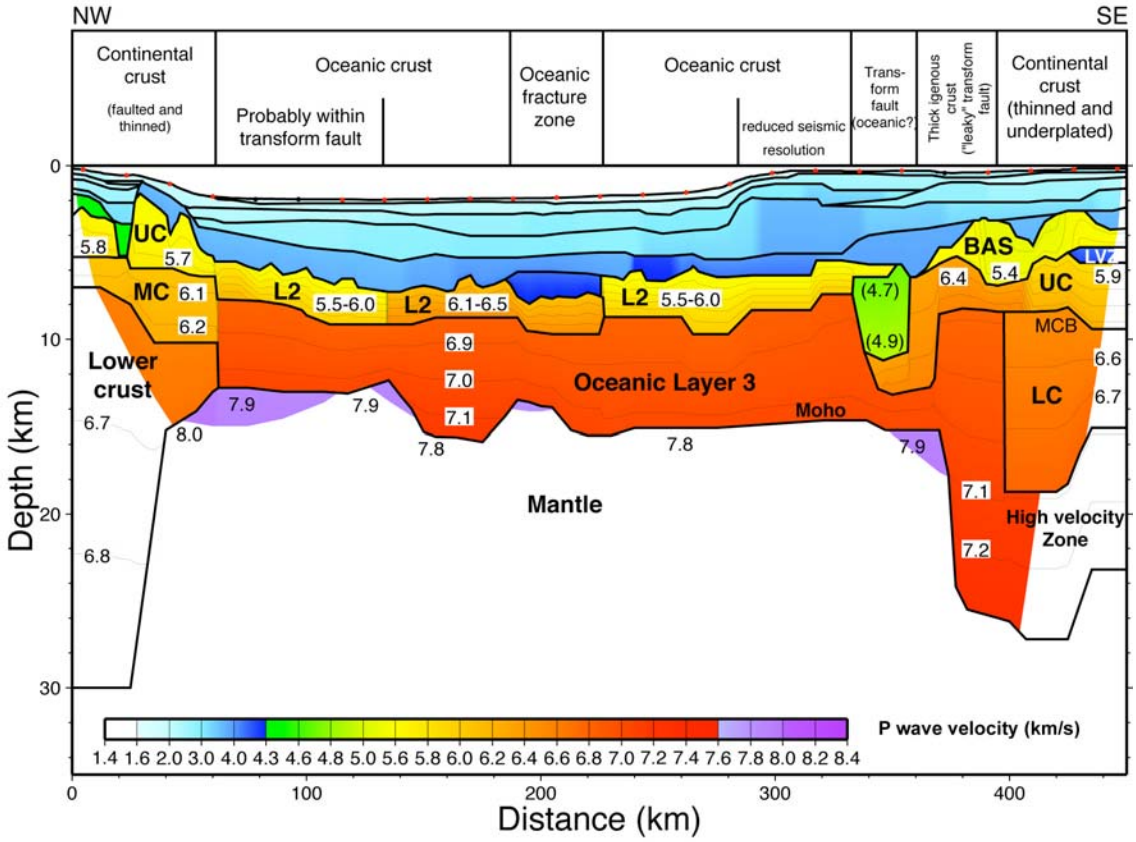

Figure 12. *Interpretation of the crustal types encountered along line 600. The lower part shows the velocity model (see also Fig. 7); the upper part summarizes the interpretation of the P-wave velocity model. The outer parts of the velocity model with no ray coverage are shown in white, velocities are specified in km/s, the velocity contour interval is 0.1 km/s. Red circles show the location of OBS that were used for the modelling, the black circles refer to non-functional OBS. Abbreviations are BAS, basalts/volcanics; MCB, mid-crustal boundary; L2, oceanic layer 2; LC, lower crust; LVZ, low-velocity zone; MC, mid-crustal layer; MCB, mid-crustal boundary; UC, upper crust.*

6.1 Continental Crust (0-60 km)

The segment between 0 and 60 km is interpreted as continental crust (Fig. 12). The velocity structure is divided into three layers with velocities that are not typical of oceanic crust.

In addition, the occurrence of mid-crustal reflections is a strong indicator for continental crust. Velocities of 5.5 to 6.3 and 6.6 to 6.9 km/s for the upper and lower crust, respectively, compare well with the range of velocities found elsewhere in West Greenland and Eastern Canada along the shores of the Labrador Sea and the Baffin Bay. For this comparison, the mid-crustal layer is considered as part of the upper crust. The Archean Nain Province in Labrador, where Funck & Louden (1998) report velocities of 5.8 to 6.5 and 6.6 to 6.9 km/s in the upper and lower crust, respectively, is very close to the study area. In the Nain Province, the uppermost crust was interpreted to have a gneissic composition based on *P*-wave velocities and a Poisson's ratio of 0.20 to 0.24. To the SE of Baffin Island along Nugget line 1, upper and lower crustal velocities of 5.8 to 6.1 and 6.4 to 6.6 km/s were reported (Funck *et al.* 2007). However, upper crustal velocities there are only poorly resolved. Farther to the east on that line (off Greenland), upper crustal velocities were as low as 5.4 km/s. This is very close to the observed 5.5 km/s on line 600. Funck *et al.* (2007) suggested a granitic composition of the upper crust on Nugget line 1. Intense faulting on line 600 as indicated by the rough basement topography between 0 and 60 km, may result in a reduction of the *P* wave velocity. Laboratory measurements of rock samples measured at pressures compatible with mid-crustal levels (3-5 kbar) indicate *P* wave velocities of 6.07 ±0.22 km/s for granite (Holbrook *et al.* 1992), which is higher than what is observed on line 600. However, on a refraction seismic line off SW Greenland, Chian *et al.* (1995b) reported upper crustal velocities of 5.4 km/s in an area that is characterized by widespread granitic intrusions.

One other interesting aspect of the continental crust at the NW end of line 600 is the abrupt transition to oceanic crust at around 60 km (Fig. 12), without any indication for a transitional crust. Transitional crust at non-volcanic continental margins is often characterized by velocities that differ from the adjacent normal continental and oceanic crust and that often are difficult to interpret. The lack of such a transition zone is interpreted to be related to the location of line 600, which is parallel to the assumed extinct spreading axis (Chalmers & Pulvertaft 2001; Chalmers & Oakey 2007; Fig. 4). The boundary from continental to oceanic crosses a transform fault. The transform margin can be recognized on the bathymetric map (Fig. 13) and even better in the gravity data (Fig. 11). To the north of line 600, the shelf break and the coast-parallel gravity high are oriented in a NW-SE direction but then step southward. Crustal thinning across transform margins is characterized by a thinning of the crust over short distance. One well-studied transform margin is the margin off Ghana in the Equatorial Atlantic. Edwards *et al.* (1997) show that the continental crust thins from 23 to 4 km over a distance of only 20 km. Such a thinning is comparable to the one observed on line 600, although it is only constrained by gravity modelling. Another example for rapid thinning of the continental crust with no transition zone is can be found at the transform margin south of Svalbard (Breivik *et al.* 2003).

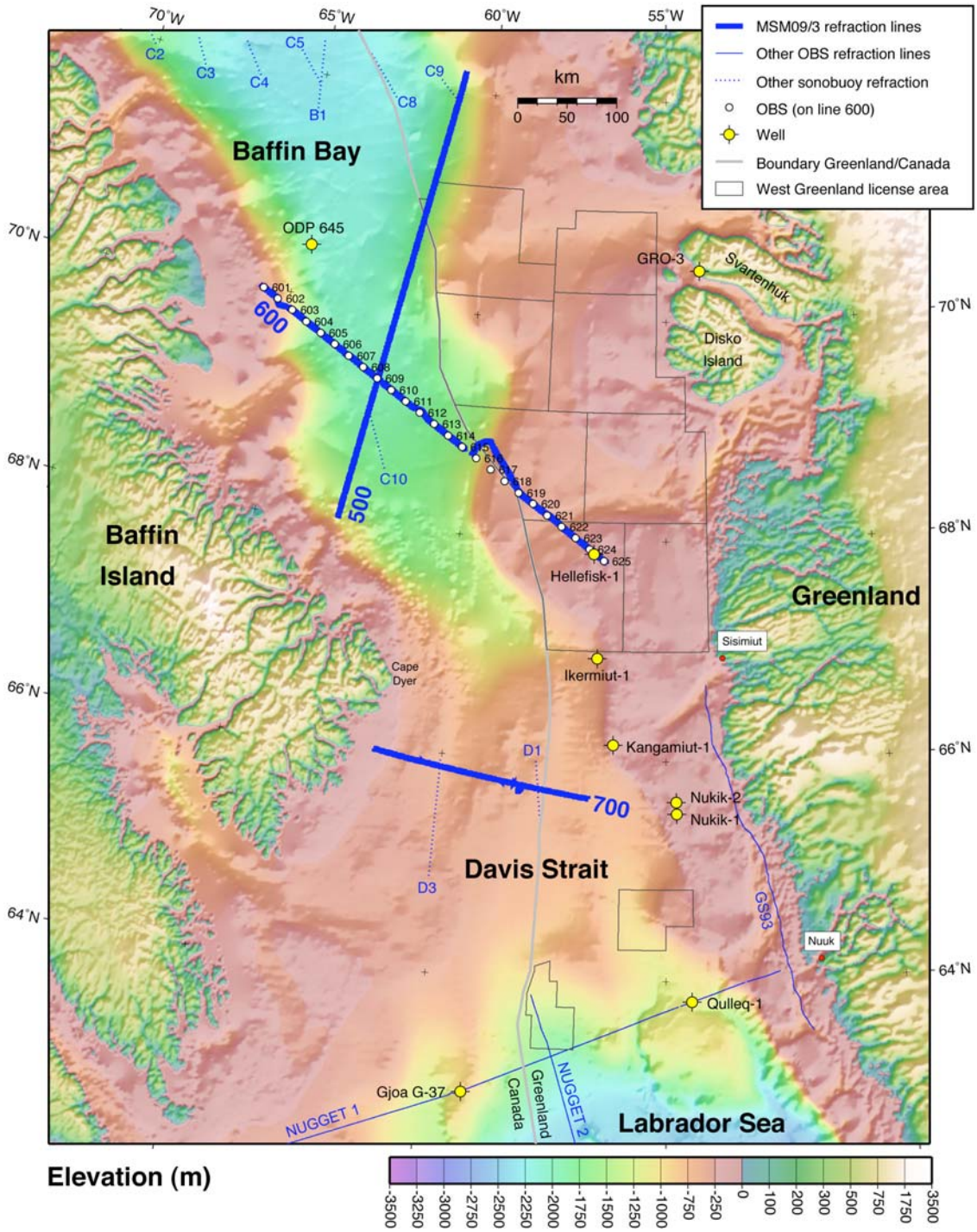

Figure 13. *Elevation map. Data source: Oakey (2001a, 2001b). Bold blue lines refer to the MSM09/3 refraction seismic lines (AWI20080[500/600/700]) (Gohl et al. 2009); thin blue lines show the location of other refraction seismic experiments: GS93 (Gohl & Smithson 1993), Nugget 1 (Funck et al. 2007), and Nugget 2 (Gerlings et al. 2009); dashed blue lines indicate sonobuoy experiments: C1 to C10, B1 and D1 (Keen & Barrett 1972), D3 (Srivastava et al. 1982).*

6.2 Oceanic Crust (60-333 km)

The zone between 60 and 333 km is interpreted as oceanic crust but displays both lateral thickness and velocity variations. Velocity variations are restricted to the upper crustal layer (oceanic layer 2). Fig. 14 shows a comparison with average oceanic crust in the North Atlantic with a crustal age between 59 and 127 Ma as compiled by White *et al.* (1992). The oceanic crust on line 600 is more likely to be of Eocene age given the proximity (30 km) to the extinct spreading axis and assuming that seafloor-spreading ceased sometime between magnetic anomalies 20 and 13 as proposed for Labrador Sea (Roest & Srivastava 1989). However, no such compilation of average crust was available for Eocene crust. The comparison shows that the layer 2 velocities of 6.1 to 6.5 km/s between 135 and 227 km are slightly higher than average. Otherwise the velocities fall well into the range of typical oceanic crust both in terms of the absolute velocities and velocity gradients. With respect to crustal thickness, the values on line 600 are typically 6 km or 9 km, which are either too low or too high when compared with average crust. White et al. (1992) found a global average thickness of 7.1 ±0.8 km.

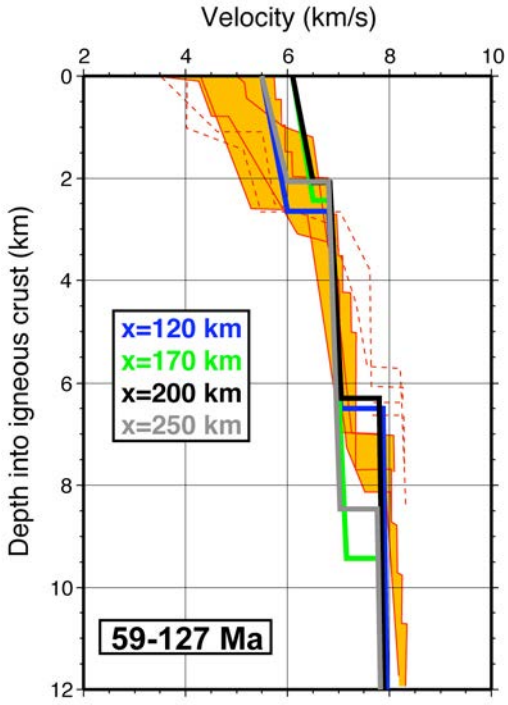

Figure 14. *Comparison of velocity-depth functions from line 600 with average oceanic crust (data taken from White et al. 1992). The shaded area shows the range of typical oceanic crust encountered in the Atlantic Ocean with a crustal age between 59 and 127 Ma. The red lines indicate individual velocity profiles that went into the compilation, the dashed red lines are from surveys that may differ from typical crust due to proximity to the continent-ocean boundary. The bold lines show the velocities from line 600, the position (km) refers to the velocity model* (*Fig. 7).*

Fig. 7 shows that the lateral velocity variations in layer 2 correlate to changes in the observed magnetic anomalies. The zone with the higher velocities (6.1-6.5 km/s) displays positive anomalies, while the lower velocities (5.5-6.0 km/s) are generally associated with negative magnetic anomalies. Changes of magnetic polarity in oceanic crust mirror the reversals of the Earth's magnetic field over time and, hence, the lateral changes observed along line 3 could indicate that the segments of oceanic crust have a different age. However, there is currently no consensus that there are seafloor-spreading magnetic anomalies in Baffin Bay (Fig. 15). Nevertheless, the positive magnetic anomalies between OBS 609 and 612 show up as a linear feature that is parallel with the spreading axis, which is itself parallel to line 600. If the anomaly is indeed related to seafloor-spreading, it may correspond to polarity chron 21n (45.3 to 47.2 Ma) as this was the last clear spreading anomaly

in Labrador Sea (Roest & Srivastava 1989) and has a similar distance to the extinct spreading axis.

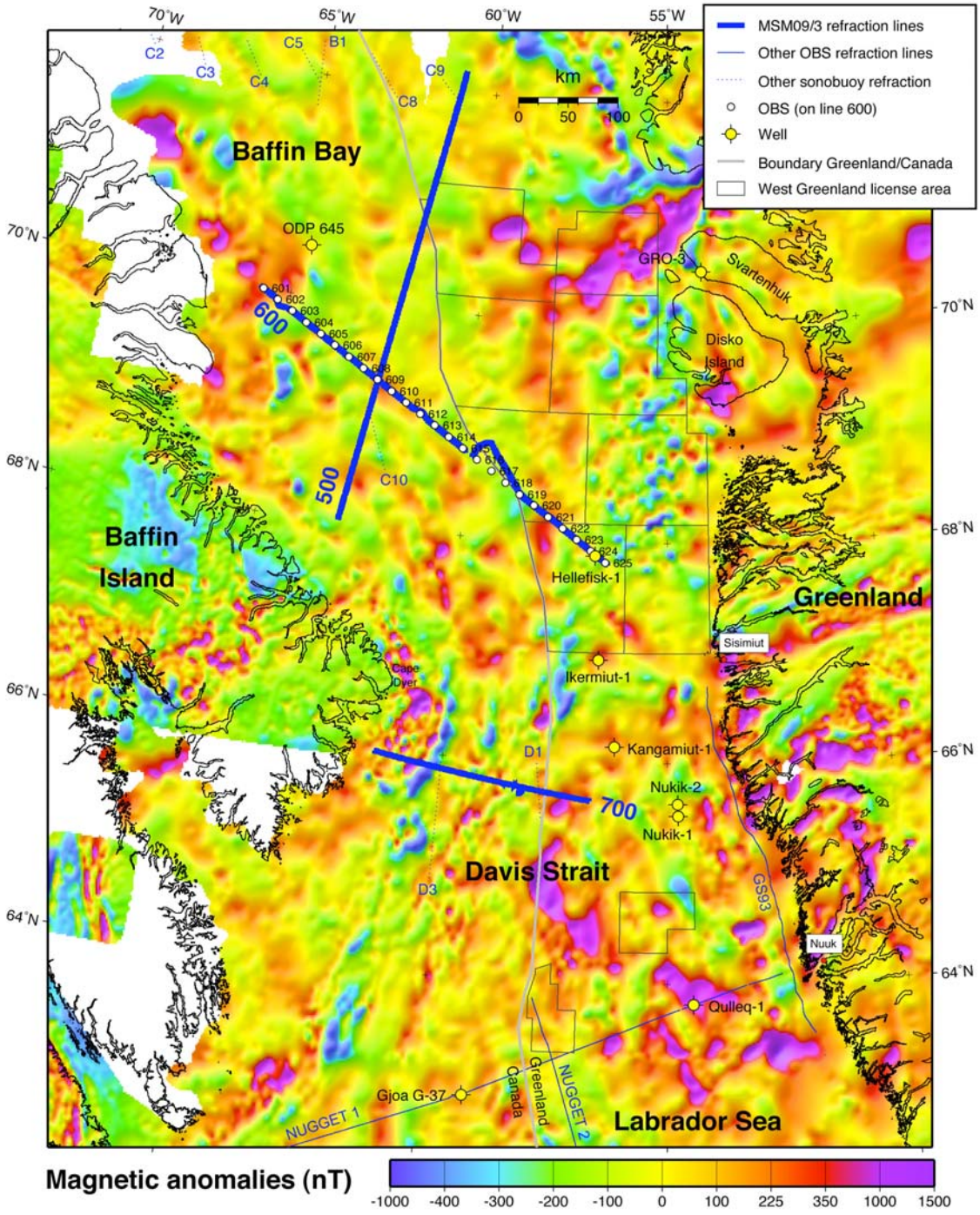

Figure 15. *Magnetic anomaly map. Data source: Verhoef et al. (1996) and Oakey (2001c). Bold blue lines refer to the MSM09/3 refraction seismic lines (AWI20080[500/600/700]) (Gohl et al. 2009); thin blue lines show the location of other refraction seismic experiments: GS93 (Gohl & Smithson 1993), Nugget 1 (Funck et al. 2007), and Nugget 2 (Gerlings et al. 2009); dashed blue lines indicate sonobuoy experiments: C1 to C10, B1 and D1 (Keen & Barrett 1972), D3 (Srivastava et al. 1982).*

On the free-air gravity map (Figs 16 and 17), the extinct spreading axis in Baffin Bay stands out as a gravity low parallel to line 600. In addition, another gravity low can be seen that continues northward from the extinct spreading axis, roughly between OBS 604 and 608. This gravity low correlates with a transform fault along which the spreading axis is displaced to the north (Chalmers & Oakey 2007; Fig. 2). It is in this zone that the oceanic crustal thickness is reduced to 6 km. A second zone with reduced crustal thickness is observed near OBS 612 and can be correlated northward to where the spreading axis shows a minor displacement. Thus, the reduced crustal thicknesses are interpreted to lie within oceanic fracture zones. The crustal thickness within transform faults and fracture zones is often anomalously thin and the observed velocities can deviate from normal oceanic crust (Detrick *et al.* 1993). Detrick *et al.* (1993) show that fracture zones in the North Atlantic are frequently quite thin (<1-2 km thick) and are characterized by low *P*-wave velocities and the absence of a normal seismic layer 3. These anomalies are explained by a reduced magma supply at the end of spreading segments. In contrast, the velocity structure within the fracture zone and transform fault on line 600 is much closer to normal oceanic crust even though it is thinner than the local average. This probably relates to the influence of the Iceland plume that provided ample magma supply in southern Baffin Bay. This extra magma supply generated the 9-km-thick oceanic crust along the line, some 2 km thicker than normal oceanic crust. Although the thickness decreases by 3 km within the fracture zone/transform fault, the resulting thickness of 6 km is still close to normal oceanic crust. Thus, the processes that cause extreme magma starvation and anomalous velocity structures in oceanic transforms were not important here.

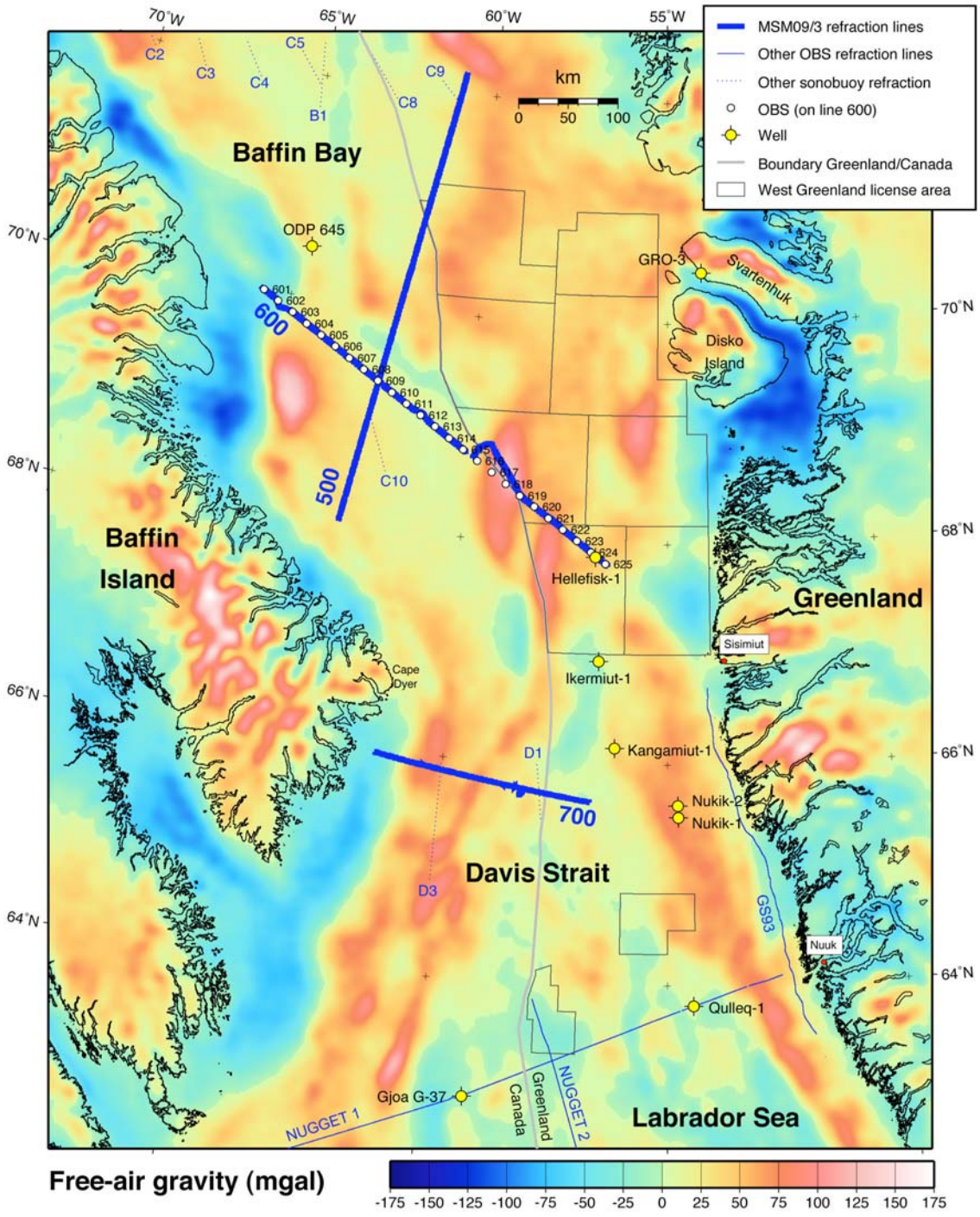

Figure 16. *Free-air gravity map. Data source: Satellite altimetry, DNSC08 1-minute grid (Andersen et al. 2008). Bold blue lines refer to the MSM09/3 refraction seismic lines (AWI20080[500/600/700]) (Gohl et al. 2009); thin blue lines show the location of other refraction seismic experiments: GS93 (Gohl & Smithson 1993), Nugget 1 (Funck et al. 2007), and Nugget 2 (Gerlings et al. 2009); dashed blue lines indicate sonobuoy experiments: C1 to C10, B1 and D1 (Keen & Barrett 1972), D3 (Srivastava et al. 1982).*

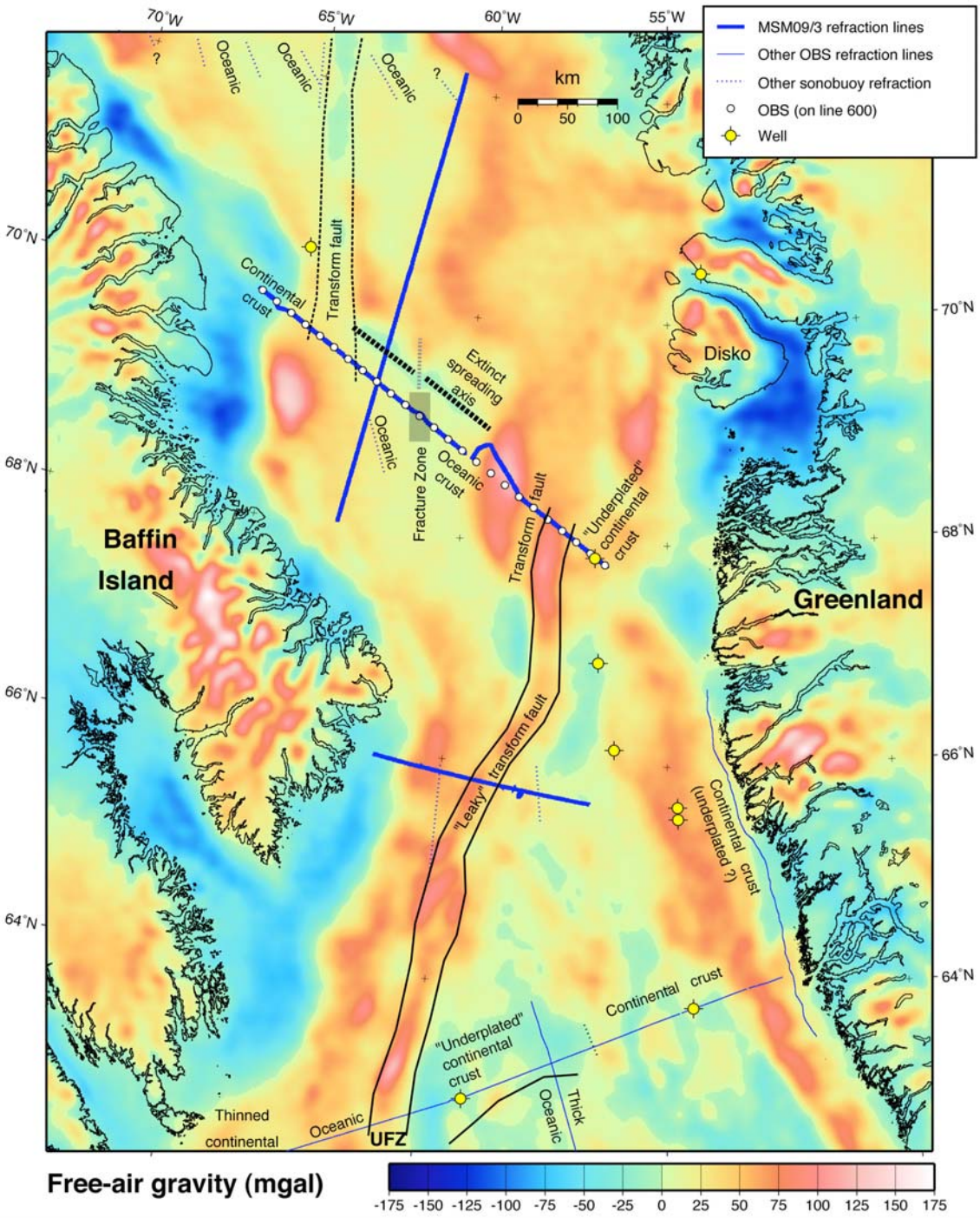

Figure 17 *Free-air gravity map with interpretation of crustal character along line 600 and along other available refraction seismic lines. Data source: Satellite altimetry, DNSC08 1-minute grid (Andersen et al. 2008). Bold blue lines refer to the MSM09/3 refraction seismic lines (AWI20080[500/600/700]) (Gohl et al. 2009); thin blue lines show the location of other refraction seismic experiments: GS93 (Gohl & Smithson 1993), Nugget 1 (Funck et al. 2007), and Nugget 2 (Gerlings et al. 2009); dashed blue lines indicate sonobuoy experiments: C1 to C10, B1 and D1 (Keen & Barrett 1972), D3 (Srivastava et al. 1982).*

One other interesting observation should be mentioned here. Storey *et al.* (1998) identified two main pulses of volcanism in West Greenland: one between 60.7 and 59.4 Ma and

one between 54.8 and 53.6 Ma. Here, the distance to the extinct spreading axis is only 40 km and an oceanic crustal thickness of 9 km is observed, indicating that the plume must have influenced the region well after 53.6 Ma to create the thicker than normal oceanic crust. While the age of the oceanic crust along line 600 is not known, some estimates can be made. Srivastava & Keen (1995), in an interpretation of a reflection seismic line across the extinct spreading axis in the Labrador Sea, assume a half-spreading rate of 3 mm/yr between magnetic anomalies 18 and 13 for an. At anomaly 13 (~33 Ma), Greenland and North America are thought to have moved as a single plate. Under the assumption that these parameters are applicable to the Baffin Bay as well, a 40 km distance to the axis at a half-spreading rate of 3 mm/yr would translate to 13 million years prior to the cessation of spreading. This yields an age estimate of 46 Ma for the oceanic crust on line 600, some 7 millions of years after the last main pulse of volcanism sampled onshore West Greenland.

6.3 Transition Zone (333-400 km)

The region between 333 and 400 km is named transition zone because its seismic character is different from both the adjacent 9-km-thick oceanic crust to the NW and the continental crust to the SE (Fig. 12). The transition zone is divided into two very distinct segments. The area that is labelled leaky transform fault is characterized by 20-km-thick igneous crust, while the basin to the NW is underlain by only 4-km-thick crust of unknown nature.

6.3.1 Leaky Transform Fault

The 20-km-thick igneous crust between 375 and 400 km lies within the area referred to as Ungava Fault Zone (UFZ) – a fault system that links the rift axis in the Labrador Sea to that in the Baffin Bay. Storey *et al.* (1998) suggested that the Davis Strait went through transtensional phases that created gaps between the Canadian and Greenlandic continental crust. These gaps were then filled with melt that formed thick igneous crust. In this sense the UFZ acted as a leaky transform fault. Storey *et al*. (1998) link the Early Eocene volcanism in west Greenland to net extension on the UFZ, caused by a change in plate kinematics as the North Atlantic opened at ~55 Ma. Funck *et al.* (2007) were the first to map the UFZ with a refraction seismic experiment. The velocity model (Fig. 18) identifies 16-km-thick igneous crust within the UFZ. Funck *et al.* (2007) favour a Paleocene age of the UFZ based on radiometric dates of the basalts (59.5 Ma; Williamson *et al.* 2001) in the nearby Gjoa G-37 well.

The igneous crust within the UFZ correlates with a gravity high that can be correlated through the entire Davis Strait (Figs 11 and 17). With the addition of this study, the oceanic or igneous character of this gravity high is confirmed at both ends (line 600 and Nugget line 1) and there can be little doubt that this feature is composed of igneous crust along its entire length. In addtion, the UFZ stands out as a prominent feature on the magnetic map (Fig. 15), although the correlation is not as good as in the gravity data. In particular, the northern part of the UFZ appears less continuous in the magnetic data.

Comparison of the velocity models of the UFZ in the north (line 600; Fig. 12) and in the south (Nugget line 2; Fig. 18) indicates some lateral changes. In the south, velocities are

lower than in the north, but these differences are close to the limit of seismic resolution. More significant seems to be the division into an upper and lower unit on the Nugget line. Here the upper unit is similar to normal oceanic crust with a total thickness of 8 km and velocities compatible with oceanic layers 2 and 3. The lower unit is a HVZ with velocities around 7.4 km/s. This could indicate a multi-phase development: first the gap was filled with normal oceanic crust and then the crust, as well as the adjacent thinned continental crust, was magmatically underplated, creating the HVZ. This magmatic underplating is consistent with geodynamic models (e.g., Nielsen *et al.* 2002) that suggest southward flow of plume material through Davis Strait along lithospheric thin spots. In the north, no such division into an upper and lower unit could be detected. However, the zone where thick igneous crust is observed, is much narrower on line 600 than on Nugget line 2. The detection of a potentially weak reflection within the igneous crust from the top of a HVZ would be significantly more difficult. The thickness decrease of the igneous crust from north to south seems to be compatible with the previously mentioned southward channelling of plume material. Including the overlying basalts, the igneous thickness is 23 km in the north compared to 17 km in the south.

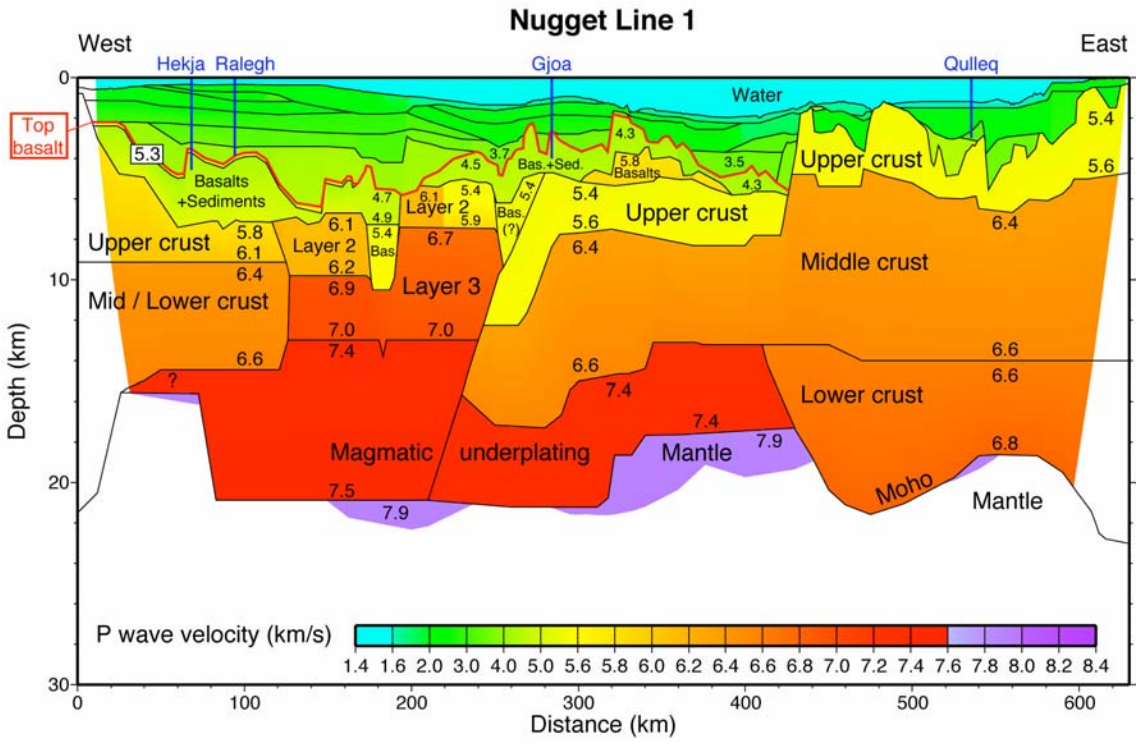

Figure 18. *Velocity model along Nugget line 1 (Funck et al. 2007) in southern Davis Strait (for location see Fig. 13). The outer limits of the model with no ray coverage is omitted; velocities are specified in km/s. The location of the four wells along the line are marked by blue lines. Abbreviations are Bas., basalts/volcanics; Sed., sediments.*

6.3.2 Basin/Transform Fault

Between 333 and 357 km, the velocity model (Fig. 12) indicates the presence of a 5-km-deep basin. As discussed earlier, velocities within the basin are poorly resolved but are

probably within ±0.2 km/s of the modelled 4.7 to 4.9 km/s. The crust immediately below the basin was not sampled by refracted waves and, hence, the velocities are unknown.

There are two possible explanations for the basin. Either this segment is a thin sliver of stranded continental crust left between the leaky transform fault and the oceanic crust or it is a transform fault, possibly associated with the UFZ. If the basin is located on continental crust, the infill could contain Cretaceous or older sediments. However, as the igneous crust of the leaky transform fault can be correlated directly to the SE flank of the basin, it appears more likely that the bulk of the infill consists of volcanic material, possibly interbedded with some non-volcanic sediments. The velocities of 4.7 to 4.9 km/s can be easily explained with volcanic rocks. Sonic log measurements in the Lopra-1 borehole on the Faroe Islands show velocities between 3.3 and 6.6 km/s in the volcanic sequence, which consists of basalts and hyaloclastites (Christie *et al.* 2006).

On the free-air gravity map (Figs 11, 16 and 17), the basin shows up as a north-south striking linear feature bordered by two gravity highs. However, this correlation is deceiving since the western gravity high (around OBS 618 or at 320 km in Fig. 10) is related to a gravitational edge effect. The anomaly is caused by the juxtaposition of the water in the deep basin and the thick sediments close to the shelf break. With a proper reduction, this anomaly disappears on a Bouguer gravity map. Tests with two-dimensional gravity models indicate that the anomaly flattens out once the water (density 1030 kg/m^3) is replaced with a density of ~2600 kg/m^3.

Seafloor spreading in a north-south direction requires a transform fault between the oceanic crust in the southernmost Baffin Bay and the continental crust observed at the SE end of line 600. Based on the gravity signature, the leaky transform fault disappears just to the north of line 600 (Fig. 17). Hence, the basin could easily form this transform fault if extended northward up to the extinct spreading axis. The interpretation as a transform fault can also explain the low crustal thickness of 4 km as is commonly observed in fracture zones and transform faults and discussed above (Detrick *et al.* 1993). In this context it is interesting to note that a similar basin was observed on Nugget line 1 (Fig. 18), where Labrador Sea oceanic crust (at a model distance of ~120 to 175 km) is separated from the leaky transform fault (UFZ between ~200 and 250 km) by a graben structure (Funck *et al.* 2007). Although the velocity structure within the graben is not very well resolved, the model for Nugget line 1 indicates a volcanic fill (velocities of 5.4 km/s) and the crust is potentially only 3 to 4 km thick (not including the underlying HVZ). However, the 5.4-km/s layer could also represent oceanic layer 2, in which case the crust would be 7 km thick; but still thinner than the surrounding crust. With the new knowledge gained from line 600 in this study, the graben structure on Nugget line 1 could also be interpreted to be related to a transform fault. However, it is unclear if the leaky transform fault in the Davis Strait is bounded by thinned crust to the west through the entire length of the fault. Results from Merian line 700 in central Davis Strait probably will answer this question.

The gravity data show very interesting similarities at either end of the leaky transform fault. In the north (Fig. 17), the gravity high associated with the leaky transform fault ends close to line 600. Another gravity high that is offset from the UFZ then continues to the north up to the position of the extinct spreading axis that is marked by a gravity low. In the northern Labrador Sea (Fig. 19), the extinct spreading axis is also characterized by a gravity low. At the NW end of the axis, a gravity high then connects northward up to the gravity anomaly associated with the UFZ. The two gravity highs are separated from each other by a small offset. Although these gravity highs seem to relate to the position of the shelf break

(gravitational edge effect, discussed above), it is interesting to note this symmetry and correlation.

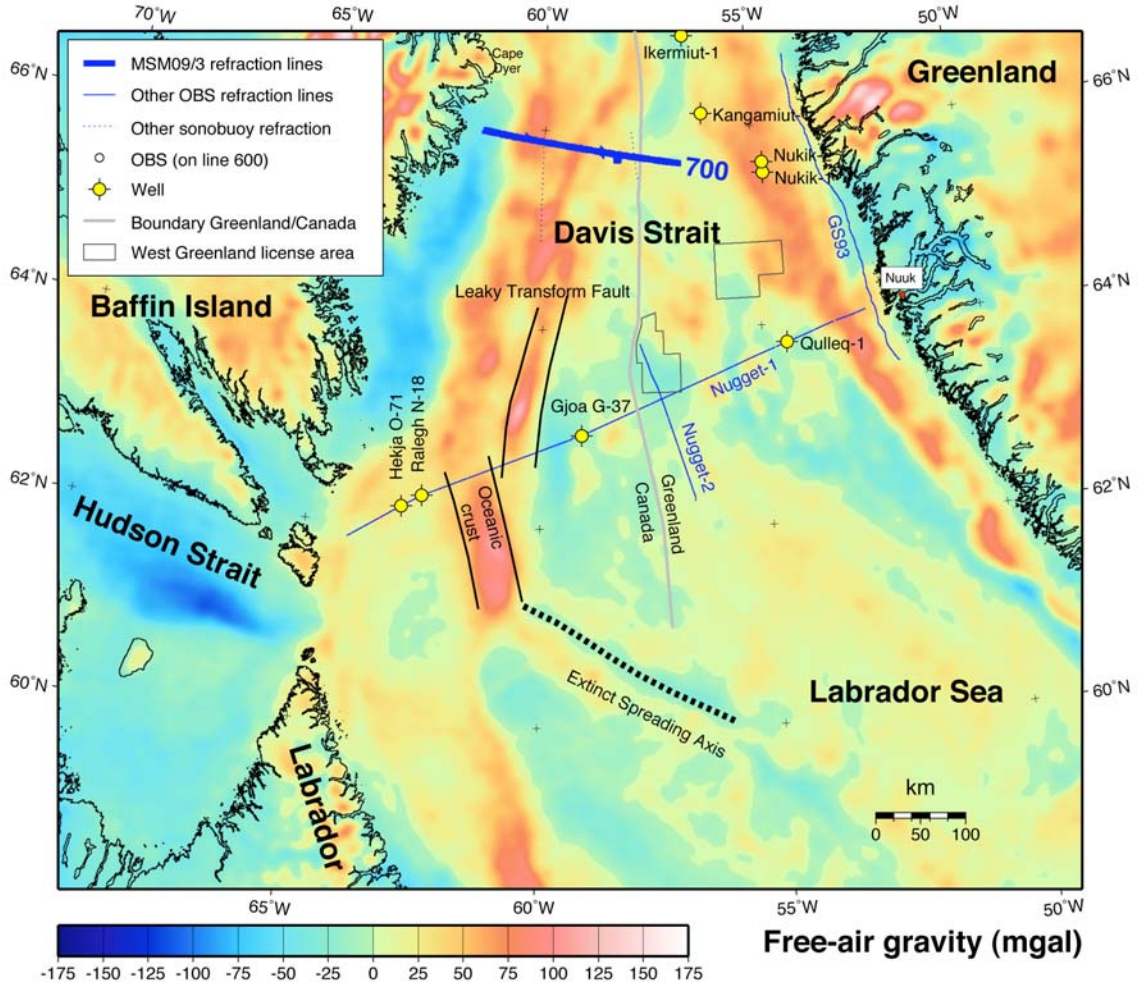

Figure 19. *Free-air gravity map. Data source: Satellite altimetry, DNSC08 1-minute grid (Andersen et al. 2008). Bold blue lines refer to the MSM09/3 refraction seismic lines (AWI20080[500/600/700]) (Gohl et al. 2009); thin blue lines show the location of other refraction seismic experiments: GS93 (Gohl & Smithson 1993), Nugget 1 (Funck et al. 2007), and Nugget 2 (Gerlings et al. 2009); dashed blue lines indicate sonobuoy experiments.*

6.4 Underplated Continental Crust (400-450 km)

Finally, the continental crust at the SE end of line 600 is discussed. Velocities in the upper and lower crust between 400 and 450 km are well-resolved (Fig. 7) and are very distinct from the oceanic and igneous crust observed elsewhere along the line. Hence, there is little doubt that this crust has a continental character with velocities of 5.9 to 6.2 km/s and 6.5 to 6.8 km/s in the upper and lower layer, respectively. Further evidence for a continental affinity comes from the observed mid-crustal reflections. While the lower crustal velocities are comparable to the ones found off Baffin Island, upper crustal velocities off Greenland are slightly lower. However, the NW and SE ends of line 600 are not conjugate. In a plate reconstruction (Skaarup *et al.* 2006), the SE end of line 600 would move southward to a posi-

tion some 100 to 200 km to the north of Nugget line 1. Hence, the Baffin Island continental crust on Nugget line 1 would come close to the continental crust off Greenland on line 600. Indeed, velocities on Nugget line 1 are 5.8 to 6.1 km/s and 6.4 to 6.6 km/s in the upper and lower crust, respectively (Fig. 18; Funck *et al.* 2007), close to the values found on line 600 (Fig. 12).

The crust at the SE end of line 600 has a continental affinity but was later modified by the Iceland plume that created the basaltic layer at the top (as drilled in the Hellefisk-1 well) and the HVZ at the base of the crust. The HVZ is interpreted as magmatic underplating. A similar layer is observed on Nugget line 1 (Fig. 18) beneath the thinned portions of the continental crust but disappears to the east where the Greenlandic continental crust thickens. This observation was interpreted by Funck *et al.* (2007) to be consistent with the channelling model of Sleep (1997) and Nielsen *et al.* (2002). In this model, buoyant plume material ponds at the base of the lithosphere and then flows laterally and preferentially along thin lithosphere. With a thickness between 9 and 13 km, the continental crust around the Hellefisk-1 well can be considered as thinned when compared with full-thickness continental crust in this area. Gohl & Smithson (1993) report a thickness of up to 40 km on a line in Davis Strait close to the coast of Greenland (for location see Fig. 13).

7. Conclusions

The data from line 600 provide new insight into the crustal affinity and geodynamic evolution in the southern Baffin Bay. The central part of the line is characterized by oceanic crust that is divided into several segments based on crustal thickness and on velocities within layer 2 (Fig. 12). In the NW near Baffin Island, the line crosses a transform margin with a sharp transition from continental into oceanic crust. The oceanic crust at this transition is 6 to 7-km thick, which is approximately the same as normal oceanic crust (7 km; White *et al.* 1992), However, it is thinner than along most of the remainder of the line. Thus, the segment is interpreted to be part of the transform fault that can be correlated northward in the gravity data (Fig. 17). An offset in the extinct spreading axis correlates with another segment of thinned oceanic crust (6 km) and is interpreted as oceanic fracture zone. From the offset in the axis and the location of the fracture zone on the line, it can be seen that the fracture zone cuts the spreading axis (defined by a gravity low) at an oblique angle, which is further confirmation for oblique seafloor spreading in Baffin Bay as suggested by Chalmers & Pulvertaft (2001).

A third zone with a reduced crustal thickness (4 km) is interpreted as a transform fault with a probable oceanic composition that separates oceanic crust in the southern Baffin Bay from 20-km-thick igneous crust and continental crust farther landward. The igneous crust coincides with a gravity high that can be correlated through the Davis Strait and into the Labrador Sea, where similar igneous crust is observed on Nugget line 1 (Fig. 18). This igneous crust is thought to form a leaky transform fault (Ungava Fault Zone) where material from the Paleogene Iceland plume filled the gaps that developed during phases of transtension. The plume also created the high-velocity zone beneath the continental crust on the Greenland side of the line. Based on its distance to the extinct spreading axis (40 km), the oceanic crust on line 600 may have an approximate age of 46 Ma. Given that the oceanic crust here is greater than the global averages (9 km outside the fracture zones and transform faults compared to 7 km for typical or average crust), the plume seems to have influenced the spreading system for a long time after the initial impact of the plume – thought to coincide with the first major volcanic pulse in West Greenland at around 60.7 to 59.4 Ma (Storey *et al.* 1998).

The continental crust at the SE end of the line is overlain by volcanic rocks that were drilled in the Hellefisk-1 well. The velocity model indicates a maximum thickness of 4 km for the basalts. A low-velocity zone observed beneath some of these basalts may indicate the presence of older sediments deposited prior to the Paleocene volcanics. However, as there are no velocity constraints at all for this LVZ, the layer may also represent basalts with a lower velocity. Although the LVZ cannot be resolved, the refraction seismic data can be used to determine the depth of the basement below the volcanic layer. A specifically designed refraction seismic experiment could probably better resolve the base of the volcanic layer, the depth to basement and the velocity in sub-basalt layers (for example by employing AVO techniques). This would require a better designed source than the one used during the MSM09/3 expedition. During future reflection seismic work in the volcanic region off West Greenland, it would be desirable to deploy sonobuoys as a cost-efficient way to obtain additional refraction seismic data. This could greatly aid the interpretation of the offshore basalt series.

8. References

Andersen, O.B., Knudsen, P., Berry, P., Freeman, J., Pavlis, N. & Kenyon, S. 2008: The DNSC07 ocean-wide altimetry-derived gravity anomaly field. Geophysical Research Abstracts **10**, EGU2008-A-07163, European Geosciences Union.

Breivik, A.J., Mjelde, R., Grogan, P., Shimamura, H., Murai, Y. & Nishimura, Y. 2003: Crustal structure and transform margin development south of Svalbard based on ocean bottom seismometer data. Tectonophysics **369**, 37-70.

Chalmers, J.A. 1997: The continental margin off southern Greenland: Along-strike transition from an amagmatic to a volcanic margin. Journal of the Geological Society **154**, 571-576.

Chalmers, J.A. & Laursen, K.H. 1995: Labrador Sea: the extent of continental and oceanic crust and the timing of the onset of seafloor spreading. Marine and Petroleum Geology **12**, 205-217.

Chalmers, J.A. & Oakey, G.N. 2007: Cretaceous-Palaeogene development of Labrador Sea and Davis Strait. Geophysical Research Abstracts **9**, 01638, European Geosciences Union.

Chalmers, J.A. & Pulvertaft, T.C.R. 2001: Development of the continental margins of the Labrador Sea: a review. In: Non volcanic rifting of continental margins: a comparison of evidence from land and sea. Edited by R.C.L. Wilson, R.B. Whitmarsh, B. Taylor & N. Frotzheim. Geological Society, Special Publications **187**, 77-105.

Chian, D. & Louden, K.E. 1994: The continent-ocean crustal transition across the southwest Greenland margin. Journal of Geophysical Research **99**, 9117-9135.

Chian, D., Keen, C., Reid, I. & Louden, K.E. 1995a: Evolution of nonvolcanic rifted margins: New results from the conjugate margins of the Labrador Sea. Geology **23**, 589-592.

Chian, D., Louden, K.E. & Reid, I. 1995b: Crustal structure of the Labrador Sea conjugate margin and implications for the formation of nonvolcanic continental margins. Journal of Geophysical Research **100**, 24239-24253.

Christie, P., Gollifer, I. & Cowper, D. 2006: Borehole seismic studies of a volcanic succession from the Lopra-1/1A borehole in the Faroe Islands, northern North Atlantic. In: Scientific results from the deepened Lopra-1 borehole, Faroe Islands. Edited by J.A. Chalmers & R. Waagstein. Geological Survey of Denmark and Greenland Bulletin **9**, 23-40.

Detrick, R.S., White, R.S. & Purdy, G.M. 1993: Crustal structure of North Atlantic fracture zones. Reviews of Geophysics **31**, 439-458.

Edwards, R.A., Whitmarsh, R.B. & Scrutton, R.A. 1997: The crustal structure across the transform continental margin off Ghana, eastern equatorial Atlantic. Journal of Geophysical Research **102**, 747-772.

Funck, T. & Louden, K.E. 1998: Wide-angle seismic imaging of pristine Archean crust in the Nain Province, Labrador. Canadian Journal of Earth Sciences **35**, 672-685.

Funck, T. & Louden, K.E. 1999: Wide-angle seismic transect across the Torngat Orogen, northern Labrador: evidence for a Proterozoic crustal root. Journal of Geophysical Research **104**, 7463-7480.

Funck, T., Louden, K.E., & Reid, I.D. 2000: Wide-angle seismic imaging of a Mesoproterozoic anorthosite complex: The Nain Plutonic Suite in Labrador, Canada. Journal of Geophysical Research **105**, 25693-25707.

Funck, T., Hopper, J.R., Larsen, H.C., Louden, K.E., Tucholke, B.E. & Holbrook, W.S. 2003: Crustal structure of the ocean-continent transition at Flemish Cap: Seismic refraction results. Journal of Geophysical Research **108** (B11), 2531.

Funck, T., Jackson, H.R., Louden, K.E., Dehler, S.A. & Wu, Y. 2004: Crustal structure of the northern Nova Scotia rifted continental margin (Eastern Canada). Journal of Geophysical Research **109**, B09102.

Funck, T., Jackson, H.R., Louden, K.E. & Klingelhöfer, F. 2007: Seismic study of the transform rifted margin in Davis Strait between Baffin Island (Canada) and Greenland: What happens when a plume meets a transform. Journal of Geophysical Research **112**, B04402.

Gerlings, J., Funck, T., Jackson, H.R, Louden, K.E. & Klingelhöfer, F. 2009: Seismic evidence for plume-derived volcanism of the continental margin in southern Davis Strait and northern Labrador Sea. Geophysical Journal International **176**, 980-994.

Gohl, K. & Smithson, S.B. 1993: Structure of Archean crust and passive margin of southwest Greenland from seismic wide-angle data. Journal of Geophysical Research **98**, 6623-6638.

Gohl, K., Schreckenberger, B. & Funck, T. (eds) 2009: The expedition of the research vessel “Maria S. Merian” to the Davis Strait and Baffin Bay in 2008 (MSM09/3). Reports on Polar and Marine Research **587**, 99 pp., Alfred Wegener Institute for Polar and Marine Research, Bremerhaven, Germany.

Hall, J., Louden, K.E., Funck, T. & Deemer, S. 2002: Geophysical characteristics of the continental crust along the Lithoprobe Eastern Canadian Shield Onshore-Offshore Transect (ECSOOT): a review. Canadian Journal of Earth Sciences **39**: 569-587.

Holbrook, W.S., Mooney, W.D. & Christensen, N.I. 1992: The seismic velocity structure of the deep continental crust. In: Continental lower crust. Edited by D.M. Fountain, R. Arculus, & R. Kay. Elsevier, Amsterdam, The Netherlands, 1-43.

Jackson, H.R. & Reid, I. 1994: Crustal thickness between the Greenland and Ellesmere Island margins determined from seismic refraction. Canadian Journal of Earth Sciences **31**, 1407–1418.

Jokat, W., Ritzmann, O., Schmidt-Aursch, M.C., Drachev, S., Gauger, S. & Snow, J. 2003: Geophysical evidence for reduced melt production on the Arctic ultraslow Gakkel mid-ocean ridge. Nature **426**, 962-965.

Keen, C.E. & Barrett, D.L. 1972. Seismic refraction studies in Baffin Bay: an example of a developing ocean basin. Geophysical Journal of the Royal Astronomical Society **30**, 253-271.

Keen, C.E., Keen, M.J., Ross, D.J. & Lack, M. 1974: Baffin Bay: small ocean basin formed by sea-floor spreading. AAPG Bulletin **58**, 1089-1108.

Kerr, J.W. 1967: A submerged continental remnant of the Labrador Sea. Earth and Planetary Science Letters **2**, 283-289.

Klose, G. W., Malterre, E., McMillan, N.J. & Zinkan, C.G. 1982: Petroleum exploration offshore southern Baffin Island, northern Labrador Sea, Canada. In: Arctic geology and geophysics. Edited by A.F. Embry & H.R. Balkwill. Memoirs of the Canadian Society of Petroleum Geologists **8**, 233-244.

Larsen, H.C. & Saunders, A.D. 1998: Tectonism and volcanism at the southeast Greenland rifted margin: A record of plume impact and later continental rupture. Proceedings of the Ocean Drilling Program, Scientific Results **152**, 503–533.

Ludwig, W.J., Nafe, J.E. & Drake, C.L. 1970: Seismic refraction. In: The Sea, volume 4, New Concepts of Sea Floor Evolution, Part I. Edited by A.E. Maxwell. Wiley-Interscience, Hoboken, New Jersey, 53-84.

Larsen, L.M., Heaman, L.M., Creaser, R.A., Duncan, R.A., Frei, R. & Hutchinson, M. 2009: Tectonomagmatic events during stretching and basin formation in the Labrador Sea and the Davis Strait: evidence from age and composition of Mesozoic to Palaeogene dyke swarms in West Greenland. Journal of the Geological Society **166**, 999-1012.

Lutter, W.J. & Nowack, R.L. 1990: Inversion for crustal structure using reflections from the PASSCAL Ouachita experiment. Journal of Geophysical Research **95**, 4633-4646.

Nielsen, T.K., Larsen, H.C. & Hopper, J.R. 2002: Contrasting rifted margin styles south of Greenland: implications for mantle plume dynamics. Earth and Planetary Science Letters **200**, 271-286.

Oakey, G.N. 2001a: Physiography, Davis Strait region, Canadian and Greenland Arctic. Geological Survey of Canada, Open File **3933b**, 1 map.

Oakey, G.N. 2001b: Physiography, Baffin Bay region, Canadian and Greenland Arctic. Geological Survey of Canada, Open File **3933c**, 1 map.

Oakey, G.N. 2001c: Magnetic anomaly, Davis Strait region, Canadian and Greenland Arctic. Geological Survey of Canada, Open File **3935B**, 1 map.

Pearson, D.G., Emeleus, C.H. & Kelley, S.P. 1996: Precise $^{40}Ar/^{39}Ar$ age for the initiation of Palaeogene volcanism in the Inner Hebrides and its regional significance. Journal of the Geological Society **153**, 815-818.

Reid, I. & Jackson, H.R. 1997: Crustal structure of the northern Baffin Bay: seismic refraction results and tectonic implications. Journal of Geophysical Research **102**, 523-542.

Roest, W.R. & Srivastava, S.P. 1989: Sea-floor spreading in the Labrador Sea: a new reconstruction. Geology **17**, 1000-1003.

Skaarup, N., Jackson, H.R. & Oakey, G. 2006: Margin segmentation of Baffin Bay/Davis Strait, eastern Canada, based on seismic reflection and potential field data. Marine Petroleum Geology **23**, 127-144.

Sleep, N.H. 1997: Lateral flow and ponding of starting plume material. Journal of Geophysical Research **102**, 10001-10012.

Srivastava, S.P. 1978: Evolution of the Labrador Sea and its bearing on the early evolution of the North Atlantic. Geophysical Journal of the Royal Astronomical Society **52**, 313-357.

Srivastava, S.P. & Keen, C.E. 1995: A deep seismic reflection profile across the extinct Mid-Labrador Sea spreading center. Tectonics **14**, 372-389.

Srivastava, S.P., MacLean, B., Macnab, R.F. & Jackson, H.R. 1982: Davis Strait: structure and evolution as obtained from a systematic geophysical survey. In: Arctic geology and geophysics. Edited by A.F. Embry & H.R. Balkwill. Memoirs of the Canadian Society of Petroleum Geologists **8**, 267-278.

Storey, M., Duncan, R.A., Pedersen, A.K., Larsen, L.M. & Larsen, H.C. 1998: $^{40}Ar/^{39}Ar$ geochronology of the West Greenland Tertiary volcanic province. Earth and Planetary Science Letters **160**, 569-586.

Talwani, M., Worzel, J.L. & Landisman, M. 1959: Rapid gravity computations for two-dimensional bodies with application to the Mendocino submarine fracture zone. Journal of Geophysical Research **64**, 49-59.

Verhoef, J., Roest, W.R, Macnab, R. Arkani-Hamed, J. & Members of the Project Team 1996: Magnetic anomalies of the Arctic and North Atlantic oceans and adjacent land areas. Geological Survey of Canada, Open File **3125**.

White, R.S., McKenzie, D. & O'Nions, K. 1992: Oceanic crustal thickness from seismic measurements and rare earth element inversions. Journal of Geophysical Research **97**, 19683-19715.

Williamson, M.-C., Villeneuve, M.E., Larsen, L.M., Jackson, H.R., Oakey, G.N. & Maclean, B. 2001: Age and petrology of offshore basalts from the Southeast Baffin Island Shelf, Davis Strait, and the Western Greenland continental margin. Paper presented at Joint Annual Meeting, Geological Association of Canada and Mineralogical Association of Canada, St. John's, Newfoundland and Labrador, Canada.

Zelt, C.A. & Forsyth, D.A. 1994: Modeling wide-angle seismic data for crustal structure: southeastern Grenville Province. Journal of Geophysical Research **99**, 11687-11704.

Zelt, C.A. & Smith, R.B. 1992: Seismic travel time inversion for 2-D crustal velocity structure. Geophysical Journal International **108**, 16-34.

Appendix A

Seismic Records and Ray Diagrams for all Ocean Bottom Seismometers

In this appendix, record sections for all OBS are shown – with exception of OBS 5, 6 and 21, which did not record any data due to technical problems. Below each record section, three other panels display the velocity model (same colour scheme as in Fig. 7) together with the ray paths, the calculated and observed travel times, as well as a record section overlain by the calculated travel times. The OBS position is indicated by a red triangle.

All record sections and travel times are displayed with a reduction velocity of 6.8 km/s; the horizontal scale is the distance along the velocity model. The observed travel times are marked by vertical lines with the height of the lines representing the estimated pick uncertainty. Ray paths and calculated travel time curves are displayed for every possible reflection and refraction in the model regardless whether such a phase could be recognized in the record section or not. That way, the eye will occasionally detect some weak phases when guided by the calculated travel time curve, which could not be picked safely just by looking at the record. For example, in the record of OBS 601 (Fig. A-1) it is difficult to identify phases between 40 to 60 km. However, when the calculated travel time curve is plotted on the seismic record, some energy can be correlated along that segment.

In some cases, a particular phase was both calculated as refraction (diving wave) and as head wave to reach proper ray coverage in areas where it was difficult to trace refracted rays. This is in particular the case for the mantle refraction P_n and sometimes for the upper crustal refraction (P_2 and P_{c1}) where steep layer geometry causes otherwise shadow zones for the diving waves.

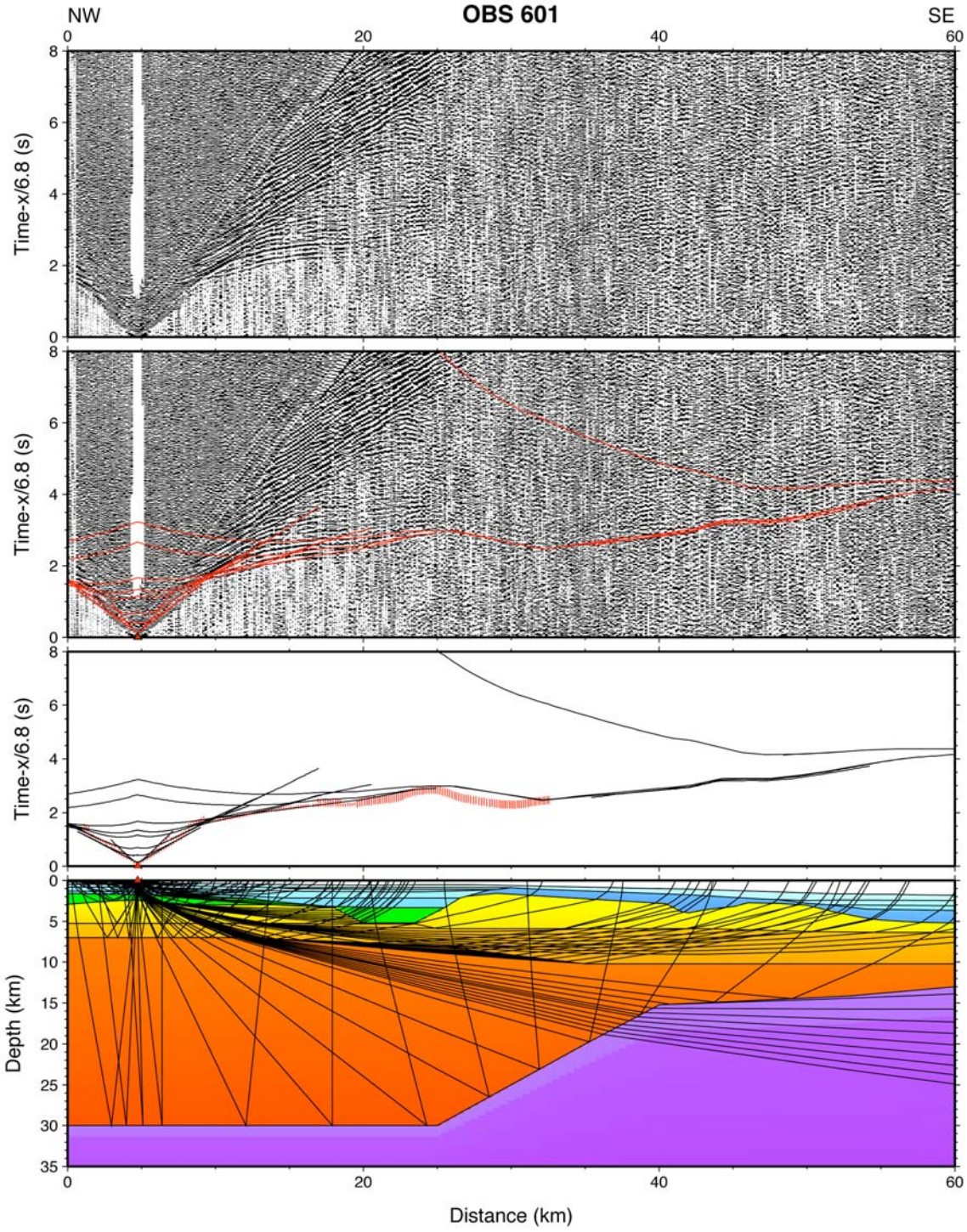

Figure A-1. *Seismic record, ray paths and travel times for OBS 601. The record shows the hydrophone component of the instrument. A more detailed description of the figure is given in the introduction to Appendix A.*

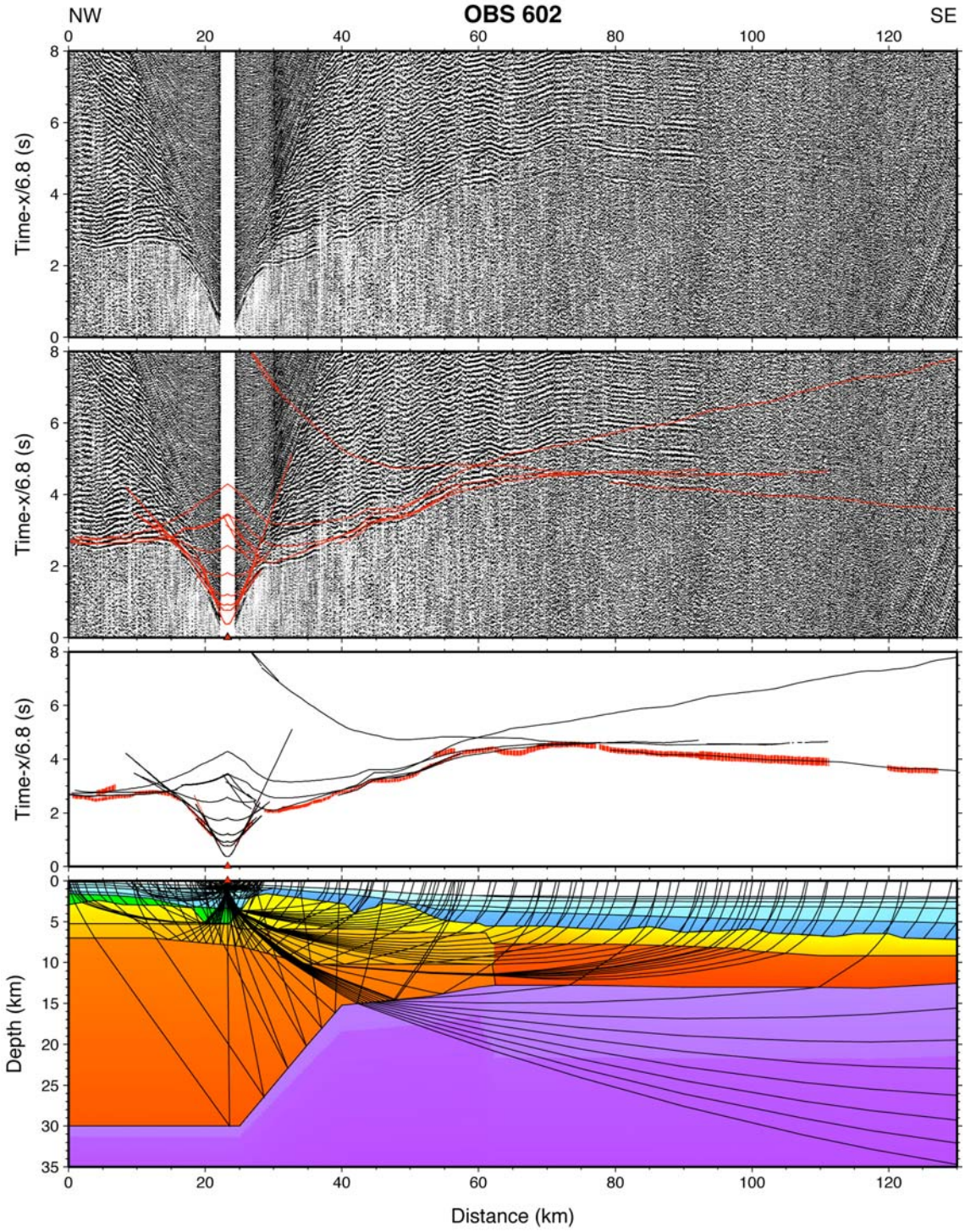

Figure A-2. *Seismic record, ray paths and travel times for OBS 602. The record shows the hydrophone component of the instrument. A more detailed description of the figure is given in the introduction to Appendix A.*

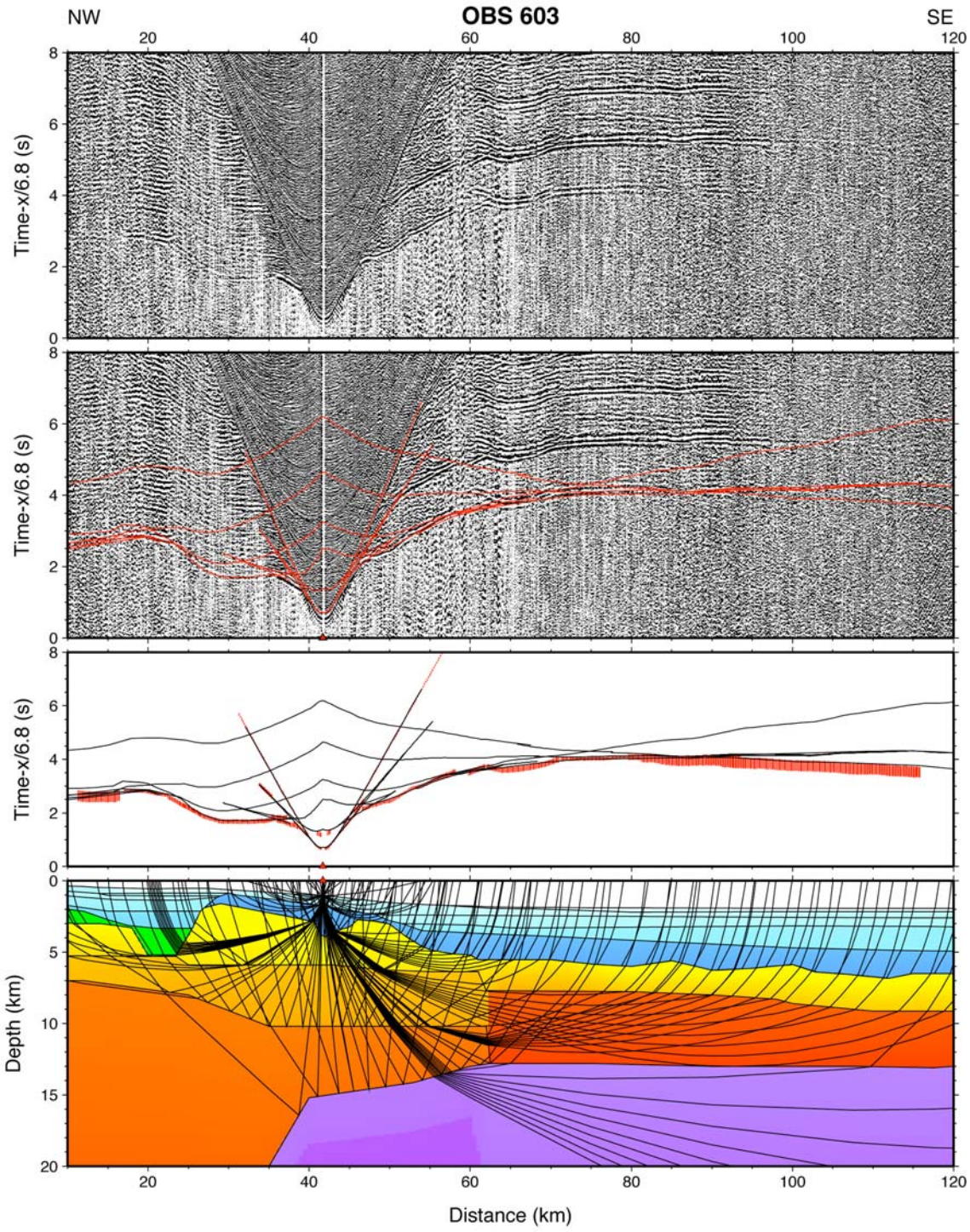

Figure A-3. *Seismic record, ray paths and travel times for OBS 603. The record shows the hydrophone component of the instrument. A more detailed description of the figure is given in the introduction to Appendix A.*

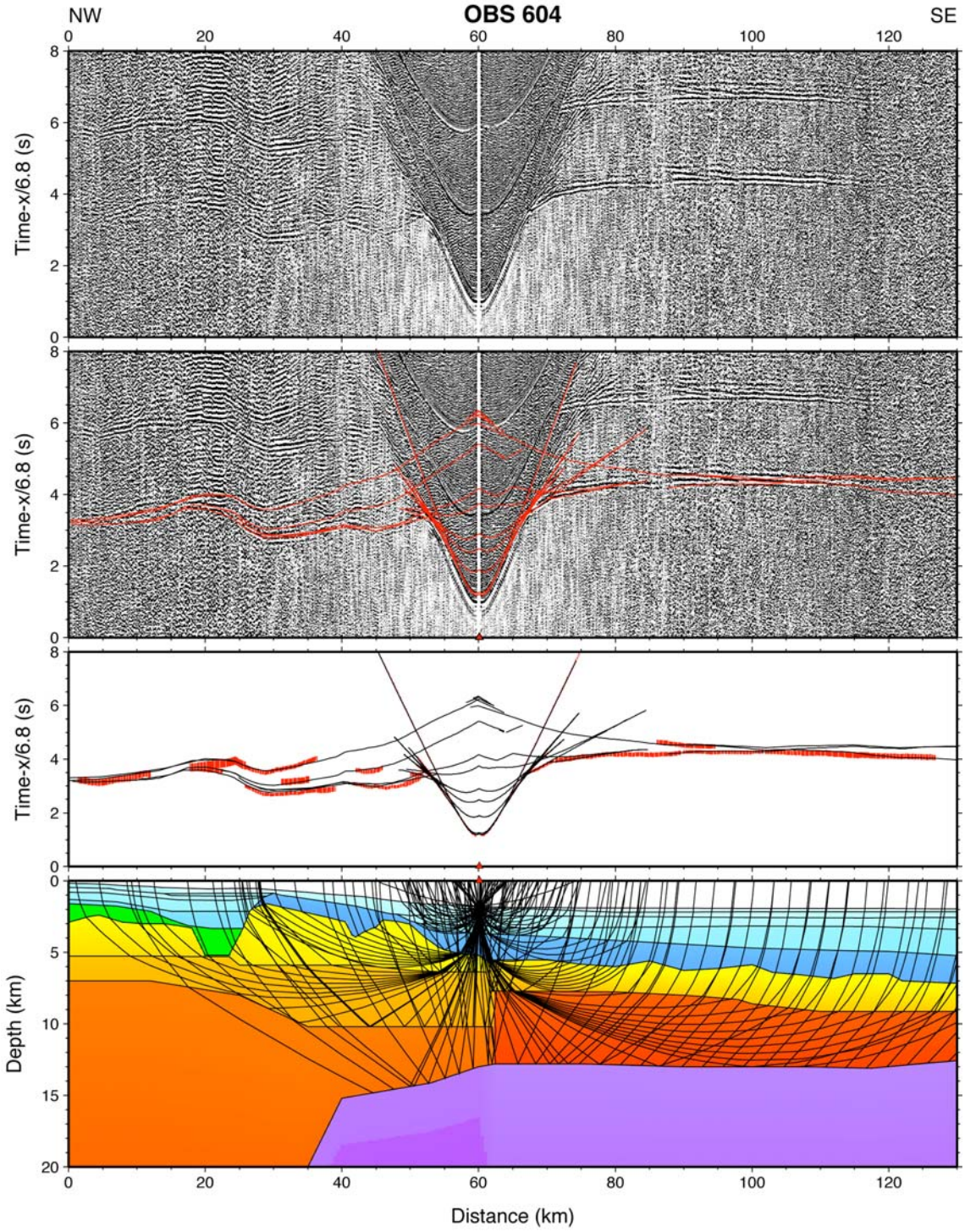

Figure A-4 *Seismic record, ray paths and travel times for OBS 604. The record shows the hydrophone component of the instrument. A more detailed description of the figure is given in the introduction to Appendix A.*

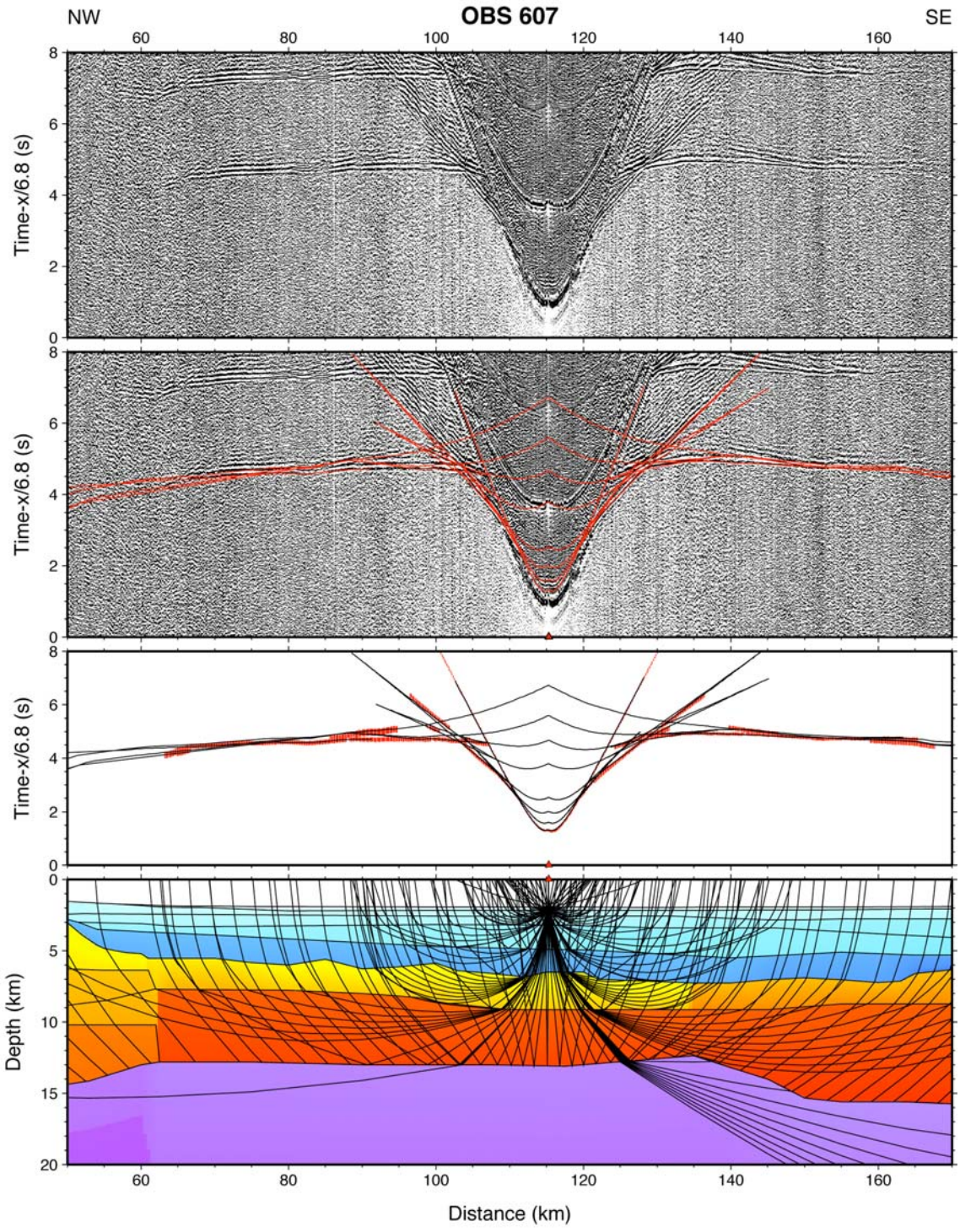

Figure A-5. *Seismic record, ray paths and travel times for OBS 607. The record shows the hydrophone component of the instrument. A more detailed description of the figure is given in the introduction to Appendix A.*

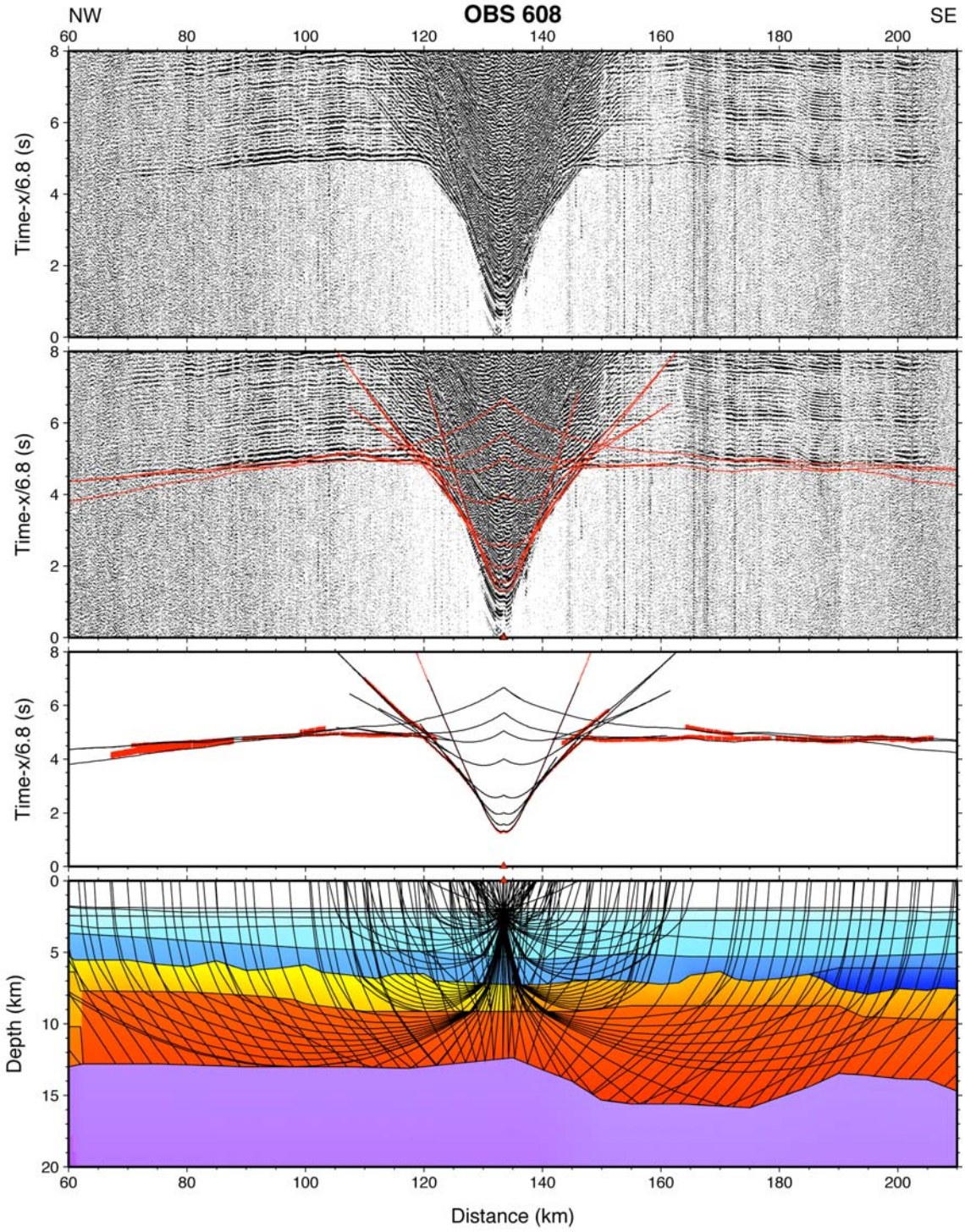

Figure A-6. *Seismic record, ray paths and travel times for OBS 608. The record shows the vertical geophone component of the instrument. A more detailed description of the figure is given in the introduction to Appendix A.*

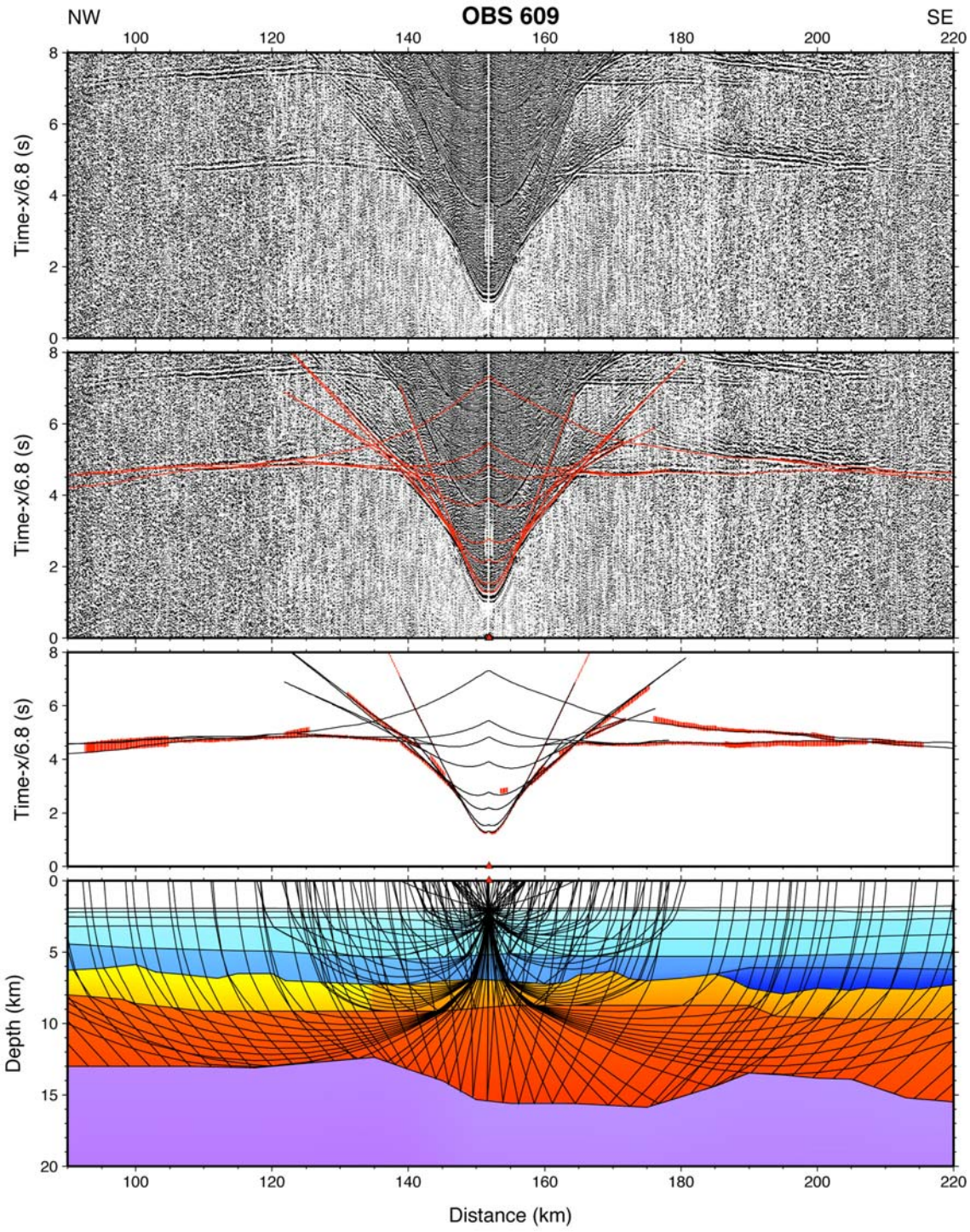

Figure A-7. *Seismic record, ray paths and travel times for OBS 609. The record shows the hydrophone component of the instrument. A more detailed description of the figure is given in the introduction to Appendix A.*

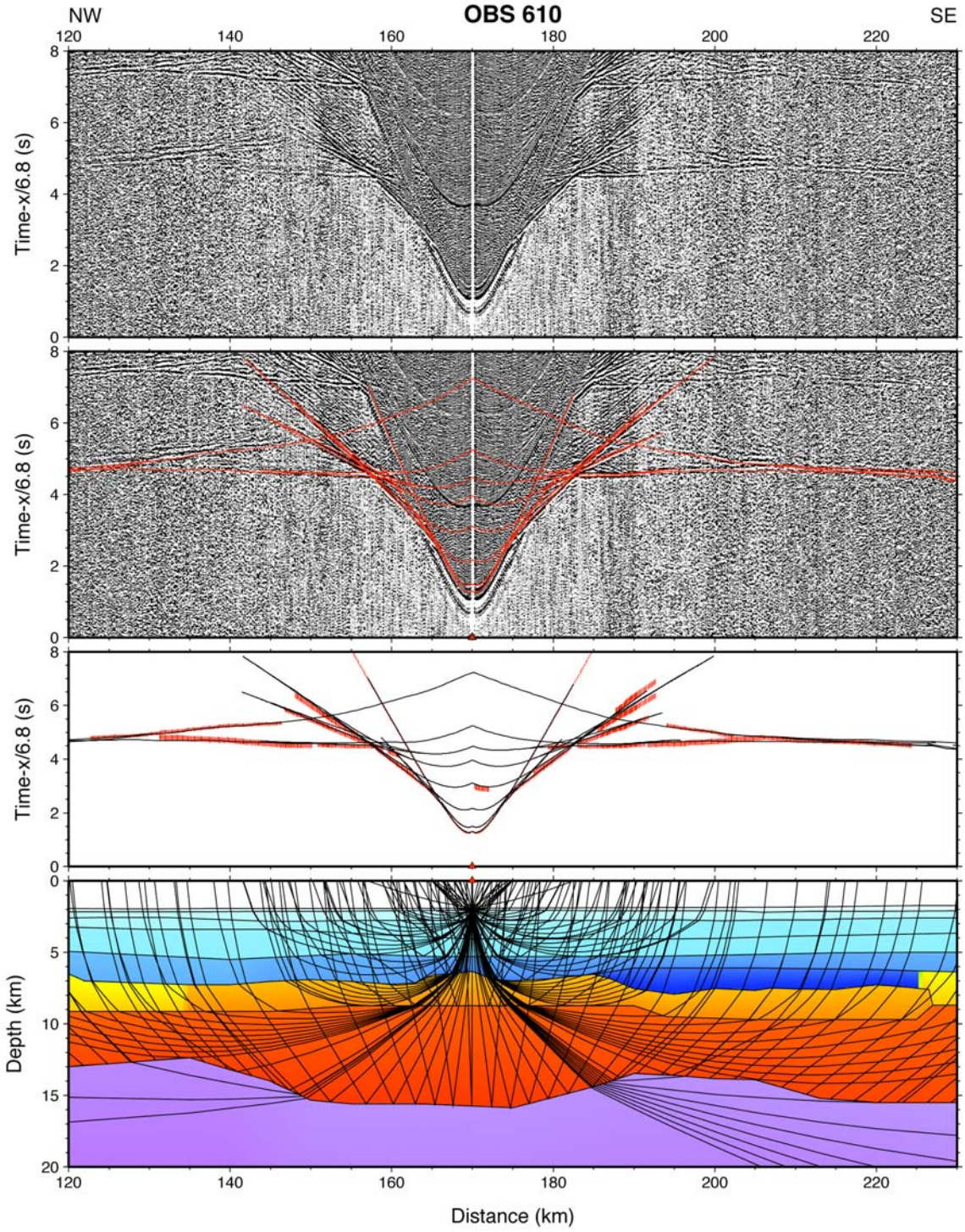

Figure A-8. *Seismic record, ray paths and travel times for OBS 610. The record shows the hydrophone component of the instrument. A more detailed description of the figure is given in the introduction to Appendix A.*

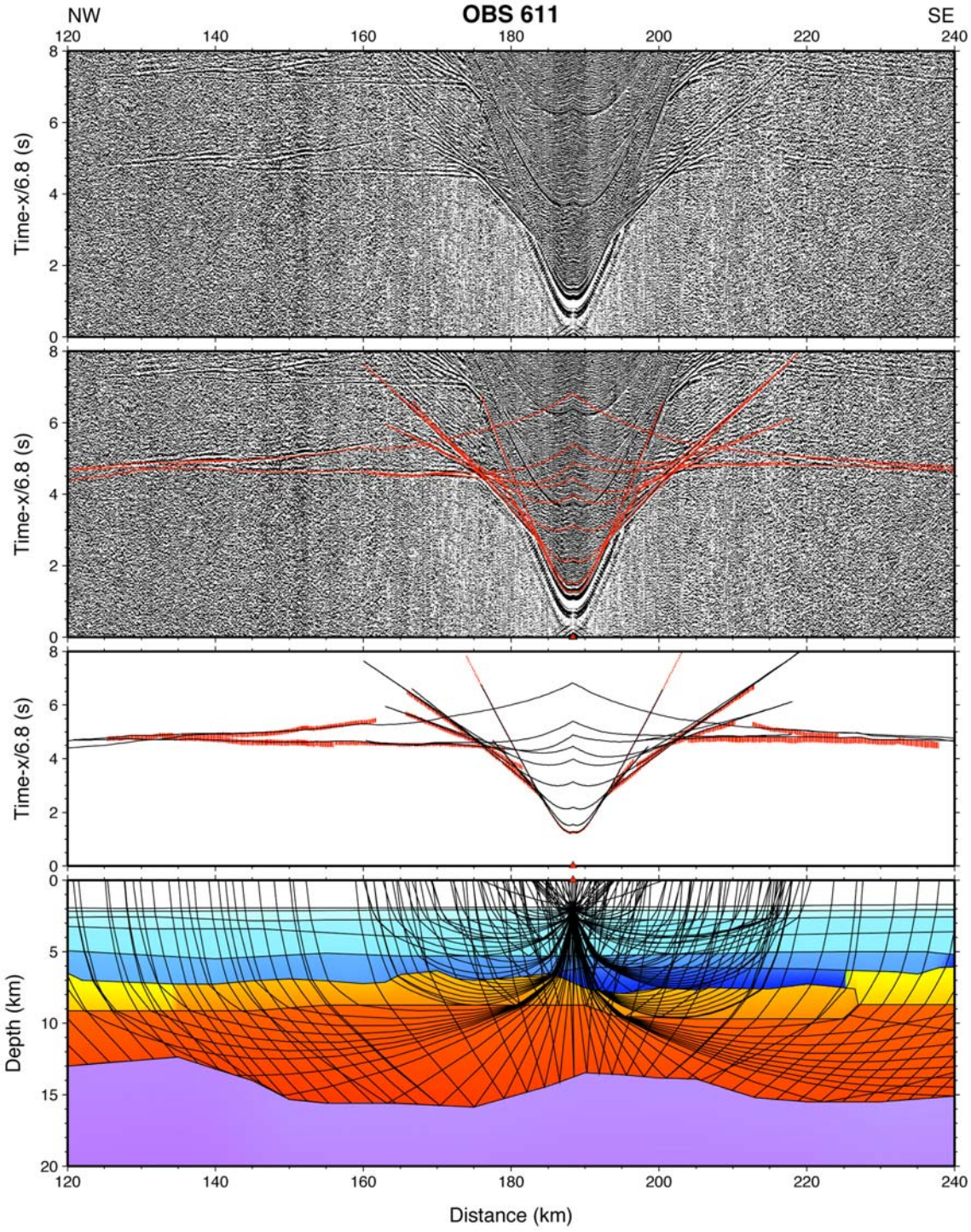

Figure A-9. *Seismic record, ray paths and travel times for OBS 611. The record shows the hydrophone component of the instrument. A more detailed description of the figure is given in the introduction to Appendix A.*

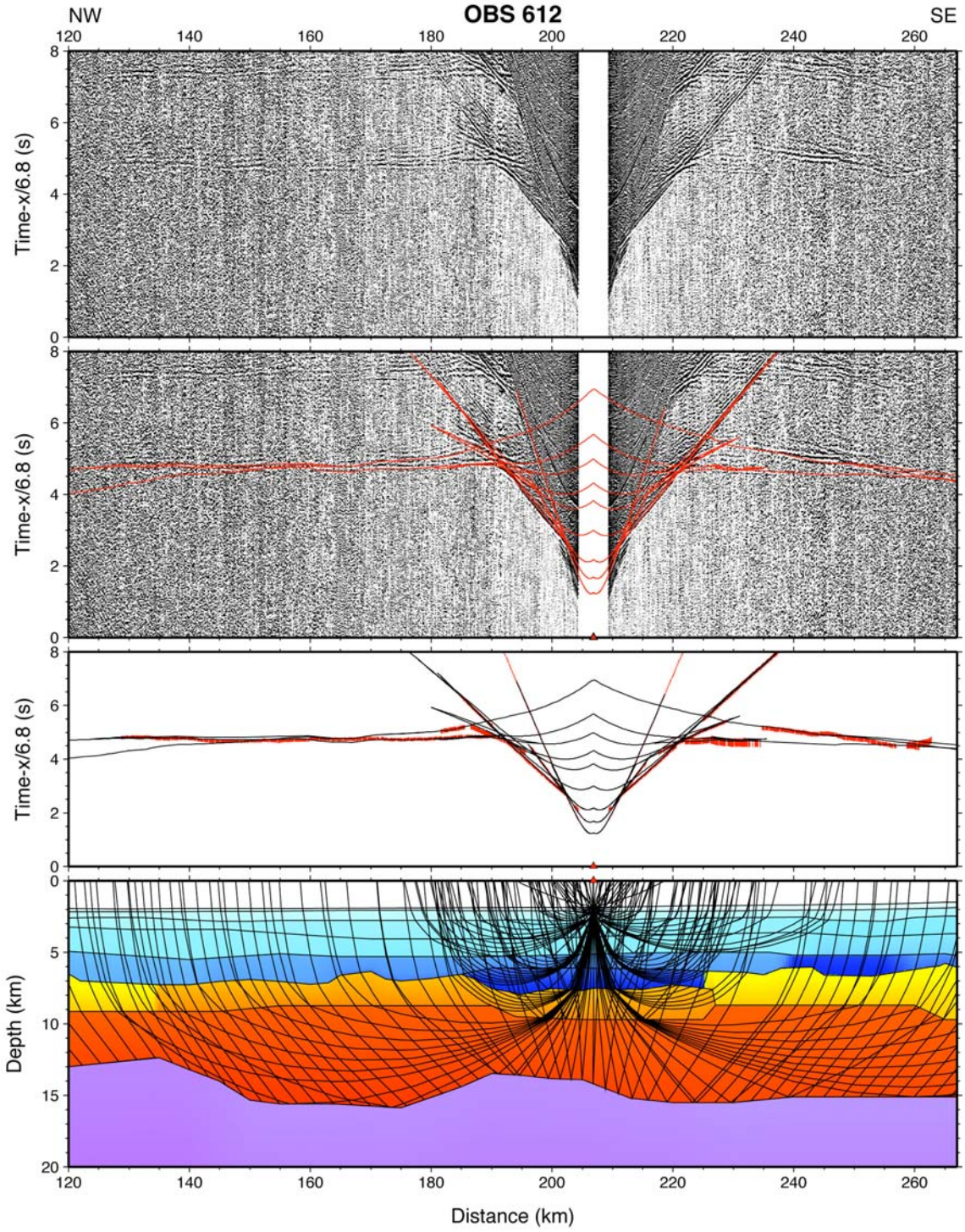

Figure A-10. *Seismic record, ray paths and travel times for OBS 612. The record shows the hydrophone component of the instrument. A more detailed description of the figure is given in the introduction to Appendix A.*

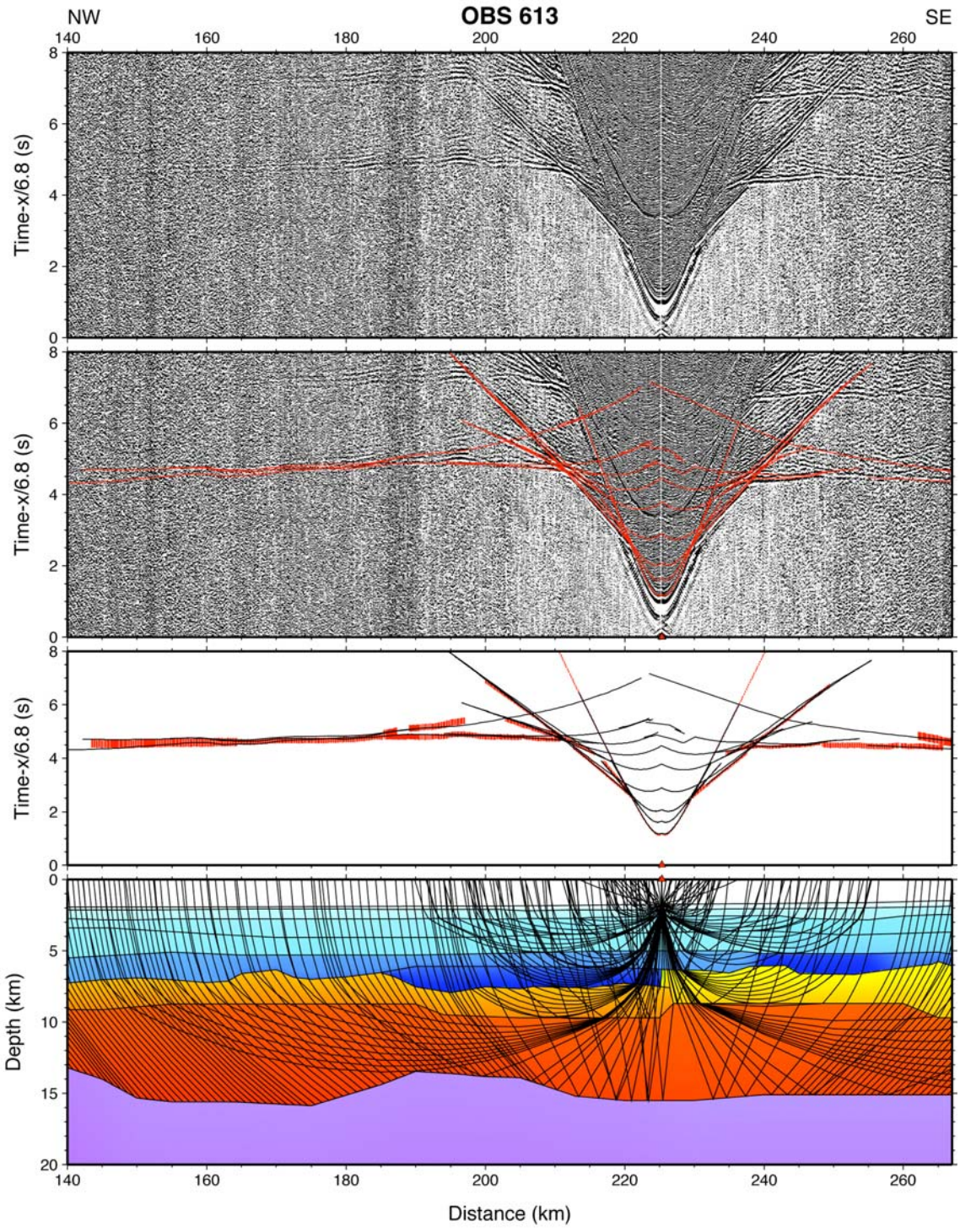

Figure A-11. *Seismic record, ray paths and travel times for OBS 613. The record shows the hydrophone component of the instrument. A more detailed description of the figure is given in the introduction to Appendix A.*

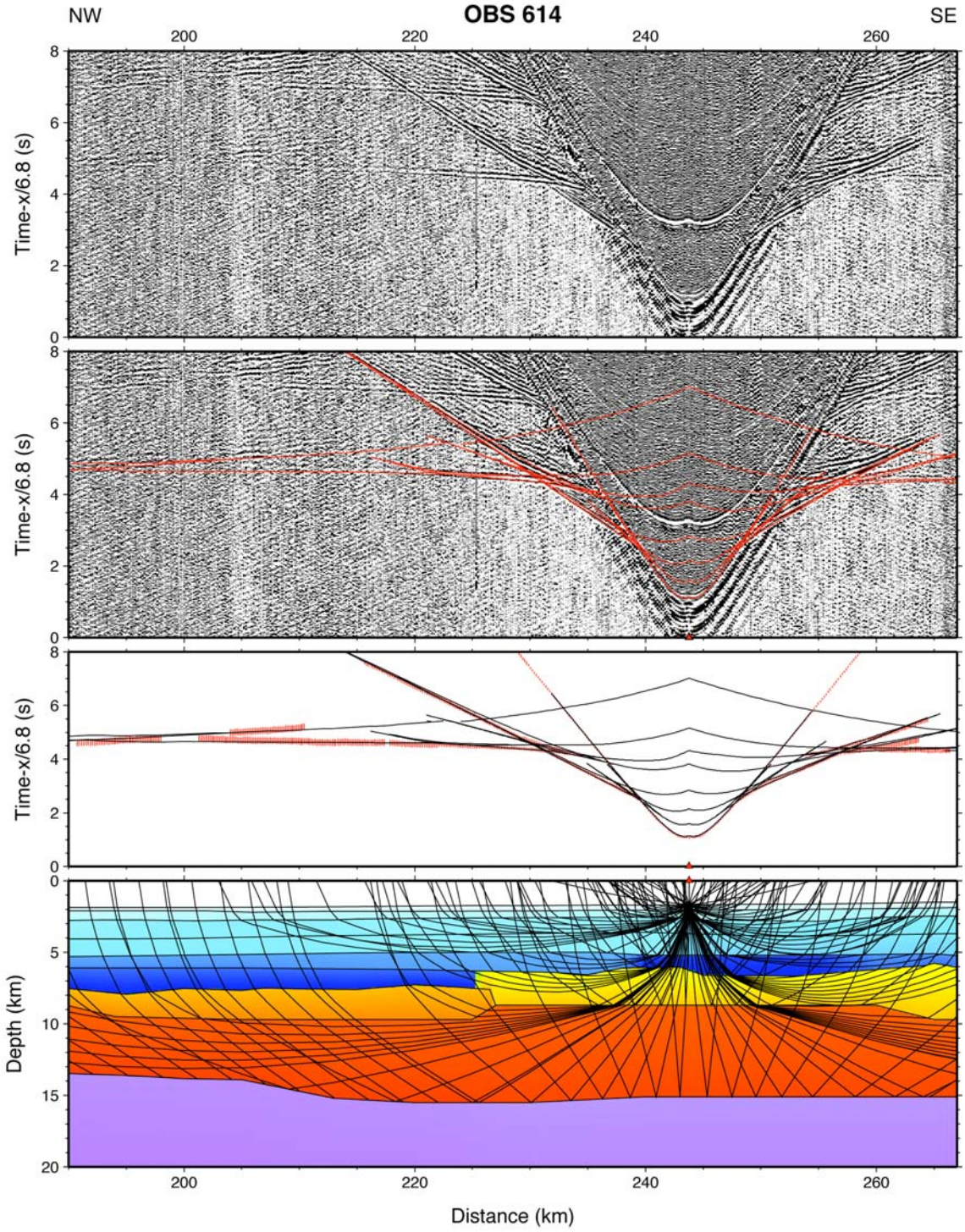

Figure A-12. *Seismic record, ray paths and travel times for OBS 614. The record shows the hydrophone component of the instrument. A more detailed description of the figure is given in the introduction to Appendix A.*

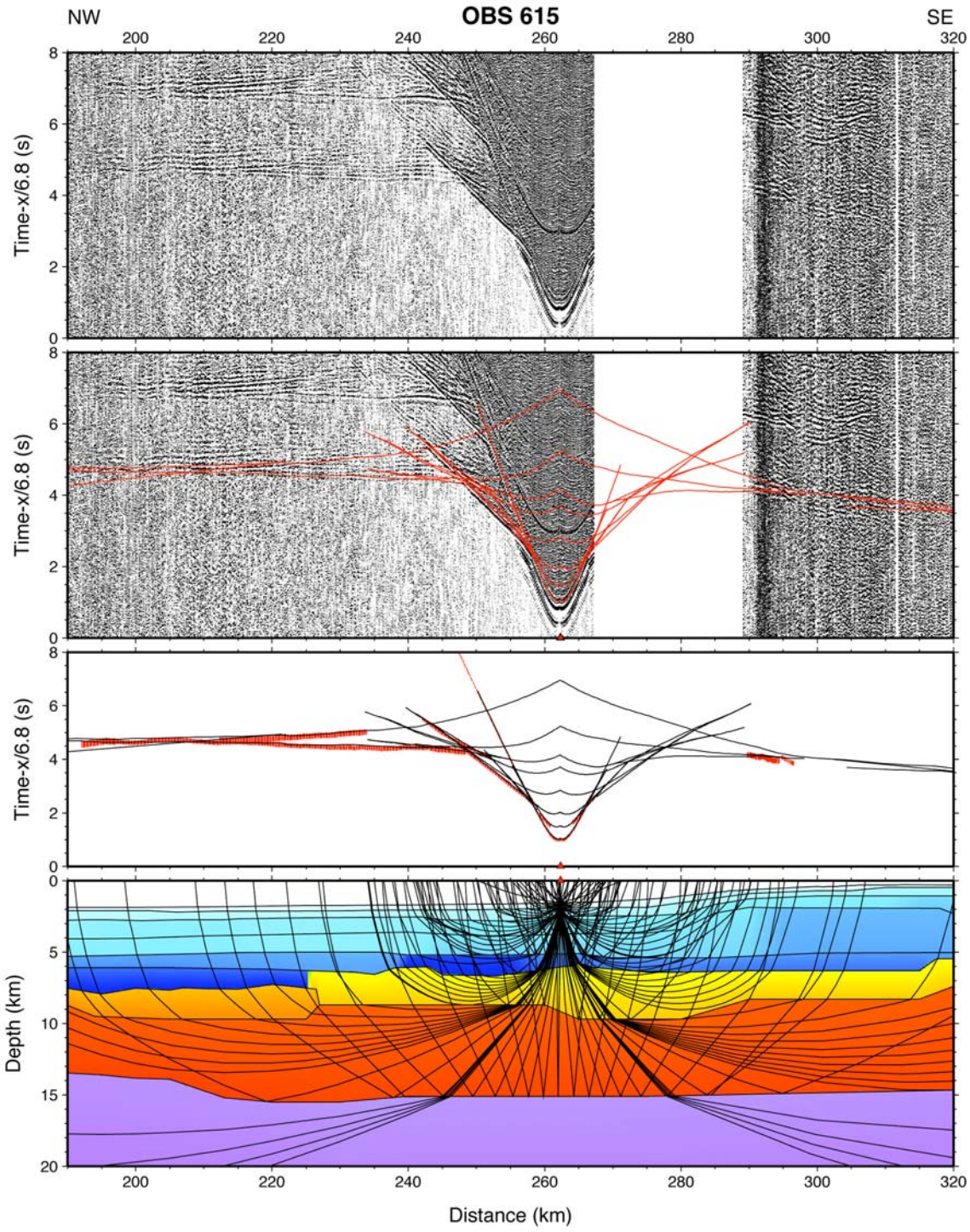

Figure A-13. *Seismic record, ray paths and travel times for OBS 615. The record shows the hydrophone component of the instrument. A more detailed description of the figure is given in the introduction to Appendix A.*

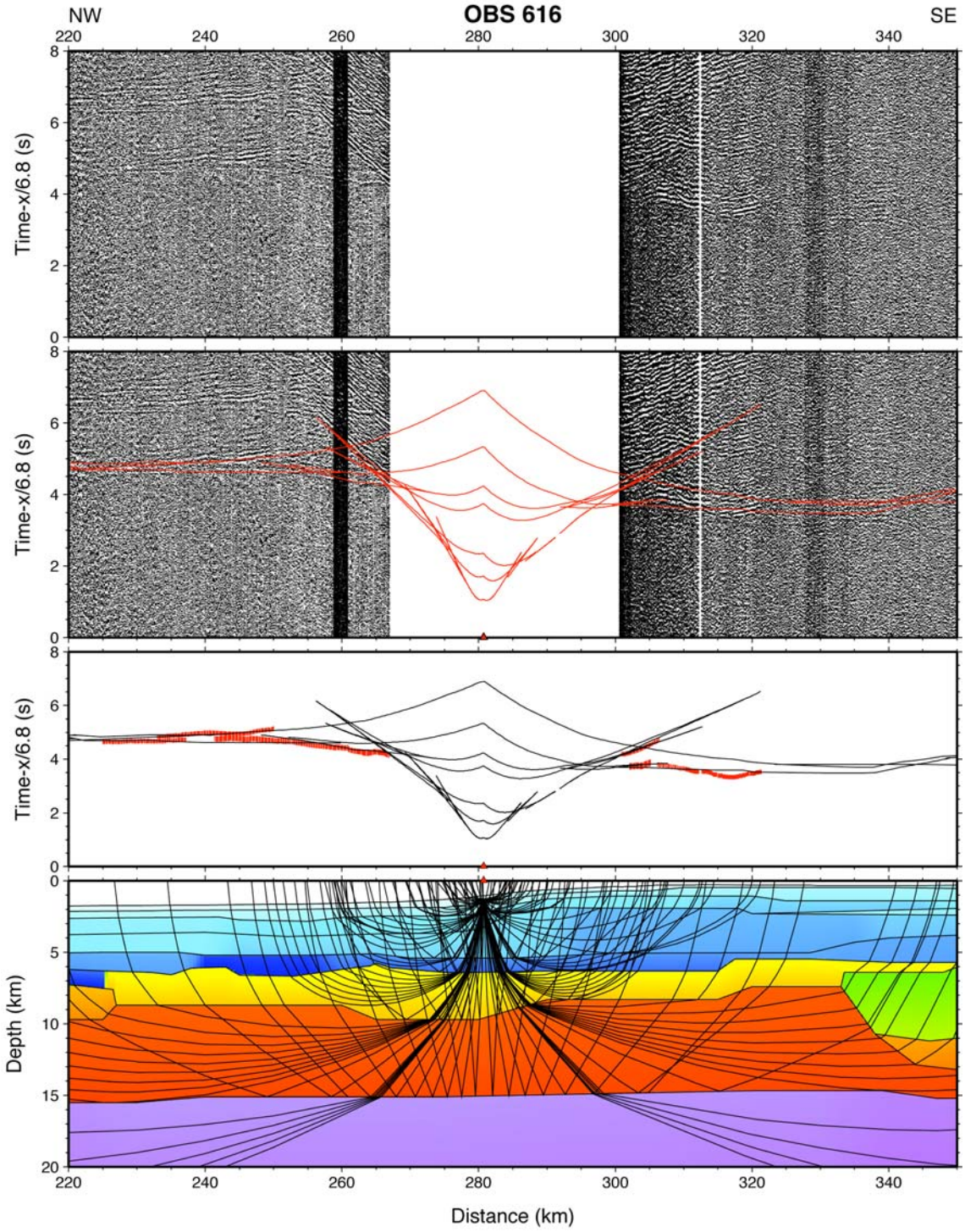

Figure A-14. *Seismic record, ray paths and travel times for OBS 616. The record shows the hydrophone component of the instrument. A more detailed description of the figure is given in the introduction to Appendix A.*

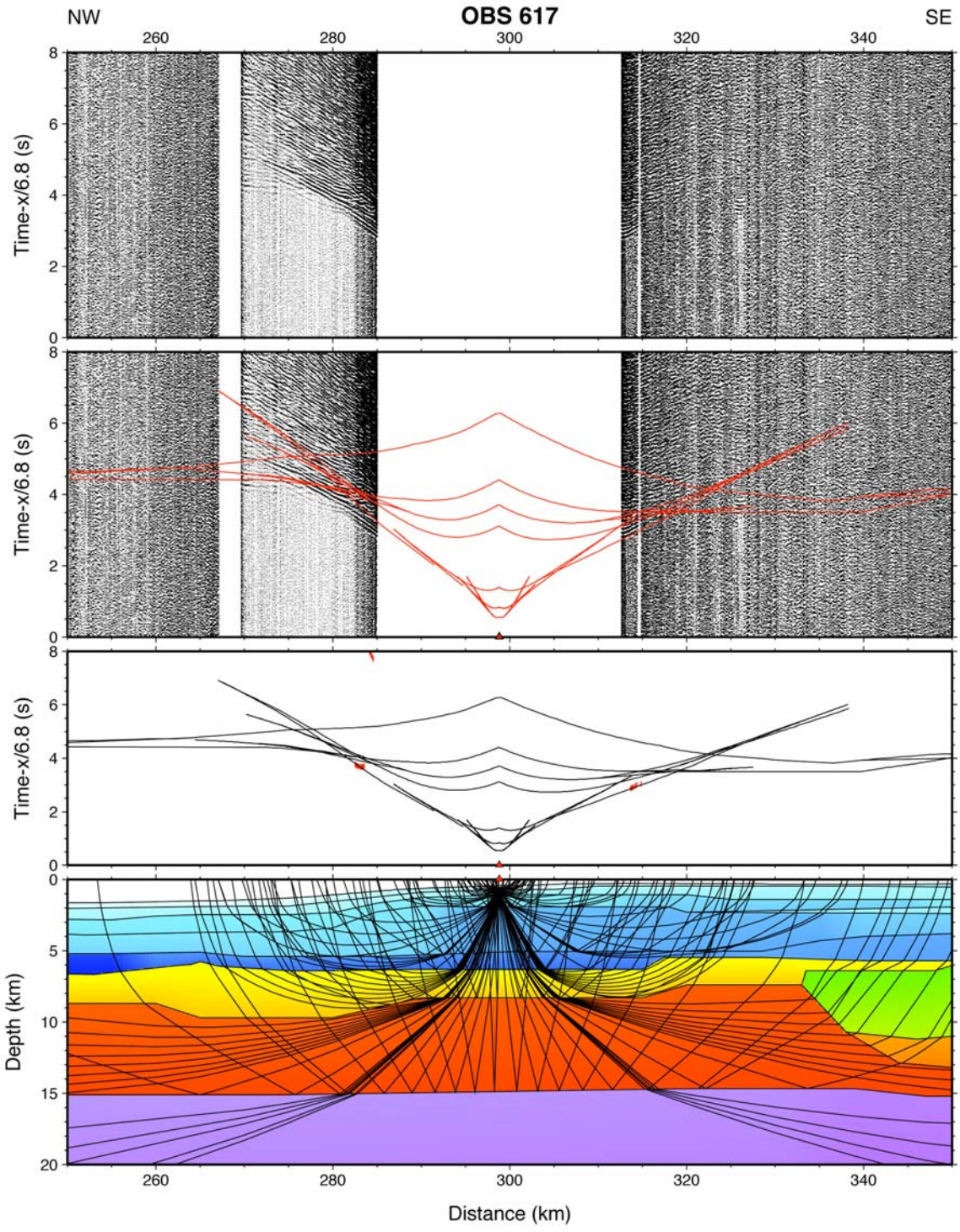

Figure A-15. *Seismic record, ray paths and travel times for OBS 617. The record shows the vertical geophone component of the instrument. A more detailed description of the figure is given in the introduction to Appendix A.*

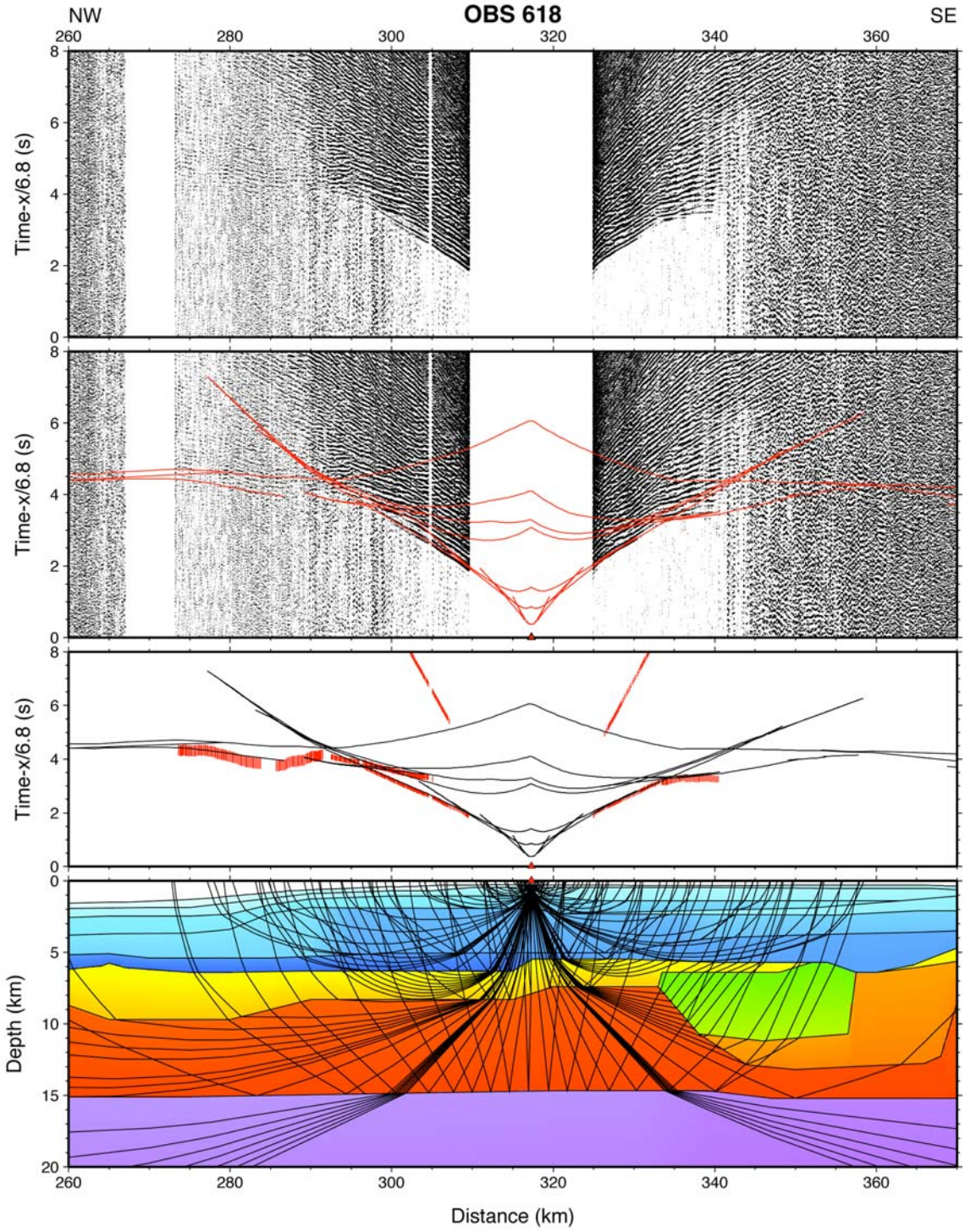

Figure A-16. *Seismic record, ray paths and travel times for OBS 618. The record shows the hydrophone component of the instrument. A more detailed description of the figure is given in the introduction to Appendix A.*

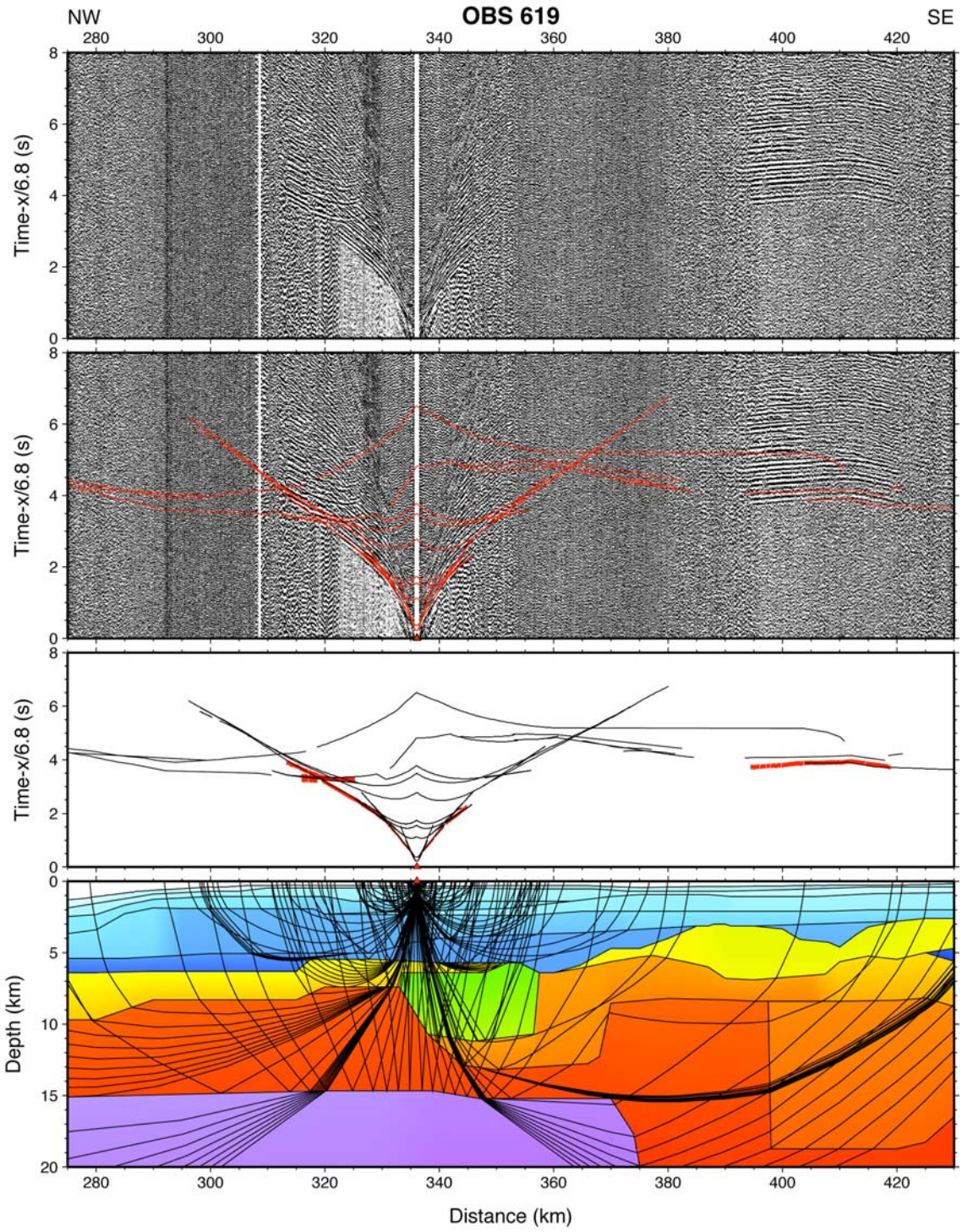

Figure A-17. *Seismic record, ray paths and travel times for OBS 619. The record shows the hydrophone component of the instrument. A more detailed description of the figure is given in the introduction to Appendix A.*

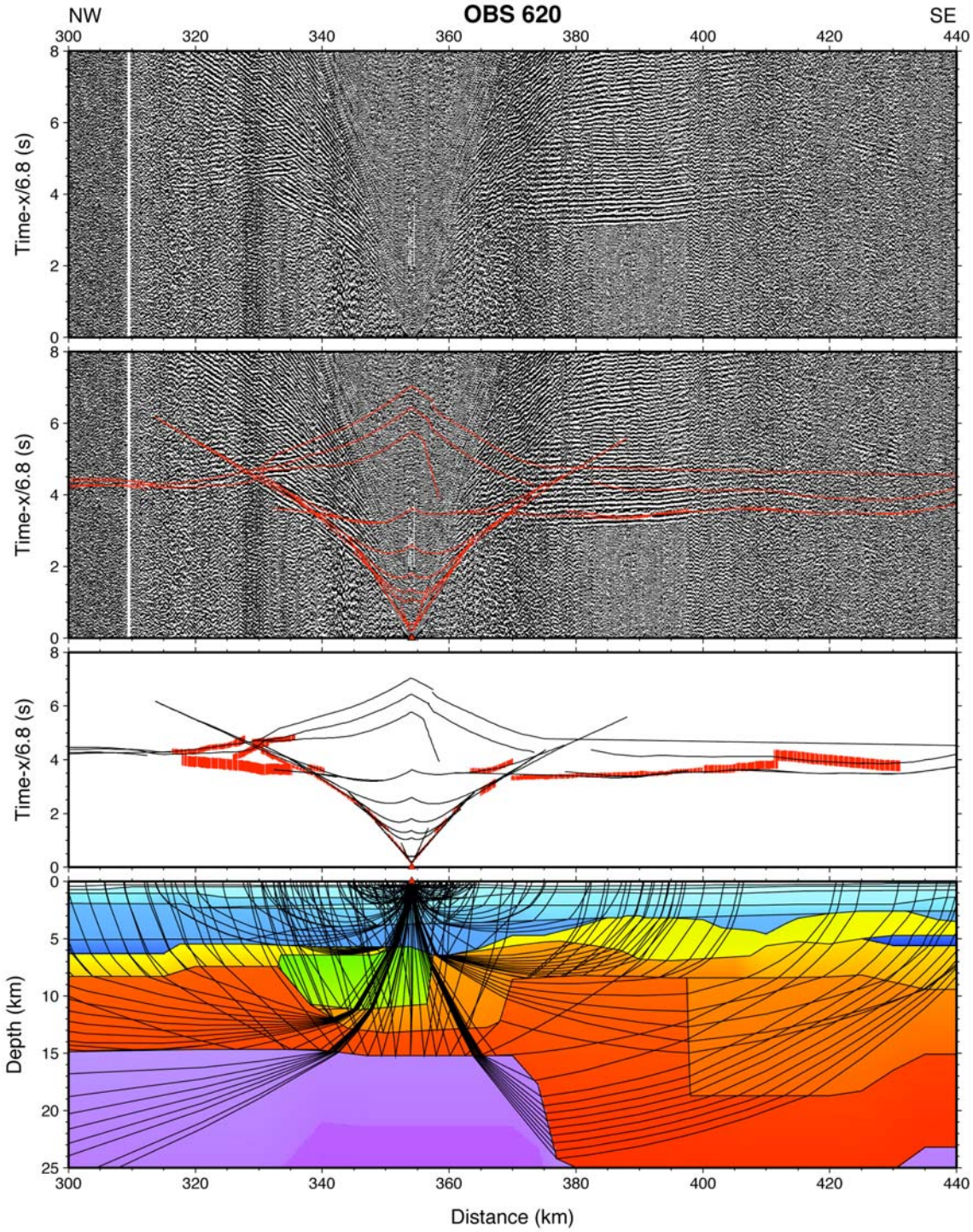

Figure A-18. *Seismic record, ray paths and travel times for OBS 620. The record shows the hydrophone component of the instrument. A more detailed description of the figure is given in the introduction to Appendix A.*

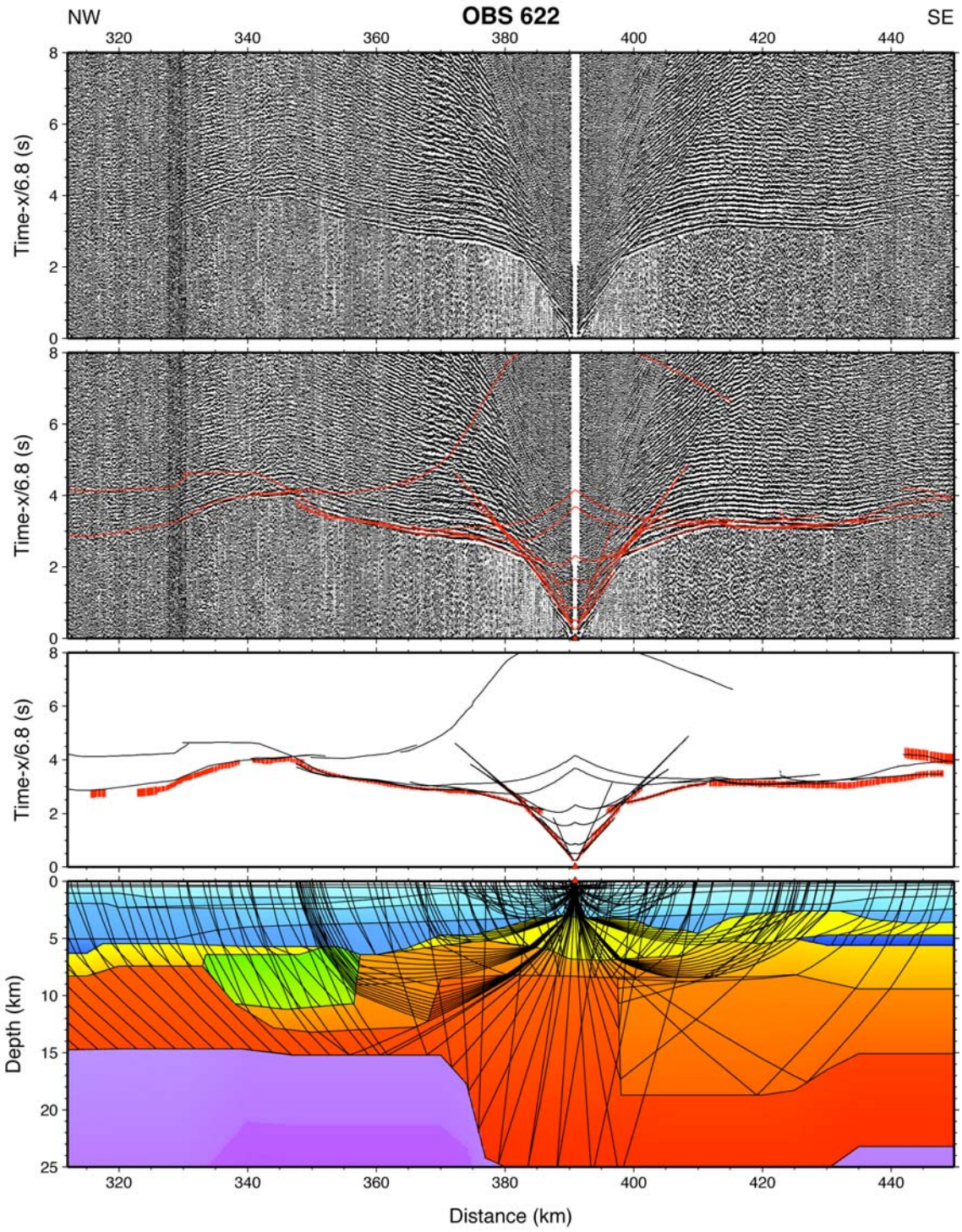

Figure A-19. *Seismic record, ray paths and travel times for OBS 622. The record shows the hydrophone component of the instrument. A more detailed description of the figure is given in the introduction to Appendix A.*

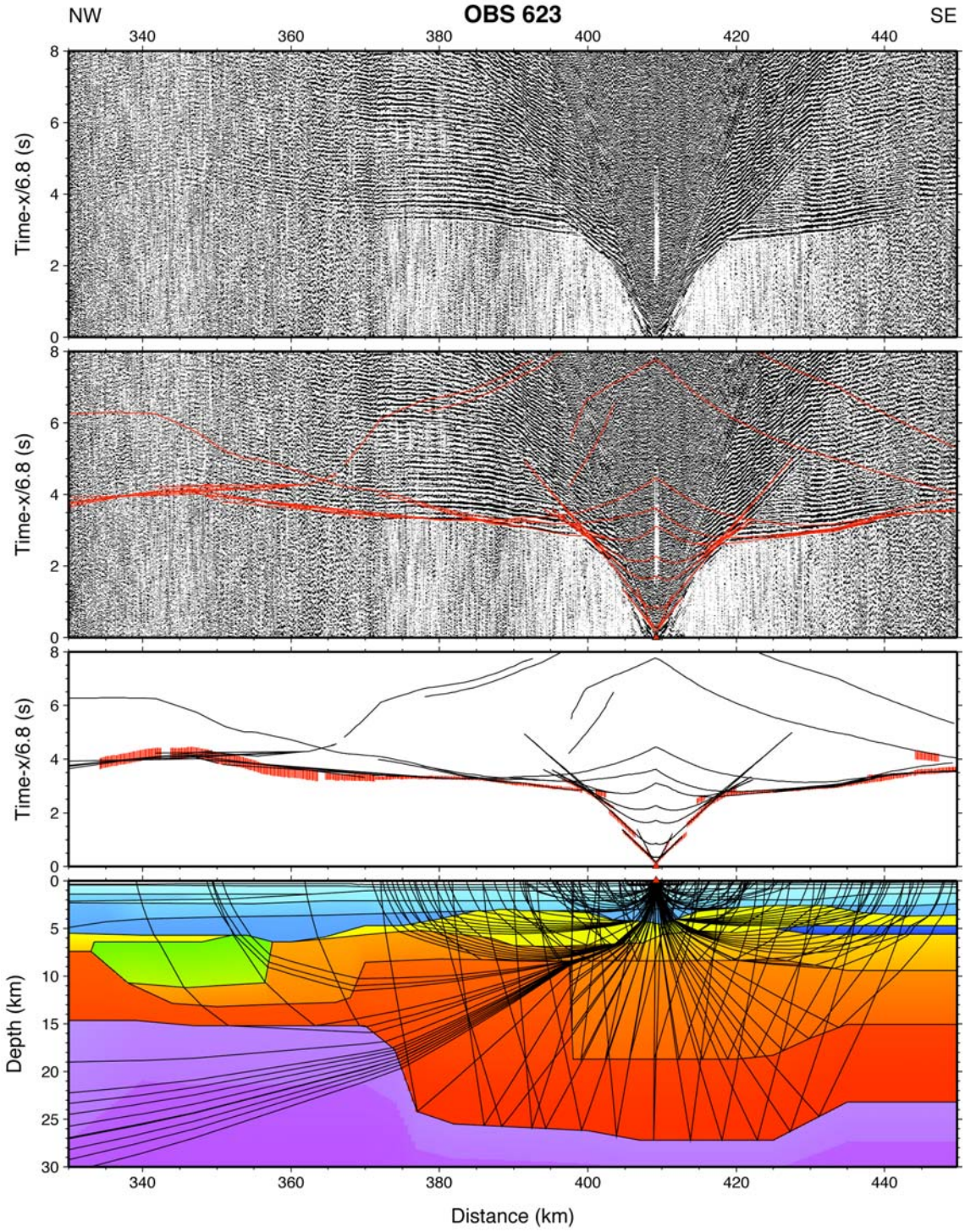

Figure A-20. *Seismic record, ray paths and travel times for OBS 623. The record shows the hydrophone component of the instrument. A more detailed description of the figure is given in the introduction to Appendix A.*

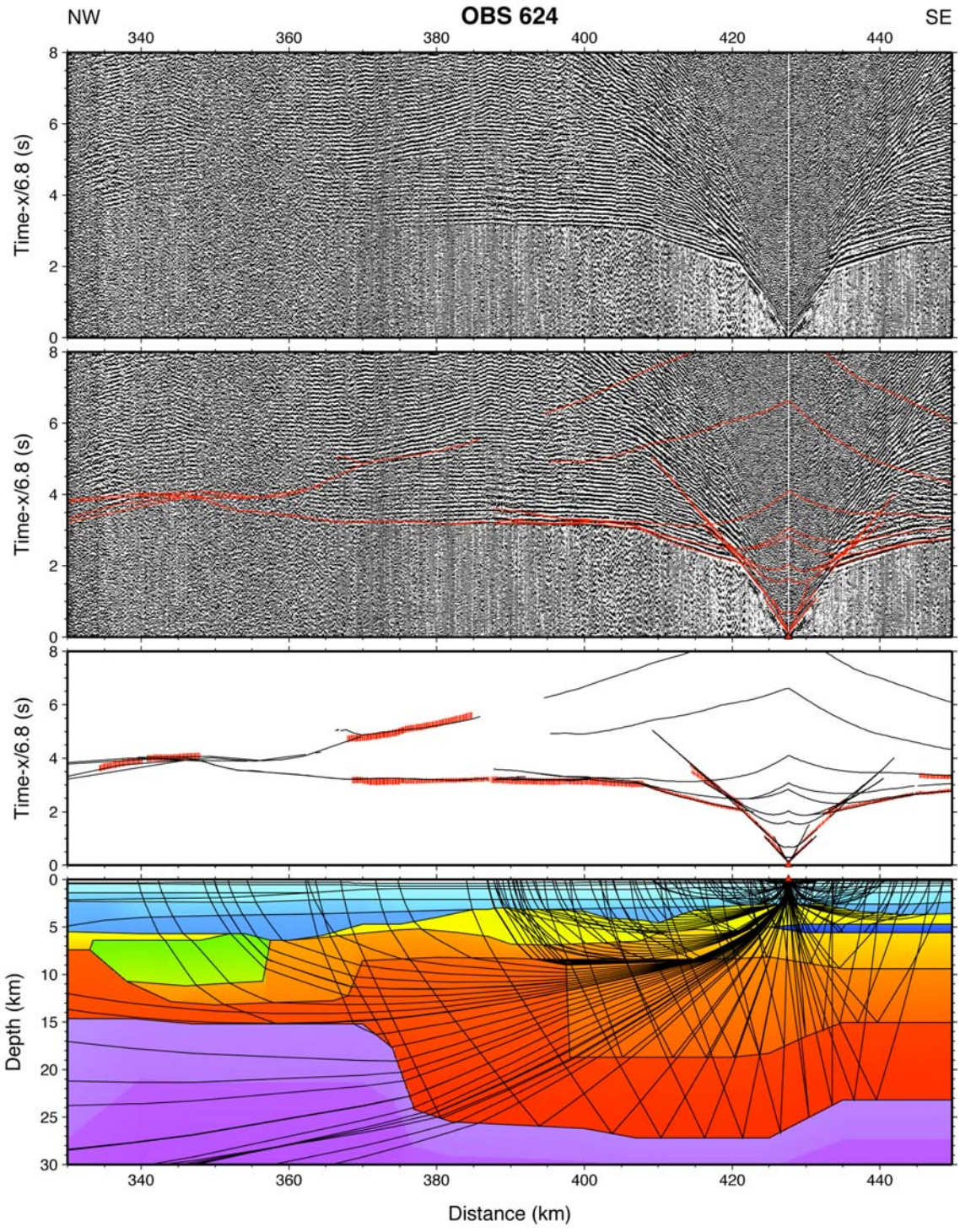

Figure A-21. *Seismic record, ray paths and travel times for OBS 624. The record shows the hydrophone component of the instrument. A more detailed description of the figure is given in the introduction to Appendix A.*

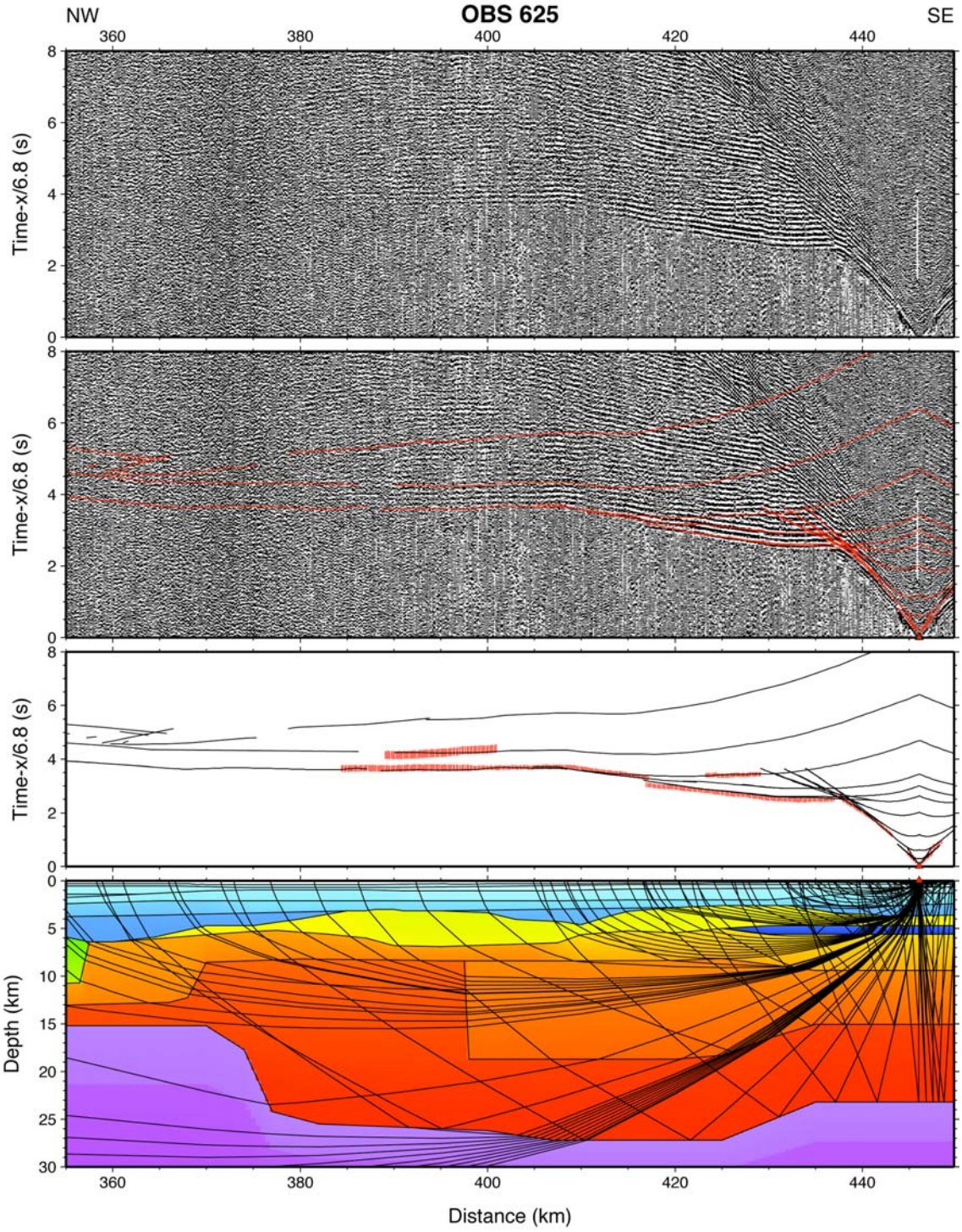

Figure A-22. *Seismic record, ray paths and travel times for OBS 625. The record shows the hydrophone component of the instrument. A more detailed description of the figure is given in the introduction to Appendix A.*

Appendix B

Reflection Seismic Records

The reflection seismic data along lines BGR08-313 and BGR08-315 were used to guide the velocity model within the sedimentary column down to basement. However, the basement could only be identified in some areas, which limited the use of the reflection seismic data to some extent as the basement is often the most difficult part to model in refraction seismic data due to the very variable depth. The reduced data quality along these two lines is caused by the large shot spacing. Due to time constraints, the reflection seismic data had to be acquired simultaneously with the refraction data. Instead of a shot spacing of 50 m as on the other reflection seismic lines, the shot interval was 1 min. As the ship's speed was not constant, the shot spacing varied as well but was in average around 150 m. The large shpt spacing resulted in a lower fold when compared with the other reflection seismic lines of the experiment. In addition, the seismic source was more low-frequent as two additional 1953-in^3 Bolt airguns were used during the refraction operation. The seafloor multiple is generally located above the basement. Hence, the data quality around basement was reduced by the multiple removal process.

The reflection seismic data are owned by the Federal Institute for Geosciences and Natural Resources (BGR; Hanover, Germany) and are shown with permission by BGR (Volkmar Damm, BGR, personal communication 2010).

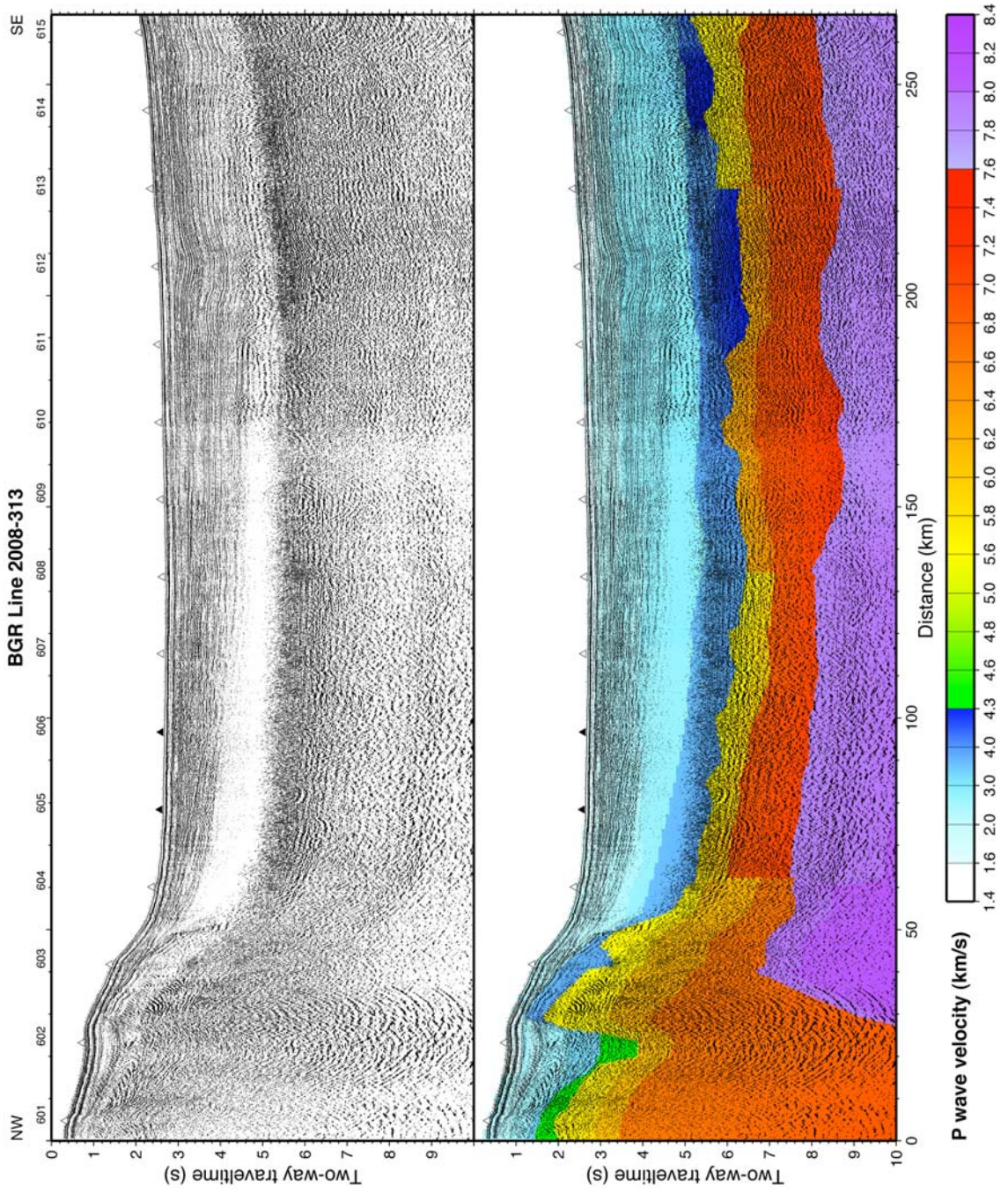

Figure B-1. *(top) Reflection seismic record (migrated) along line BGR08-313. (bottom) The same record shown together with the time-converted velocity model along line 600. Horizontal scale is distance along the velocity model. White and black triangles show the location of functional and non-functional OBS, respectively. OBS numbers are indicated at the top.*

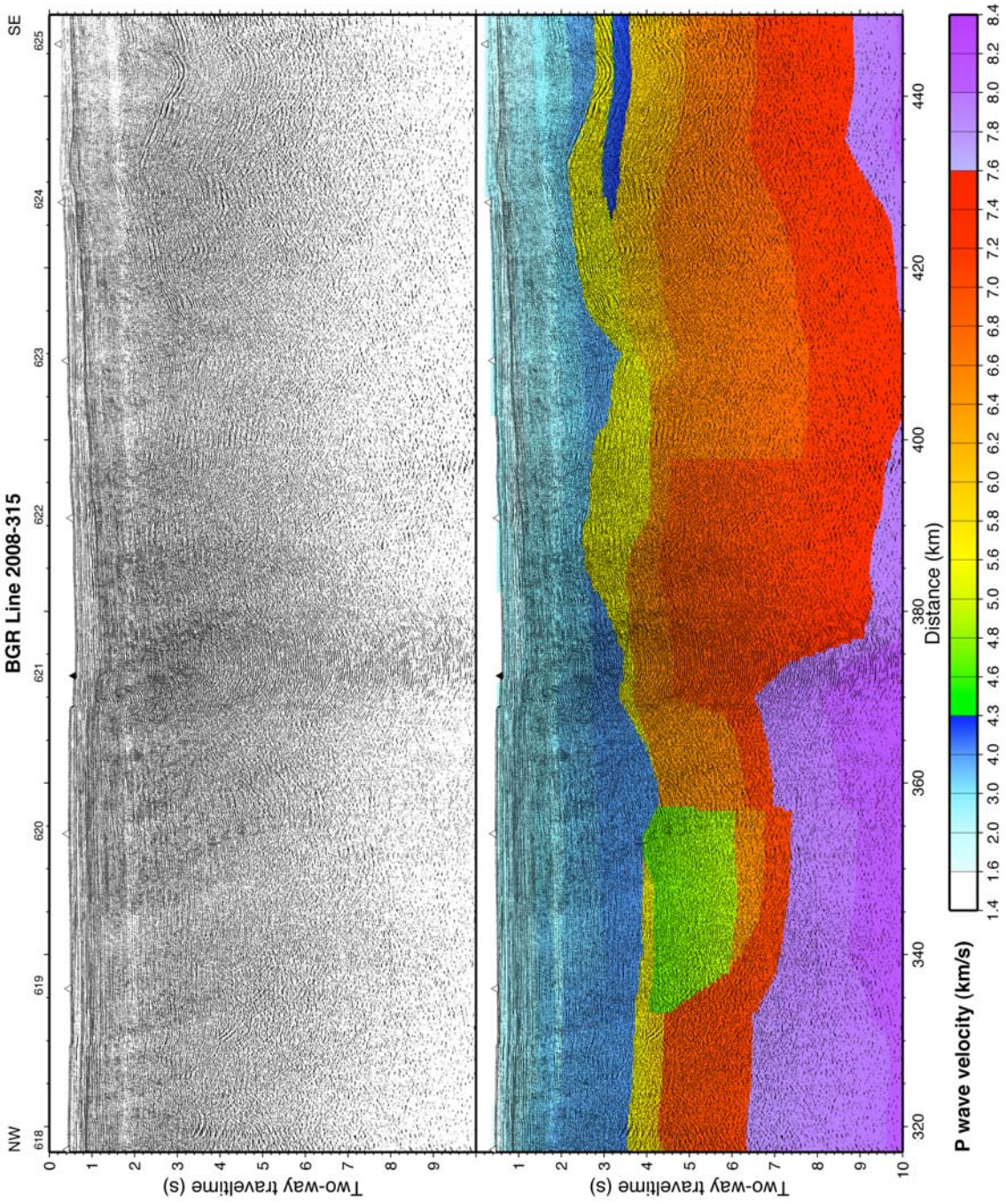

Figure B-2. *(top) Reflection seismic record (migrated) along line BGR08-315. (bottom) The same record shown together with the time-converted velocity model along line 600. Horizontal scale is distance along the velocity model. White and black triangles show the location of functional and non-functional OBS, respectively. OBS numbers are indicated at the top.*

Appendix C

CD-ROM

This report includes a CD-ROM that contains

- this report in PDF format,
- the velocity model of line 600 as a grid file in Network Common Data Format (NetCDF),
- the velocity model of line 600 in ASCII format (c.in format, a description is given on the CD-ROM),
- a grid of the diagonal values of the resolution matrix of the *P* wave velocity model along line 600 in Network Common Data Format (NetCDF) – for velocity nodes only,
- an ASCII table with the diagonal values of the resolution matrix of the *P* wave velocity model – for both the velocity and boundary nodes,
- the deployment positions of the ocean bottom seismometers (ASCII table with latitude, longitude and the OBS number),
- the recalculated positions of the ocean bottom seismometers at the seafloor,
- the shot positions along line 600.